2024

Estrogen Receptor (ER) Alpha Regulatory Mechanisms and Therapeutic Strategies in ER+ Breast Cancer

Bianca A. Romo
Dartmouth College, bianca.a.romo.gr@dartmouth.edu

Estrogen Receptor (ER) Alpha Regulatory Mechanisms and Therapeutic Strategies in ER+ Breast Cancer

A Thesis
Submitted to the Faculty
in partial fulfillment of the requirements for the
degree of

Doctor of Philosophy

in

Cancer Biology

by **Bianca A. Romo**

Guarini School of Graduate and Advanced Studies
Dartmouth College
Hanover, New Hampshire

May 2023

Examining Committee:

Chairman_____
Todd W. Miller, Ph.D.

Member_____
Arminja Kettenbach, Ph.D.

Member_____
Xiaofeng Wang, Ph.D.

Member_____
Christy R. Hagan, Ph.D.

_____
F. Jon Kull, Ph.D.
Dean of the Guarini School of Graduate and Advanced Studies

PREFACE

Abstract

Breast cancer is among the most frequently diagnosed cancers in the U.S. and is one of the leading causes of cancer-related mortalities, second to lung cancer. Estrogen receptor alpha-positive (ER+) breast cancer accounts for 2/3 of diagnosed cases. Patients diagnosed with this subtype of breast cancer typically undergo endocrine therapy that aims to mitigate the growth-promoting effects of estrogen/ER. While therapies are effective, 1/3 of patients will experience recurrence. To begin addressing this drug-resistant patient population, we investigated potential drug targets involved in response to treatment.

Coregulators have been implicated in the regulation of ER transcriptional activity and subsequently affecting the success of treatment with endocrine therapies. Using the mutant biotin ligase labeling system TurboID, we profiled the ER interactome in response to estrogen to identify novel regulators of ER activity. By identifying novel targets, we aim to identify new therapeutically targetable vulnerabilities.

Upon cancer recurrence with endocrine therapies, patients are often switched to an alternative endocrine therapy combined with another targeted therapeutic such as a phosphatidylinositol 3,4,5-trisphosphate (PI3K) inhibitor. To further address the potential mechanisms of resistance to targeted therapies such as PI3K inhibitors, we have generated resistance models under various genetic mutations (*PIK3CA* and *PTEN*) in the setting of fulvestrant resistance to

ascertain kinases that could potentiate tumor survival. Phosphoproteomic analysis of *PTEN* deficient tumors resistant to PI3K inhibition identified ATM as a top kinase for further validation as to its role in the development of PI3K resistance. For clinical relevance we are also investigating *PIK3CA* mutants to determine if results observed from phosphoproteomic analyses in a *PTEN*-deficient model could be extended to models with other forms of PI3K pathway activation and resistance to other subtypes of PI3K inhibitors. Preliminary work has identified that *PI3KCA* mutant cell lines resistant to both fulvestrant and GDC-0941 show increased sensitivity to ATM inhibition. These findings promote further investigation as to ATM inhibition's effects on *PTEN* deficient lines.

ACKNOWLEDGMENTS

As I begin to thank everyone that has helped me on this journey, I have to begin with my mentor, Dr. Todd W. Miller. Words cannot express how thankful I am to have found myself as a member of his lab. Todd genuinely cares for each and every one of his students and does his best to mentor each student in a way that will best support their success. The memory that stands out to me in the process of my Ph.D. was during my 4th year IDP meeting when Todd asked me what my career goals were, and I responded with a career as a professor. He immediately started typing on his computer putting me in contact with his colleagues so I could begin networking. This is but one instance of Todd's willingness to help his students meet their goals. I have learned a great deal during my time in Todd's lab and would not be the scientist I am today without his guidance. So once again Todd thank you. I would also like to extend my thanks to my committee members, Arminja Kettenbach, Xiaofeng Wang, and Christy Hagan. Thank you for your scientific suggestions and guidance throughout this process.

Thank you to my parents for their constant support especially in these last few months. Thank you for pushing me to demand more out of life and to ultimately do what will bring me happiness. I love you very much and to answer your question, yes, I am officially done with school.

Shoutout to my STMU crew, Luis C., Diana D., Keyera R., and Raul R. Although we may be separated by miles this group of people were there from the start of all of this. Thank you for your support and encouragement. We all

decided to do this crazy thing called grad school. I'll forever remember our Zoom movie nights during COVID.

Thank you to all of the friends that I have made along the way here at Dartmouth. From visiting the Ice Castles, paint nights, dinners on The Green, and movie nights, we shared so many laughs and stories. I wish you all the best as you continue on in your journeys. I look forward to seeing your successes.

Finally, I have to say thank you to my lab. I cannot fully express the gratitude, appreciation, and love that I have for my fellow lab mates. Being so far away from family could have been so detrimental, but I am so fortunate to have created another family. These people are some of the best that you could ever hope to meet. As a Ph.D. student you spend countless hours working towards your project, spending more time together than you ever have with your own family. It truly makes coming into lab so enjoyable when you have people that you can not only have intellectual conversations one second and shift to taking a quiz about the type of fictional character you are. It is so valuable to have people in your life that understand the challenges that you face and can commiserate with you. They see you at your best of times and the worst of times and in the worst of times help to pick you up and support you. Thank you to Nicole for being an amazing student mentor when I first started in the lab, helping to answer my million and one questions. Thank you, Charlotte, for all of your support and encouragement. Thank you to Steven for always being ready to engage in a philosophical conversation and providing guidance whether that be in life or in science and always asking if I was getting enough sleep. Thank you to Abby for

always being willing to lend a listening ear and just being a genuine human being that you can't help but feel happy and seen when you're around her. Thank you to Anneka for being such an optimistic presence and amazing support and always reminding us to "trust yourself". I am so thankful to you for keeping me accountable and helping to push through to finish writing. Thank you to Alyssa for tolerating all the funny videos that I send you and engaging in witty and sarcastic banter. Thank you to Huijuan for all the help that you gave me in these last few months, you helped to alleviate so much stress. You are just such a kind human being. Very rare is it that you find such genuine people to move through life with but also to have the privilege of working with every day. Some might think we are a little weird with how close we are, but we're just The Miller Lab.

"How lucky I am to have something that makes saying goodbye so hard" – A.A. Milne

Table of Contents

ABREVIATIONS

AI – aromatase inhibitor

AKT – protein kinase B

ATCC – American Type Culture Collection

BC – breast cancer

BCA – bicinchoninic acid assay

BSA – bovine serum albumin

CDK4/6 – cyclin dependent kinase 4/6

CHX – cycloheximide

DAB – 3,3'-diaminobenzidine

DCC-FBS – dextran-coated-charcoal-treated FBS

DMEM – Dulbecco's Modified Eagle's Medium

E2 - 17β-estradiol

ERα – estrogen receptor alpha

EREs – estrogen response elements

HD – hormone deprivation

HER2 – human epidermal growth factor receptor 2

HR - Homologous recombination

IHC – immunohistochemistry

mTORC – mammalian target of rapamycin

PI3K – phosphatidylinositol 3, 4, 5-triphosphate

PARP – poly(ADP-ribose) polymerase

PR – progesterone receptor

PTEN – phosphatase and tensin homolog

Rb -retinoblastoma

SERM – selective estrogen receptor modulator

SERD – selective estrogen receptor downregulator

shRNA – short hairpin ribonucleic acid

SRB – sulforhodamine B

S6 – ribosomal protein S6

TNBC – triple negative breast cancer

TRIM33 – tripartite motif containing 33

TUNEL – terminal deoxynucleotidyl transferase dUTP nick end labeling

LIST OF TABLES

LIST OF FIGURES

CHAPTER 1: INTRODUCTION

1.1 Breast Cancer

Breast cancer is the most frequently diagnosed cancer in women in the United States, accounting for about 30% of all diagnosed cancer cases[1]. Diagnosis of breast cancer before the age of 40 accounts for about 2% of the diagnosed population with the highest rate of incidence being 31% in women age 60-69, at which point incidence decreases to 20% at age 70-79[1]. Over the years, breast cancer incidence has shifted as a result of informed treatment practices. Breast cancer-related mortality accounts for about 15% of all cancer cases, second to lung cancer[1]. The mortality rates of breast cancer showed a steady increase from 1975 – 1989, which have ultimately decreased since 2017 as a result of advances in methods of detection and treatment[2,3]. The 5-year survival rate in the US is 91%, with 84% and 80% being the 10- and 15-year survival rates, respectively[3].

In the 1980s, breast cancer incidence was observed to increase due to increased mammography screening as well as increased use of hormonal therapy for the treatment of menopause[4]. In the early 2000s, this incidence experienced a decrease due to halting of hormonal therapy[4]. From patient data from 2015-2019, breast cancer incidence rates have been shown to vary among ethnicities, with White patients at 133.7 per 100,000, Black patients at 127.8 per

100,000, and Hispanic patients at 99.2 per 100,000[1]. In recent years, early-stage disease has seen an increased incidence, while late-stage (*de novo* metastatic) incidence, experienced a drastic increase from 2004-2011 (2.4% incidence rate per year) but has since leveled at 0.9% increase per year, highlighting the potential role of imaging for detecting early metastasis[1].

Efforts to prevent breast cancer have identified modifiable lifestyle risk factors, which include maintaining a healthy weight, moderating alcohol intake, regular physical activity, and avoiding hormonal therapy post-menopause. Additionally, breastfeeding has been identified to lower risk of triple-negative breast cancer[5,6]. As an additional means to prevent breast cancer, patients can elect to have prophylactic surgery, as especially directed by The National Comprehensive Cancer Center Network (NCCN) for patients with cancer-predisposing *BRCA1/2* mutations.

1.2 Breast Cancer Management

The more common areas that breast cancer can originate from are within the lobules and ducts. Cancers of the lobules and ducts are termed adenocarcinomas and can be further subdivided on the basis of their invasiveness: *in situ* (non-invasive) or invasive. When examining patients, consideration must be taken for the presence of masses to nearby lymph nodes, potentially indicating the spread (metastasis) of cells to distant sites. Upon initial

detection of a mass, patients will undergo testing by fine-needle aspiration, core biopsy, or surgical removal for further analysis by pathology.

A combination of immunohistochemistry (IHC) and fluorescent *in situ* hybridization (FISH) will be used to subtype a tumor based on molecular profiling for the presence or absence of hormone receptors (estrogen receptor alpha [ERα] and progesterone receptor [PR]) and human epidermal growth factor receptor 2 (HER2). From molecular profiling, breast cancer is commonly divided into 4 groups: Luminal A, Luminal B, Human epidermal growth factor receptor 2 positive (HER2+), and triple-negative. Luminal cancers can be separated by the level of expression of hormone receptors. Luminal A is ER+/PR+/HER2-ve with low markers of proliferation (Ki67); Luminal B also express ERα but have higher expression of Ki67 with variable expression of PR[7]. ER+ breast cancer accounts for about 2/3 of diagnosed breast cancers[8]. ER+ breast cancers are dependent on estrogen hormones for growth and tumor progression.

The presence or absence of the above-mentioned markers dictates the course of treatment that patients undergo. Patients with ER+ breast cancer will typically be administered endocrine therapies designed to specifically interrupt estrogen's growth-promoting capabilities. Currently available adjuvant treatments (A) target ERα for degradation (SERD- selective estrogen receptor downregulator), (B) competitively bind to ER over natural ligand estrogens

(SERM- selective estrogen receptor modulator), or (C) inhibit endogenous production of estrogen (AI- aromatase inhibitor).

1.3 Cellular Functions of Estrogen Receptor Alpha

ERα is encoded by the *ESR1* gene on chromosome 6 locus 6q25.1 and is a nuclear hormone receptor responsive to estrogen steroid hormones. ER consists of four functional domains: the ligand-binding domain, the hinge domain, the DNA-binding domain, and the amino-terminal domain. The amino-terminal domain contains a transcription activation function 1 (AF-1) which plays a role in ligand-independent activation, while the activation function 2 (AF-2), located in the DNA-binding domain, is responsible for ligand-dependent activation[9]. ER can engage in ligand-dependent or ligand-independent transcriptional regulation. In the canonical ligand-dependent pathway, estrogens such as 17b-estradiol (E2) (or the less potent ligand estrone) will bind the estrogen receptor alpha at the ligand binding domain. This binding results in the reversal of the repressive effects of heat shock proteins (HSP70 and HSP90), allowing conformational changes exposing the nuclear localizing domain located in the hinge domain. The estrogen receptor is then able to homodimerize via the D-box located in the DNA binding domain[10]. Once in the nucleus, the DNA binding domain will promote interaction with estrogen response elements (EREs) for modulation of gene transcription.

To elicit transcriptional regulation, chromatin structure may need to be altered for ER to access regulatory sites. For this process, the estrogen receptor relies on the action of pioneer factors such as FOXA1[11] to open chromatin via their ability to bind nucleosomes[12,13]. With the ligand binding of the estrogen receptor, this leads to a conformational change exposing helix-12 that promotes interactions with coactivators for further modulation of transcription[14–16]. Examples of additional coactivators that promote modulation of ER-regulated transcription include *p300*, *SRC-3, BRG-1, CARM1,* and *TET2*[17–23]*.* Further action by transcription factors like GATA3 promote estrogen receptor activation and engage in a positive regulatory loop necessary for estrogen mediated growth of breast cancer cells [24,25]. The estrogen signaling pathway promotes tumor growth via inducing transcription of genes that are involved in cell cycle progression *(MYC* and *CCND1)*[26,27]. In addition to activating components necessary for cell cycle progression, ERα also promotes the induction of genes responsible for inhibiting apoptosis (*BCL2*[28–30] and *BCL2L1*[31]*)*. In parallel to upregulating genes upon E2, many more genes are downregulated. Such classes of genes include: transcriptional repressors (Mad4 and JunB), antiproliferative (cyclin G2), and proapoptotic (BCL-2 antagoinist/killer 1, caspase 9, TGFβ growth inhibitory factors), further promoting breast cancer cell proliferation with E2 administration[32].

In addition to direct signaling, the estrogen receptor can modulate gene expression via indirect genomic signaling relying on the conditions of protein-

protein interactions in the nucleus[33]. For genes that do not contain estrogen response elements, ER is able to indirectly bind to DNA via interaction with co-factors like SP-1, AP-1, and NF-κB[15,34]. When in complex with the cofactor AP-1, ERα is able to modulate the transcription of genes like insulin-like growth factor-1 (*IGF1*), IGF-1 receptor (*IGF1R*), and cyclin D1 (*CCND1*)[35]. The DNA binding domain in this indirect genomic signaling does not need direct binding to DNA; however, it is believed that this domain is necessary for the protein-protein interactions characteristic of this signaling mechanism, or is involved in recruitment of proteins necessary for coregulation[36].

Within the cell, there exist numerous signaling pathways that upon induction elicit a kinase cascade, resulting in phosphorylation and activation of downstream effector proteins. One such consequence of this cascade is the activation of the estrogen receptor in a ligand-independent manner. An example of a post-translational modification that can initiate ER activity is phosphorylation[37]. The N-terminal domain of ER has been shown to be highly phosphorylated with Ser118 being the most well characterized site[38–43]. Epidermal growth factor (EGF) can lead to activation of ERα via MAPK activation, and more recently this phosphorylation event has been implicated in increasing cell proliferation through complex with AP-1 and pre-B-cell leukemia transcription factor 1 (PBX1)[43–46]. Furthermore, the IGF-1R and fibroblast growth factor receptor (FGFR) can lead to the activation of phosphatidylinositol 3-kinase (PI3K) pathway, resulting in phosphorylation of ERα at Ser167 by p90RSK and

AKT[33–35]. Due to this crosstalk between the ER and PI3K and MEK/ERK pathways, this exists as an important consideration for the treatment of patients diagnosed with ER+ breast cancer.

1.4 Regulation of ER Stability

The transcriptional activity of ER can be altered via interactions with coregulators and post-translational modifications such as phosphorylation and ubiquitination. Estrogen administration induces the polyubiquitination of ERα beginning the process of ER degradation through the ubiquitin proteasome pathway[47–49]. For processing through the ubiquitin proteasome system, a substrate will typically first be phosphorylated or methylated to be recognized by ubiquitin ligases for addition of ubiquitin to lysine residues in a sequential process to build polyubiquitin chains[49]. Several E3 ubiquitin ligases have been identified to be responsible for ubiquitination of ER: CHIP[50], E6AP[51], BRCA1[52], BARD1[53], SKP2[54], MDM2[55], and Hbo1[56]. This ubiquitination and degradation of the estrogen receptor are necessary processes in the transcriptional cycle of ER whereby liganded ER promotes cycling on ERE sites for transcriptional activation/repression[57,58,59].

In addition to their protein degradation capabilities, some E3 ubiquitin ligases act as coactivators for ER. E6AP has been shown to be recruited to promoters alongside ER to ERE sites[51,57]. MDM2 in conjunction with ER can

promote binding to the promoter of the canonical ER-inducible gene *TFF1*[57]. These are just two examples of the potential of E3 ubiquitin ligases possessing transcriptional activating capabilities in a context dependent manner that are able to influence ERα activity. In later chapters, I will discuss my work done to identify a novel E3 ubiquitin ligase's role in the regulation of ER signaling.

1.5 Mechanisms of Resistance to Treatment in ER+ Breast Cancer

In the treatment of ER+ patients, 1/3 of patients will eventually develop resistance. Resistance to treatments can present as several clinical scenarios: (1) a patient is resistant to all hormonal therapies or no longer responds to treatment or subsequent endocrine treatment (*de novo* resistance), (2) resistance to a select group of endocrine therapies but not others (*de novo* resistance), (3) response to initial endocrine therapy and subsequent alternative endocrine therapies before complete failure to respond to all endocrine treatments (acquired resistance), (4) progression following endocrine therapy with partial response when administered the same reagent after several years[60]. Mechanisms that lead to the above-mentioned schemes of resistance include alterations to ER, co-regulator dysregulation, growth factor receptors, and cell cycle regulators.

1) Alterations to ERα: Loss of ER expression has been implicated in the development of resistance to endocrine therapies in 17% of patient

samples[61]. A potential explanation for the loss of ERα is due to epigenetic regulation with methylation of the estrogen receptor gene[62] . Alternative alterations include *ESR1* mutations. Mutations specifically occurring in the ligand binding domain promoting an agonistic conformation resulting in estrogen independent growth[63] . *ESR1* mutations were observed to occur in about 20% of patients with the predominant mutation being D538G with Y537S being the next most common[63,64] . Finally, *ESR1* fusions such as, *ESR1-CCDC170* (fusion of the 5' untranslated region of *ESR1* to the *CCD170* coding region) generating truncated CCDC170[65], have been shown to provide ligand-independent growth[66], anchorage independent growth advantages, assist in motility, and provide reduced sensitivity to endocrine treatments[66]. The fusion *ESR1-YAP1* has also been shown to induce downstream ER signaling leading to estrogen independent growth[67].

2) Co-Regulator Dysregulation: The estrogen receptor is a nuclear hormone receptor transcription factor. Upon binding of estrogen to the ligand binding domain, ER homodimerizes and is shuttled from the cytoplasm to the nucleus[68]. Once in the nucleus, ERα will bind to regions on DNA known as estrogen response elements (ERE) to elicit modulations to gene expression[69]. Additional modulations to ER can occur via interaction with cofactors.

In the case of enhancing transcription, one of the first co-activators to be identified as enhancing ER driven transcription was steroid receptor coactivator-1 (SRC-1)[70]. In opposition to this, co-repressors function to repress transcription. Dysregulation of the expression of these coactivators has been shown to be a driving factor in the progression of breast cancer. Examples of this include AIB1, whose overexpression and amplification has been shown to contribute to cancers whose growth is driven by hormones[71]. Further manipulation of ER activity can be accomplished by altering the association with co-regulators. Examples include overexpression of HOXB7, leading to increased HER2 expression and downstream ERα target genes contributing to resistance to tamoxifen[72]. Mediator of DNA damage checkpoint 1 (MDC1) was identified to distinctly act as a novel regulator of ER in the context of invasive lobular carcinoma (ILC), and was observed to affect proliferation and response to tamoxifen[73]. Oct-4 overexpression was shown to be necessary for tamoxifen resistance via complex formation with ER, Skp2, and p38MAPK to promote expression of tamoxifen resistance genes[74]. The above-mentioned co-factors are but a few examples of the unfortunate consequences that can arise from the dysregulation in protein interactions.

3) Receptor Tyrosine Kinases and Signaling Pathway Activation: Receptor tyrosine kinases can have broad reaching effects leading to a cascade of downstream intracellular signaling. Dysregulation to levels/activation of

receptors (EGFR, ERBB3, FGFR1, IGF-1R, insulin receptor, HER2) have been shown to play a role in the development of resistance to endocrine therapies and be used as potential biomarkers for response to long-term treatment [75,76,77,78]. In addition to direct alteration/activation of these kinases, they can in turn activate downstream intracellular pathways including PI3K/AKT/MTOR. A consequence of activation of the PI3K/AKT/MTOR pathway is the potential to phosphorylate ERα, resulting in ligand independent activation[79]. Mechanisms that lead to aberrant activation are mutations to *PIK3CA* (the p110a catalytic subunit of PI3K) and the tumor suppressor *PTEN* [80]. Within luminal breast cancer, *PIK3CA* mutations range from 32-49% and *PTEN* mutations/loss range from 13-24%[80].

HER2 provides another mechanism by which endocrine resistance may develop. Overexpression/amplification of HER2 occurs in about 10% of ER+ patients. This promotes agonistic effects of the anti-estrogen tamoxifen[81] as well as loss of ERα when combined with overexpression of MAPK[82].

4) Cell Cycle Regulators: The cell cycle is a delicately coordinated process and aberrant regulation can lead to disastrous proliferation. Retinoblastoma (RB) protein is a modulator of the cell cycle and is hyperphosphorylated by cyclin D1/CDK4 and cyclin D3/CDK6 to promote

expression of cell cycle-driving genes. RB loss was shown to decrease time to recurrence in patients receiving SERM treatment [83]. Cyclin D1 was amplified in a range of 29-58% of luminal breast cancer patients [80]. CDK4 was observed to be amplified in 14-25% of luminal patients[80].

1.6 Management of Endocrine Resistant ER+ Breast Cancer

Upon the development of resistance to endocrine therapies, patients are switched to either an alternative endocrine therapy and/or begin treatment with a targeted therapeutic. As mentioned in the previous section, there exist several FDA approved drugs against components such as PI3K (p110a), CDK4/6, and mTOR for use in combination with endocrine therapies to treat advanced breast cancer. The MTOR inhibitor everolimus in combination with exemestane was FDA approved for postmenopausal hormone receptor positive, HER2 negative women based on results of the BOLERO-2 trial showing an increase of median progression-free survival by 4.1 months compared to exemestane/placebo [84].

Palbociclib, a CDK4/6 targeting therapy, received FDA approval in 2015 followed by the approval of CDK4/6 targeting agents ribociclib and abemaciclib in 2017. Approval for Palbociclib was based on the findings of two studies: PALOMA-2 showed increased progression free survival from palbociclib when used in combination with letrozole as a first line treatment in women with advanced ER+ breast cancer[85]; PALOMA-3 showed increased overall survival in patients who previously responded to endocrine therapy[86].

For patients with PI3K pathway activation, the p110a targeting drug alpelisib was FDA approved in combination with fulvestrant in 2019 from findings of the SOLAR-1 trial for postmenopausal hormone receptor positive HER2 negative patients, specifically with *PIK3CA* mutation. Fulvestrant plus alpelisib showed an increase in progression-free survival of 11 months compared to the 5.7 months of fulvestrant plus placebo[87].

The above listed treatment modalities are but a few of the available treatment options for patients experiencing resistance to treatment. In later chapters, I will discuss the work that we are carrying out in the lab to investigate methods of resistance to combination treatment with PI3K pathway inhibitors and the SERD, fulvestrant, as well as novel targets for further investigation.

CHAPTER 2: GENERAL METHODS

2.1 Cell Culture, reagents, and drug treatments

MCF-7, T47D, BT-549, MDA-MB-415, CAMA-1, ZR75-1, CAOV3, EFO21, OVCAR4, EFO27, IGROV1, SKOV3, BT20, HCC70, and HCC1806 cell lines were obtained from the American Type Culture Collection (ATCC). CAL-51 and CAL-120 cells were obtained from DSMZ (Braunschweig, Germany). LentiX cells were obtained from Clontech (Mountain View, CA, USA). Cell lines were cultured in Dulbecco's Modified Eagle's Medium (DMEM; Corning) with 10% fetal bovine serum (FBS; R&D Systems). MCF-7/FR cells were obtained from Matthew Ellis (Washington Univ., St. Louis, MO). MCF-7/FR, T47D/FR, MDA-MB-415/FR, ZR75-1/FR cells were maintained in DMEM supplemented with 10% FBS with continuous treatment of 1 uM fulvestrant (Tocris Biosciences). MCF-7/FR/BR, and MCF7/FR/GR cells were generated from MCF-7/FR obtained from Matthew Ellis (Washington Univ., St. Louis, MO). MCF-7/FR/BR, T47D/FR/BR, and MCF7/FR/GR, and T47D/FR/GR cells were maintained in 1 uM fulvestrant (Tocris Biosciences) and 1 uM BYL-719 (Selleck Chemical) or 1 uM GDC-0941 (Selleck Chemical) in DMEM supplemented with 10% FBS. Cells were passaged using 0.25% phenol-red free trypsin (Gibco) with 2.21 mM EDTA. For experiments done in hormone deprived conditions (HD), cells were cultured for the specified time in phenol-red free DMEM (Corning) supplemented with 10% dextran coated

charcoal-treated FBS (DCC-FBS; R&D Systems) and 2 mM GlutaMAX (ThermoFisher Scientific).

Drugs used in experimental conditions were reconstituted in ethanol, DMSO, or sterile water. Reconstituted drugs were stored at -20°C. Refer to Table 2.1 for drug dilutions for *in vitro* and Table 2.5 for *in vivo* experiments. Ribociclib and abemiciclib were obtained from Alibaba.

Table 2.1 Drug Concentrations and Vehicles for *in vitro* experiments

Drug	Vehicle	Vendor	Working Concentration
17b-estradiol	Ethanol	Sigma	1 nM
Palbociclib	DMSO	Pfizer	200 nM
Ribociclib	DMSO	Alibaba	2 uM
Abemaciclib	DMSO	Alibaba	500 nM
Fulvestrant	Ethanol	Tocris Biosciences	1 uM
AT13387	DMSO	Astex Therapeutics, Ltd.	0.1 uM
S63845	DMSO	APExBio	0-2 uM
ABT-737	DMSO	APExBio	0-2 uM
ABT-199	DMSO	APExBio	0-2 uM
A1155463	DMSO	APExBio	0-2 uM
GDC-0941	DMSO	Selleck Chemical	1 uM
BYL-719	DMSO	Selleck Chemical	1 uM
AZD1390	DMSO	Selleck Chemical	10 nM
Puromycin	DMSO	Sigma	1 ug/ml

2.2 Immunoblot

Chemicals were purchased from Sigma (exceptions will be specified). Cells were rinsed twice with PBS, then lysed using RIPA buffer (20 mM Tris, pH 7.4, 150 mM NaCl, 1% NP-40, 10% glycerol, 1mM EDTA, 1mM EGTA, 5mM NaPPi, 50mM NaF, 10mM Na β-glycerophosphate) plus fresh HALT protease inhibitor cocktail (Pierce) and 1mM Na_3VO_4 (New England Biolabs). Lysates were sonicated at 30% power for 10 s, then centrifuged 17,000 x g for 10 min at 4°C. Protein content was quantified from lysate supernatant by bicinchoninic acid (BCA) assay (Pierce) and diluted to equivalent concentrations across samples. Protein extracts were reduced with 1.25% β-mercaptoethanol and denatured with 4X NuPAGE buffer (ThermoFisher Scienctific) and heating to 95°C for 1min. Proteins were separated using an SDS-PAGE gel at a constant 130 V. Proteins were transferred from separated gels to nitrocellulose membranes by a semi-dry transfer apparatus (Bio-Rad) for 10 min, 25 V. Membranes were stained with Ponceau S to confirm even protein loading and transfer. Membranes were blocked with 5% BSA for 1 h, then probed with primary antibody (Table 2.2) diluted in 5% BSA overnight at 4°C. Membranes were washed 3 x 5 min in TBST, incubated in secondary antibody for 1 h at room temperature, and rinsed 3 x 10 min. Signal was detected using horseradish-peroxidase labeled secondary antibodies (GE Healthcare) and ECL substrates (Pierce) with imaging using the ChemiDoC MP (Bio-Rad), or DyLight conjugated secondary antibodies (Cell Signaling Technology) or IRDye® conjugated secondary antibodies (LI-COR

Biosciences) with imaging using the LI-COR Odyssey system (LI-COR Biosciences).

Table 2.2 Antibodies for Immunoblot

Antibody	Vendor	Catalog Number	Dilution
Estrogen Receptor α	Santa Cruz Biotechnology	SC-8002	1:1000
Vinculin	Cell Signaling Technology	13901	1:5000
β-actin	Cell Signaling Technology	3700	1:5000
FLAG	Millipore Sigma	F3165	1:1000
IRDye® 800CW Streptavidin	LI-COR Biosciences	926-32230	1:7000
AKT p473	Cell Signaling Technology	4060	1:1000
AKT p308	Cell Signaling Technology	13038 4056	1:1000
pS6 240/244	Cell Signaling Technology	5364L	1:1000
pKAP1 S824	Bethyl Laboratories	A300767AT	1:2000
TRIM33	Cell Signaling Technology	90051S	1:500
Bim	Cell Signaling Technology	C3C45	1:1000
Bak	Cell Signaling Technology	D4E4	1:1000
Bax	Cell Signaling Technology	2774	1:1000
Mcl-1	Cell Signaling Technology	4572	1:1000
Puma	Cell Signaling Technology	D3040	1:1000
Bcl-2	Cell Signaling Technology	2872	1:1000
Bcl-xL	Cell Signaling Technology	11E3	1:1000
Bid	Cell Signaling Technology	2002	1:1000

2.3 Immunohistochemistry

Formalin-fixed and paraffin-embedded (FFPE) blocks were cut into 5-micron sections and placed on slides. Sections on slides were deparaffinized and rehydrated in xylene and graded ethanol washes (100%, 90%, 70%, 50%, and 0%, 5 min each), respectively. Heat-induced epitope retrieval was performed using either Tris-EDTA (pH 9) or Citrate (pH 6) buffers for 20 min on 'high' in a pressure cooker (Cuisinart). Sections were then permeabilized with 0.2% Triton X-100 in TBST and rinsed in TBST. Sections were blocked in 5% goat serum in PBS for 1 h, then incubated in blocking solution containing primary antibody overnight at 4°C. A list of antibodies used can be found in Table 2.3. The following day, sections were washed 3 x 5 min in TBST, then blocked in 0.3% hydrogen peroxide in methanol for 10 min. Sections were washed for an additional 3 x 2 min in TBST to remove excess hydrogen peroxide. Signal was developed using VectaStain Elite ABC-HRP kit and DAB substrate (Vector Laboratories) according to protocol. In brief, slides were incubated in biotinylated secondary antibody for 1 hr, followed by several washes, then a 30 min ABC reagent incubation. Sections were counterstained with hematoxylin for 7 min. Slides were washed with water to remove excess hematoxylin, then incubated with Scott's solution for 7 min. Sections were dehydrated in a graded ethanol series (50%, 70%, 90%, 100% ethanol, 3 min each) and xylene (4 x 3 min washes), then mounted in Cytoseal XYL (Richard-Allan Scientifc). Proportions of positively stained cells were quantified in 3 representative 200x-magnification

microscopic images from each sample using HALOVelocity software (Indica Labs).

Table 2.3 Antibodies, Stains, and Enzymes used for Immunohistochemistry

Name	Vendor	Dilution	Antigen Retrieval	Staining
Hematoxylin	Vector Labs	1:1	-	Nuclear
Ki67	Biocare Medical (CRM325B)	1:200	TrisEDTA pH 9.0	Nuclear
TUNEL	Promega	1:100	-	Nuclear
pHistone H3 Ser10 9701	Cell Signaling Technology	1:200	Citrate buffer pH 6	Nuclear
pCHK2 T68 (82263)	Cell Signaling Technology	1:400	pH 9	Nuclear
pKAP1 S824	Bethyl Laboratories	1:2000	pH 9	Nuclear

2.4 RNA interference

Lenitviral vectors encoded constitutively expressed shRNA targeting TRIM33 (sh#5 catalog V2LHS-134255 and sh#6 V2LHS-134259) from Dharmacon or non-targeting shRNA control (catalog #SHC002) from Sigma Aldrich. Lentix cells (Clontech) were used for generation of lentivirus using standard protocols with pMD2.G (#12259) and psPAX2 (#12260) plasmids (gifted from Didier Trono; obtained from Addgene). Cells that were stably transfected were selected for one week with 1 ug/ml puromycin.

Table 2.4 Plasmid and RNA Constructs

Name	Type	Vendor	Catalogue	Target Sequence
Mission shRNA ctrl	Lentiviral	Sigma Aldrich	SHC002	Non-targeting
TRIM33 sh#6	Lentiviral	Dharmacon	RHS4430200207911	TTATCTTCAAAGTACAATG
TRIM33 sh#5	Lentiviral	Dharmacon	RHS4430200189072	ATTGACTACATTCTTTGCC
PMD2.G	Lentiviral	Addgene	12259	-
PSPAX2	Lentiviral	Addgene	12260	-

2.5 Sulforhodamine B (SRB) Growth Assay

Cells were plated in triplicate in 96-well plates at specified numbers of cells per well dependent on growth rate of cells. Cells would be seeded such that on the day of plating, cells were ~20% confluent. Cells were treated with growth media and specified drug treatment. Assays were run for 7-8 d, unless otherwise specified. Drug/media was refreshed every 4 d. Cell growth was monitored and when vehicle treated wells reached 70%-90% confluence, cells were fixed with 10% trichloroacetic acid (TCA) for 30 min at 4°C. Wells were washed with water and allowed to dry. Wells were stained with 0.4% sulforhodamine B (SRB) dye for 10 min. Wells were rinsed with 1% acetic acid and allowed to dry. SRB dye was solubilized with 10 mM Tris (pH 7.5), and signal was measured at an absorbance of 490 nm via a microplate reader (Bio-Rad).

2.6 Mouse Studies

2.6.1 Surgeries

All animal studies were approved by the Dartmouth College IACUC. For all studies, immune compromised NOD/SCID/IL2Rγ-/- (NSG) mice were used. Mice were obtained from the Norris Cotton Cancer Center Mouse Modeling Shared Resource. At 3-4 wk of age, mice for estrogen withdrawal (EW) studies were ovariectomized. To prepare for surgery, animals were shaved using fine clippers, and the surgical area was cleaned with povidone-iodine swab and an alcohol swab. Mice received a 5-mg/kg subcutaneous (s.c.) injection of ketoprofen and were anesthetized with isoflurane. An incision less than 5 mm was made in the skin on each shaved flank (left and right) and another incision was made in the body wall (left and right) for access to uterine tubes and ovaries. The uterine tubes were ligated by suture. The ipsilateral ovary was exteriorized with forceps and removed with scissors. The body wall incision was closed with a 4-0 nylon suture, and the skin incision was closed with a wound clip. Animals recover from anesthesia on a heating pad, and following recovery were returned to their cage. Animals were monitored for behavior following surgery and the day after surgery. If animals appeared distressed during recovery, the animal was euthanized, or a veterinarian was consulted.

Orthotopic tumor cell injections were done at the time of ovariectomy through the same incision site. For animals not undergoing ovariectomy, two <1-cm incisions were made in the skin on the flank over the #4 mammary fat pad.

Cells for injection were prepped on the day of surgery. In brief, cells were trypsinized into a single-cell suspension and washed with sterile PBS three times. Cells were resuspended in an appropriate volume of PBS. 50 uL of the resuspended tumor cells were bilaterally injected into the mammary fat pads.

2.6.2 Treatments and Tumor Monitoring

To stimulate tumor growth, mice received E2 treatment at the time of ovariectomy. A small skin incision was made near the upper scruff on the back. A beeswax pellet containing 17β-estradiol (E2, 1 mg) approximately 5 mm in diameter was implanted under the skin with forceps. For periods of hormone withdrawal, the pellet was removed by an incision in the skin and removal with forceps. Incisions in the skin were closed using wound clips. Treatments by oral gavage (p.o), subcutaneous (s.c) injection, and intraperitoneal (i.p.) injection were administrated while mice were under hand-held restraint.

Tumor growth was monitored biweekly via calipers (volume = length x length x width/2). Mouse body weights were measured once per week. Drug treatments are described in Table 2.5.

2.6.3 *In vivo* Luciferase Imaging

Mice were injected i.p. with 100 uL of *in vivo*-grade D-luciferin (Promega) in PBS. Mice were placed under isoflurane anesthesia. Following a 15-min uptake period, mice were imaged for bioluminescence with a Xenogen IVIS 200

System (Perkin Elmer). Signal was quantified with LivingImage software (Perkin Elmer) using regions of interest (ROIs) around tumors and a tumor-free (background) region for each image.

2.6.4 Specimen Processing

At specified experimental endpoints, mice were euthanized by carbon dioxide asphyxiation followed by cervical dislocation. Tumor specimens were harvested and cut into pieces and snap-frozen for downstream analysis. For immunohistochemistry purposes, tumor cross-sections were fixed in 10% formalin overnight, rinsed 3 x with water and stored in 70% ethanol. Specimens were submitted to Norris Cotton Cancer Center Pathology Shared Resource for processing and paraffin embedding.

Table 2.5 *In vivo* Drug Treatments

Name	Dose	Vendor	Vehicle	Route of Administration
Palbociclib	100 mg/kg/d	Pfizer	Saline	p.o
Ribociclib	100 mg/kg/d	Alibaba	Methyl Cellulose	p.o
Abemaciclib	100 mg/kg/d	Alibaba	Methyl Cellulose	p.o
Fulvestrant	5 mg/kg/wk	Tocris	10% ethanol, 90% castor oil	s.c.
GDC-0941	100 mg/kg/d	Selleck	Methyl Cellulose	p.o.

CHAPTER 3: TRIM33: A NOVEL REGULATOR OF ERα

Work described in this chapter is being prepared for peer-reviewed manuscript submission.

Romo BA, Karakyriakou B, Cressey LE, Brauer BL, Yang H, Warren A, Johnson AL, Kettenbach AN, Miller TW

ABSTRACT

Estrogen receptor alpha-positive (ER+) breast cancer is responsible for over 60% of breast cancer cases in the U.S. Among patients diagnosed with early-stage ER+ disease, 1/3 will experience recurrence despite treatment with adjuvant endocrine therapy. ER is a nuclear hormone receptor responsible for estrogen-driven tumor growth. ER transcriptional activity can be modulated by interactions with coregulators. Dysregulation of the levels of these coregulators is involved in the development of endocrine resistance. To identify ER interactors that modulate ER activity, we utilized the TurboID proximity profiling tool to create a TurboID-ER construct for profiling of ERα interactomes. LC-MS/MS analysis revealed the E3 ubiquitin ligase TRIM33 as an estrogen-dependent interactor of ERα. shRNA knockdown showed that TRIM33 promotes estrogen-dependent cell growth by promoting ERα transcriptional activity. Additionally, TRIM33 increases ER protein stability. TRIM33 provides a novel target for inhibiting estrogen-induced cell growth and provides rationale for targeting in cases of endocrine resistance that rely on high ER levels.

3.1. Introduction

Breast cancer is one of the leading diagnosed cancers in women in the United States, affecting about 30% of all cancer patients[88]. Breast cancer is subtyped based on molecular profiling for the expression of hormone receptors: progesterone receptor (PR), estrogen receptor (ER), and human epidermal growth factor receptor 2 (HER2). Among diagnosed patients, 2/3 of breast cancer cases are ER-positive (ER+)[8]. Patients affected by ER+ breast cancer typically receive endocrine therapies that target the estrogen/ER signaling axis to mitigate estrogen's tumor growth-promoting effects.

ER+ tumor growth is induced by estrogen steroid hormones including 17b-estradiol (E2). ER is a nuclear transcription factor encoded by the gene *ESR1* that upon binding of estrogens will homodimerize and be shuttled into the nucleus. Once in the nucleus, ER will bind to estrogen response elements (EREs) within DNA to modulate gene expression[69]. As an added layer of gene regulation, the liganded ER will undergo conformational changes exposing helix 12, allowing for binding of coregulatory proteins that modulate ER transcriptional activity[14–16,89,58]. Coactivators that have been identified to be involved in ER transcriptional activity include *p300*, *SRC-3, BRG-1, CARM1, TET2*[17–23]. In a paradoxical manner, E3 ubiquitin ligases have been identified to have coactivator abilities in the context of ER signaling. E6AP has been identified to interact with ER in a ligand-dependent manner and even localize to EREs alongside ERα[51,57].

MDM2 has been shown to promote expression of the ER-inducible gene *TFF1* by co-binding with ER at the gene promoter[57].

The process of transcription can be dysregulated and lead to the development of therapeutic resistance. One-third of ER+ patients being treated with endocrine therapies experience recurrence 15 years after initial diagnosis[90]. One such mechanism of resistance is alterations to co-regulator levels. Homeobox B7 (HOXB7), mediator of DNA damage checkpoint 1 (MDC1), and Oct-4 are co-regulators shown to modulate ER function, contributing to the development of endocrine resistance[72–74]. In the case of HOXB7, SERM treatment resistance was observed to have increased expression of HOXB7 that when in complex with ER was able to further drive increased expression of not only ER target genes but elevate expression of HER2[72]. Oct-4 in the presence of tamoxifen assisted in the binding of ER to regulatory sites to promote tamoxifen dependent gene activation and cell proliferation of resistant cells[74].

In an effort to identify novel interactors that may modulate ER interactions, we utilized the technique of proximity-dependent biotin labeling[91]. This system takes advantage of a mutant biotin ligase from *Escherichia coli,* biotin ligase (BirA) that has undergone yeast-display directed evolution, resulting in the 35 kD biotin ligase, TurboID[92]. The benefits of using this updated BioID system allows for labeling of transient and weak interactions on the order of minutes rather than hours without affecting the viability of cells, providing a road map of interactions

as the ligase moves through the cell[93,94,95]. Using the proximity labeling capabilities of TurboID, a TurboID-ER fusion construct was generated to profile ER interactomes. Profiling identified the E3 ubiquitin ligase tripartite motif containing 33 (TRIM33) as an interactor of ER. TRIM33 has been implicated in cancer progression and prognosis in liver, pancreatic, lung, and prostate[96–99]. However, in breast cancer the role of TRIM33 remains controversial. One report cites TRIM33 levels as being decreased in breast tumors relative to normal breast tissue[100], while another report cites tumor TRIM33 overexpression as being associated with poor prognosis in patients with breast cancer[101]. With these contradictory findings, it is clear that more investigation is warranted to determine the specific context of TRIM33's role in ER+ breast cancer. Our findings show that TRIM33 promotes ER activity and stabilizes ERα protein.

3.2 Methods

3.2.1 Plasmids and Cloning

3XF TurboID plasmid was a gift from Arminja Kettenbach (Dartmouth College). pHAGE-ESR1 was a gift from Gordon Mills & Kenneth Scott (Addgene plasmid # 116737) and was used for cloning of wild-type ESR1. pLenti PGK V5-LUC Puro (w543-1) was a gift from Eric Campeau & Paul Kaufman (Addgene plasmid # 19360) and underwent restriction digest with SalI and XbaI to remove luciferase and was used for plasmid generation below. For a complete list of primers used for construct generation, reference Table 3.2. For Flag-Turbo-Control: 3XF TurboID was cloned into digested pLenti PGK V5 (w543-1) using Hifi DNA assembly Master Mix (NEB). ESR1 was cloned from pHAGE-ESR1 for fusion with 3XF TurboID (Flag-TurboID-ESR1WT) using Hifi DNA assembly Master Mix (NEB) and insertion into pLenti PGK V5 (w543-1). TRIM33 cDNA was cloned from HA-TRIM33_pInducer20 (Genescript) into pLenti PGK V5. Lentiviral vectors encoded constitutively active shRNA targeting TRIM33 (sh#5 catalog # V2LHS-134255, and sh#6 catalog # V2LHS-134259) from Dharmacon or non-targeting shRNA control (catalog # SHC002) from Sigma Aldrich. Lentivirus was created using Lentix cells with plasmid of interest (Flag-TurboID-ESR1, shRNA ctrl, TRIM33 sh#6, TRIM33 sh#5), and pMD2.G (#12259) and psPAX2 (#12260). pMD2.G and psPAX plasmids were gifted from Didier Trono; obtained from Addgene). Transduced cells were selected with puromycin (1 μg/ml) for 7 d.

3.2.2 Immunoblotting

Immunoblotting procedure carried out as detailed in Chapter 2. Membranes were probed for ERα (1:1000, Sc-8002, Santa Cruz), TRIM33 (1:500, 90051, Cell Signaling Technology), β-actin (1:5000, 3700, Cell Signaling Technology), vinculin (1:5000, 13901, Cell Signaling Technology), FLAG (1:1000, F3165, Millipore Sigma), IRDye® 800CW Streptavidin (1:3000, 926-32230, LI-COR Biosciences).

3.2.3 Cycloheximide Assay

Cells were hormone-deprived for 3 d and reseeded. On Day 4, cells were administered 100uM cycloheximide and 1 nM 17β-estradiol over an 8 hr time course. Baseline cells did not receive drug treatment. At specified time points, lysates were harvested for immunoblot. MCF-7 shCtrl and MCF-7 sh#6 cells kept in 0.5 ug/ml of puromycin. Puromycin was not administered during assay.

3.2.4 RT-qPCR

Cells were hormone deprived for 3 d and reseeded. On Day 4, cells were treated +/- 1 nM E2 for 24 h. RNA was harvested using RNeasy Universal Plus Mini Kit (Qiagen) according to manufacturer's protocol. RNA was reverse transcribed with iScript cDNA Synthesis kit (Bio-Rad). Real-time qPCR was done with iQ SYBR Green SuperMix (Bio-Rad) with Bio-Rad CFX96 thermocycler. Data was analyzed by ΔΔCT method. Reference Table 3.1. for primer sequences.

3.2.5 SRB Growth Assay

Cells were hormone deprived for 3 d and reseeded. On Day 4, cells were administered increasing doses of E2 (0, 0.1, 1, 10, 100, 1000 pM). Cells were treated for 7 d and processed as previously stated in Chapter 2.

3.2.6 Biotinylated Protein Pulldown

For mass spectrometry assays, cells were hormone deprived for 8 d and treated for 1 h with 100 uM biotin +/- 1 nM E2. For immunoblot, cells were hormone-deprived for 4 d and treated with 100 uM biotin +/- 1 nM E2 x 24 h. Cells were rinsed with PBS and lysed with base lysis buffer (50 mM Tris pH 7.5, 500 mM NaCl, 0.5% Triton X-100, 5 mM β glycerophosphate, 2 mM NaF, 2 mM molybdate) with 1:500 Protease Inhibitor Cocktail (Research Products International). Samples were centrifuged at 17,000 x *g* for 10 min at 4ºC. Protein concentrations were determined by BCA assay (Pierce). Concentrations were equalized across samples. Strep-Tactin® Sepharose® 50% suspension beads (IBA Lifesciences) were used for biotinylated protein pulldown. Lysate was incubated with beads for 3 h at 4ºC. Beads were washed and protein was eluted in 100 uL 2% SDS, 50 mM Tris pH 8.0, and 5 mM biotin at 85ºC for 15 min. Eluted protein was analyzed by MS as in 3.2.9 for further downstream analysis or used for immunoblot.

3.2.7 RNA-Seq

Cells were hormone deprived for 4 d and subsequently treated +/- 1 nM E2 for 24 h. RNA was harvested using RNeasy Universal Plus Mini Kit (Qiagen) according to manufacturer's protocol. RNA for RNA-seq was quantified by qubit and integrity measured on a fragment analyzer (Agilent). 200 ng RNA was hybridized to FastSelect probes (Qiagen) for ribodepletion, followed by library preparation using the RNA HyperPrep kit (Roche) following manufacturer's instructions. Libraries were pooled for sequencing on a NextSeq2000 instrument (Illumina) targeting 30M, paired-end 50bp reads/sample. Sequencing reads were trimmed for low quality reads, and adapter contamination with Cutadapt[102]. Trimmed reads were aligned using the STAR aligner (v2.7.1a) and indexed with samtools index [103,104]. Raw gene read counts were generated using featureCounts (v2.0.5)[105]. Differential analysis was performed using DESeq2 (V1.41.0)[106].

3.2.8 Label-free LC-MS/MS Analysis

Proximity-labeled samples were analyzed on a Q-Exactive Plus quadrupole Orbitrap mass spectrometer (ThermoScientific) equipped with an Easy-nLC 1000 (ThermoScientific) and nanospray source (ThermoScientific). Peptides were resuspended in 5% methanol / 1% formic acid and loaded onto a trap column (1 cm length, 100 µm inner diameter, ReproSil, C18 AQ 5 µm 120 Å pore (Dr. Maisch, Ammerbuch, Germany) vented to waste via a micro-tee and eluted across a fritless analytical resolving column (35 cm length, 100 µm inner diameter, ReproSil, C18 AQ 3 µm 120 Å pore) pulled in-house (Sutter P-2000,

Sutter Instruments, San Francisco, CA) with a 45 minute gradient of 5-30% LC-MS buffer B (LC-MS buffer A: 0.0625% formic acid, 3% ACN; LC-MS buffer B: 0.0625% formic acid, 95% ACN).

The Q-Exactive Plus was set to perform an Orbitrap MS1 scan (R=70K; AGC target = 1e6) from 350 – 1500 m/z, followed by HCD MS2 spectra on the 10 most abundant precursor ions detected by Orbitrap scanning (R=17.5K; AGC target = 1e5; max ion time = 50ms) before repeating the cycle. Precursor ions were isolated for HCD by quadrupole isolation at width = 1 m/z and HCD fragmentation at 26 normalized collision energy (NCE). Charge state 2, 3, and 4 ions were selected for MS2. Precursor ions were added to a dynamic exclusion list +/- 20 ppm for 15 seconds. Raw data were searched using COMET (release version 2014.01) in high resolution mode[107] against a target-decoy (reversed)[108] version of the human proteome sequence database (UniProt; downloaded 2/2020, 40704 entries of forward and reverse protein sequences) with a precursor mass tolerance of +/- 1 Da and a fragment ion mass tolerance of 0.02 Da, and requiring fully tryptic peptides (K, R; not preceding P) with up to three mis-cleavages. Static modifications included carbamidomethylcysteine and variable modifications included: oxidized methionine. Searches were filtered using orthogonal measures including mass measurement accuracy (+/- 3 ppm), Xcorr for charges from +2 through +4, and dCn targeting a <1% FDR at the peptide level. Quantification of LC-MS/MS spectra was performed using MassChroQ[109] and the iBAQ method[110]. Missing values were imputed from a

normal distribution in Perseus to enable statistical analysis and visualization by volcano plot[111].

3.2.9 Statistical Analysis

For proximity labeling experiments, statistical analysis was carried out in Perseus by two-tailed Student's t-test. Growth assays and RT-qPCR were analyzed by ANOVA with Bonferroni-adjusted post-hoc testing. Growth assays, RT-qPCR, and immunoblots experiments were repeated on at least 2 separate occasions.

Table 3.1 Primers for RT-qPCR

Gene	Sequence
AREG FWD	5'tga tcc tca cag ctg ttg ct 3'
AREG REV	5' tcc att ctc ttg tcg aag ttt ct 3'
PDZK FWD	5' gtccgggtggttgagaagt 3'
PDZK1 REV	5' ttgatcctaagaactctgtctcca 3'
PR FWD	5'gat tca gaa gcc agc cag ag 3'
PR REV	5' tgc ctc tcg cct agt tga tt 3'
IRS1 FWD	5'gca acc aga gtg cca aag tga 3'
IRS1 REV	5' gga gaa agt ctc gga gct atg 3'
β-*actin* FWD	5' tga cag gat gca gaa gga gat 3'
β-*actin* REV	5' gcg ctc agg agg agc aat 3'

Table 3.2 Primers for Generation of Flag-Turbo-ESR1 and TRIM33/OVEXP Constructs

Primer	Sequence
(Flag-Turbo-Control) Lenti-Turbo Fwd	5’ agggggatccaccggttcgatggactacaaagaccatga 3’
(Flag-Turbo-Control) Turbo-Lenti Rev	5’ tgcggtctgccgaaaagtagacccagctttcttgtacaaa 3’
(Flag-Turbo-ER) Turbo-ESR1 FWD	5’ gtctgcggtctgccgaaaagggtggaggcggttctaccat 3’
(Flag-Turbo-ER) ESR1-Lenti Rev	5’ gtttccctgccacagtctagacccagctttcttgtacaaa 3’
(Flag-Turbo-ER) Turbo-ESR1 Rev	5’ gtctgcggtctgccgaaaagggtggaggcggttctaccat 3’
(Flag-Turbo-ER) Turbo-ESR1 FWD	5’ gtctgcggtctgccgaaaagGgtggaggcggttctaccat 3’
(TRIM33 OVEXP) TRIM33 OVEXP FWD	5’ gatccaccggttcgGCCACCatggcggaaaacaaaggcgg 3’
(TRIM33 OVEXP) TRIM33 OVEXP REV	5’ gaccagtacatataaagtaaacccagctttcttgtacaaa 3’

Table 3.3 RNA Interference Constructs

Name	Type	Vendor	Catalogue	Target Sequence
Mission® shRNA ctrl	Lentiviral	Sigma Aldrich	SHC002	Non-targeting
TRIM33 sh#6	Lentiviral	Dharmacon	RHS4430200207911	TTATCTTCAAAGTACAATG
TRIM33 sh#5	Lentiviral	Dharmacon	RHS4430200189072	ATTGACTACATTCTTTGCC

3.3 Results

3.3.1 – Development of BioID-ER Constructs for the Identification of the ER Interactome

The first iteration of this project began with the first-generation BioID in collaboration with the Kettenbach lab. In beginning to identify interactors of ER, I set out to generate a series of BioID constructs: empty vectors (to account for non-specific biotinylation), and BioID fused to ER (Figure 3.1A). When beginning to develop the BioID-tagged ER constructs, special consideration was given to the labeling of either the N-terminus or C-terminus of ER. The C-terminal domain (AF-1) of ER is involved in ligand-independent interactions while the C-terminus is involved in the binding of estrogens and co-activators necessary for the modulation of transcriptional activity[112]. When beginning to determine which construct (either the N-terminal or C-terminal fusion) to move forward with for profiling of the ER interactome, preference was given to the N-terminally labeled construct as labeling at the N-terminus is commonly used when monitoring ER protein function[113–115]. This construct development stems from minimizing alterations to the biological function carried out by the ligand-binding domain that could be inhibited by tagging the C-terminus. Additionally, profiling of the interactome was to be done under ligand-dependent estrogen stimulation. For this reason, preliminary work set out to generate constructs that were labeled on the N-terminus (Figure 3.1B). Although outside of the scope of this project, the

ER-BioID (C-terminally labeled) construct could be used in the future to profile protein interactions occurring in a ligand-independent manner.

MCF-7 cells were stably transduced with BioID-x1-ER or BioID-x4-ER. The level of both endogenous and exogenous ER proteins were examined to determine the effects of transduction on the overall levels of ER that would be expressed within cells (Figure 3.1B). It was observed that ER levels were increased in comparison to levels of endogenous ER found in parental cells; this could lead to problems with proper ER activity which could thereby influence accurate identification of interacting proteins. To address this issue, targets selected for follow-up studies would need to be validated for their biological relevance in parental cell lines via immunoprecipitation to validate protein interactions.

Linkers between BioID and ER consisted of four glycine residues followed by 1 serine residue (G_4S1) varied linker lengths allowed for increased flexibility and increased labeling radius. Two linker lengths were arbitrarily chosen ranging from a single G_4S1 repeat (“x1”) to 4 repeats (“x4”). Protein linkers provide separation of protein domains and allows for independent folding; however, linkers have the potential to influence protein function[116]. The labeling radius of BioID is less than 20 nm[117]. This labeling radius can be further extended by the introduction of an extended linker (G_4S)[95]. Longer linker lengths can potentially introduce interactions that are not true interactions with bait proteins, and too short of a linker can fail to profile interactions that occur in a larger complex[95] To determine the effects of linker length on construct function, I assessed the level

of biotinylation across stably transduced MCF-7 cells: non-tagged BioID (Myc-BioID), BioID-x1-ER, BioID-x4-ER, and parental cell lines (Figure 3.1C). It was observed that the construct containing the G_4Sx4 linker was failing to induce biotinylation. In addition, there were concerns that this linker was too long and could potentially introduce false interactors. For these reasons, the G_4Sx1 linker was chosen to pursue further.

Further motivation for this decision was supported by the results from a luciferase transcriptional reporter assay. HEK293T cells were transiently transfected with plasmids containing BioID constructs or wild-type ER to determine the ability to drive ER-inducible transcription at estrogen response elements (ERE) (Figure 3.1D). Results indicated that both BioID-ER constructs are estrogen-responsive and are able to bind EREs. However, results from the biotinylation assay suggest better labeling by BioID-x1-ER. Potential explanations for the poor biotinylation by BioID-x4-ER could be that the increased linker length is preventing shuttling through the cell, the biotin molecules are failing to encounter free primary amines to label, or more simply the biotin ligase is non-functional in this construct.

Following identification of the appropriate construct for interactome profiling, further optimization was carried out to determine the volume of Streptavadin Sepharose beads to use when performing pulldown of biotinylated proteins. A dilution series was carried out using 0, 5, 7, and 10 uL of beads in cells treated with 100 uM biotin for 20 h (data not shown). When samples were analyzed by mass spectrometry, samples were observed to have too much biotin

contamination, preventing proper protein identification. Based on these results, Strep-Tactin® Sepharose® beads were utilized. Strep-Tactin® has a lower affinity for biotin than streptavidin, so bound proteins can be eluted from Strep-Tactin® beads by supplementation with excess levels of biotin[118]. These beads are able to bind to biotinylated proteins in a reversible manner and additionally solved the problem of biotin contamination present in samples being processed for mass spectrometry.

In preliminary optimization experiments with BioID-ER constructs, mass spectrometry of biotin pulldown samples consistently showed low quantification of biotinylated ESR1 protein levels. This can potentially be explained by the slow kinetics of the first generation of BioID. In our experimental design, we examined the molecular changes that occur from estrogen addition after 24 h. The prolonged labeling time needed for BioID is thought to miss crucial interactions taking place in the earlier time frame following estrogen administration. For this reason, I diverted to using the next-generation TurboID construct to take advantage of its rapid temporal labeling capabilities (see Section 3.3.2).

In parallel to experiments attempting to identify the ER interactome under estrogen conditions, I also investigated the interactome of ER in endocrine-resistant settings. I generated stable BioID-ER constructs (of both short and long linker lengths) in MCF-7 fulvestrant resistant cell lines (Figure 3.2A). However, a concern was that the fulvestrant treatment in endocrine-resistant cell lines leads to a decrease in the levels of Bio-ER which could inhibit the overall ability for BioID-ER to accurately generate an interactome profile. I aimed to test the ability

of the construct to biotinylate proteins both in the parental and resistant cells (Figure 3.2B). Biotinylation levels in the resistant cell line are increased, but in comparison to parental cells treated with fulvestrant, this biotinylation is much lower, validating my concern for the accurate generation of an ER interactome under fulvestrant resistance.

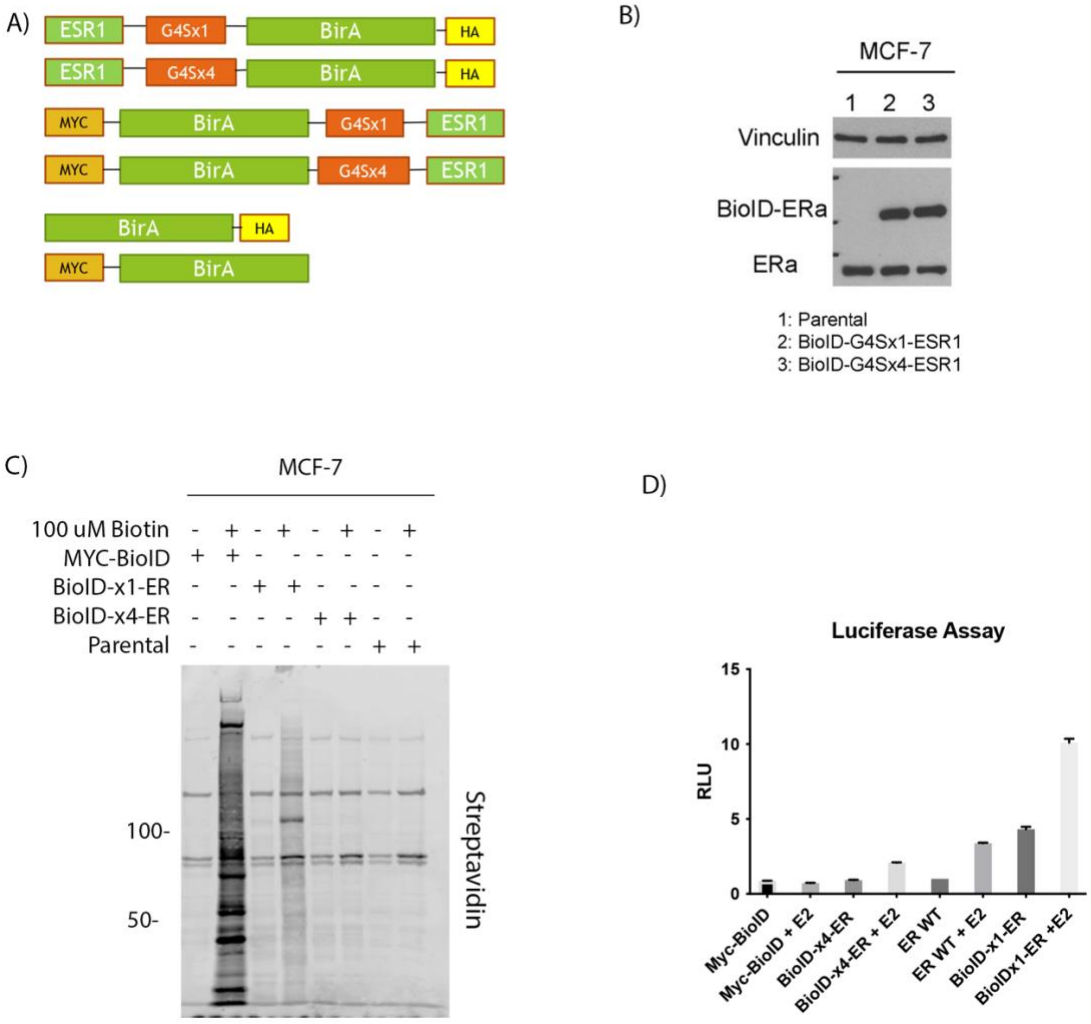

Figure 3.1. Preliminary Investigation of BioID for ER Interactome Profiling. **A)** Maps for proposed BioID constructs for labeling at N- or C- Terminals. **B)** MCF-7 cells stably transduced with N-terminally labeled BioID-ER constructs containing variable linker lengths. **C)** MCF-7 cells treated with 1 nM E2 +/- 100 uM biotin for 24 hrs and immunoblotted for streptavidin. **D)** Lentix cells were HD for 3 days and subsequently transiently transfected with plasmids containing: wildtype ER, Myc-BioID, BioID-x1-ER, BioID-x4-ER. Cells were treated +/- 1 nM E2. All values were normalized to ER WT (no E2 treatment).

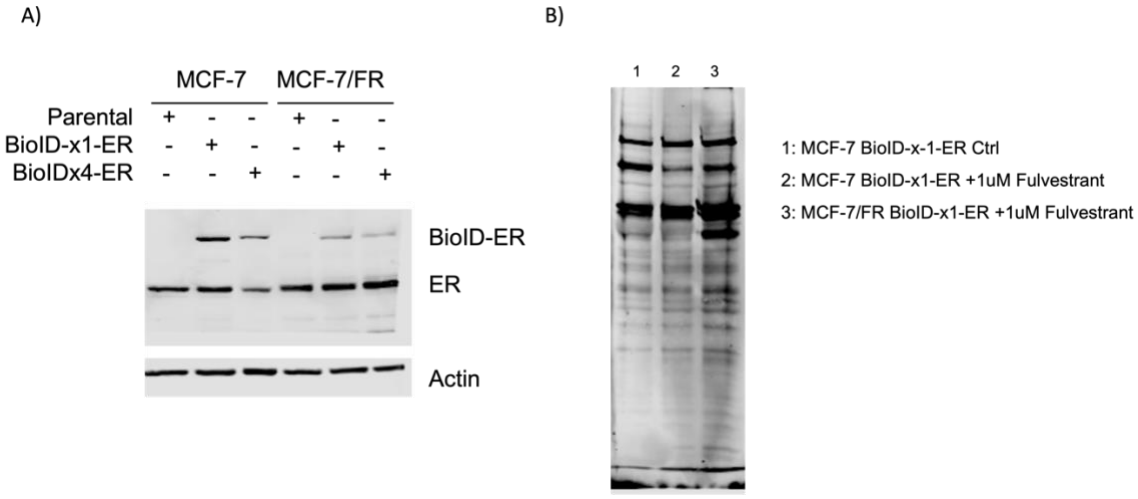

Figure 3.2 Development of BioID-ER in Fulvestrant-Resistant ER+ BrCa cells. A) MCF-7 and MCF-7/fulvestrant-resistant (FR) cells stably transduced with BioID-ER constructs or no vector. Immunoblots were probed for levels of ER in protein lysates. **B)** Biotinylation levels of MCF-7 and MCF-7/FR cells expressing BioID-x1-ER following treatment +/- 1 uM fulvestrant for 24 h.

3.3.2- Proximity Labeling of ER Identifies TRIM33 as an Interactor

To begin profiling the interactome of ER, we generated an N-terminally TurboID-labeled ER construct (Turbo-G4Sx1-ER) and a non-specific TurboID control (Turbo-Control) (Fig. 3.3A). These constructs were used to generate stable cell lines using the ER+ breast cancer cell line MCF-7 (Fig. 3.3A). Transduction with TurboID-ER did not yield drastically increased ER protein levels. The use of TurboID-labeled proteins can influence protein function if the fusion construct is expressed at a significantly increased level. Further investigation in parental cells will provide further validation of results identified via TurboID screening. Initial validation steps were carried out to determine the biotinylation capabilities of both constructs over a period of 24 h (Fig. 3.3B). The control construct was observed to retain promiscuous biotinylation ability with saturation occurring as early as 10 min after biotin treatment. Turbo-ER did not reach levels of saturation even after 24 h. To ascertain the early interactors associating with ER upon E2 supplementation, E2 was administered for 1 h and protein was subsequently harvested. From proximity labeling experiments under E2-treated conditions, TRIM33, an E3 ubiquitin ligase, was observed to be a significant ER interactor in Turbo-ER cells compared to Turbo-Control (Fig. 3.3C, Table 3.4). To further validate LC-MS/MS findings, proximity labeling was again carried out with MCF-7/Turbo-ER cells this time following 24 h of E2 stimulation (Fig. 3.3E); results recapitulated the significant TRIM33 interaction with ER under prolonged E2-induced conditions. Comparing our findings of ER interactomes with those previously reported[115,119], TRIM33 was observed to be a common ER

interactor in all profiles (Fig. 3.3D). Differences between interacting proteins between of studies can be explained by differing technique (RIME vs biotin labeling) and duration of E2 signal induction. Of the statistically significant hits identified by my screen, statistically significant molecular functions[120] include: nuclear steroid receptor activity, chromatin binding, transcription coregulator activity (Figure 3.4A); all molecular functions that reflect E2-stimulated signaling. Comparing the molecular functions identified by my screen to that of other interactomes cited herein, the most functional overlap exists between the targets identified by Agbo et al. 2022 using the TurboID-focused method. No current reports have investigated TRIM33 interaction with ER, providing rationale for target selection and further investigation.

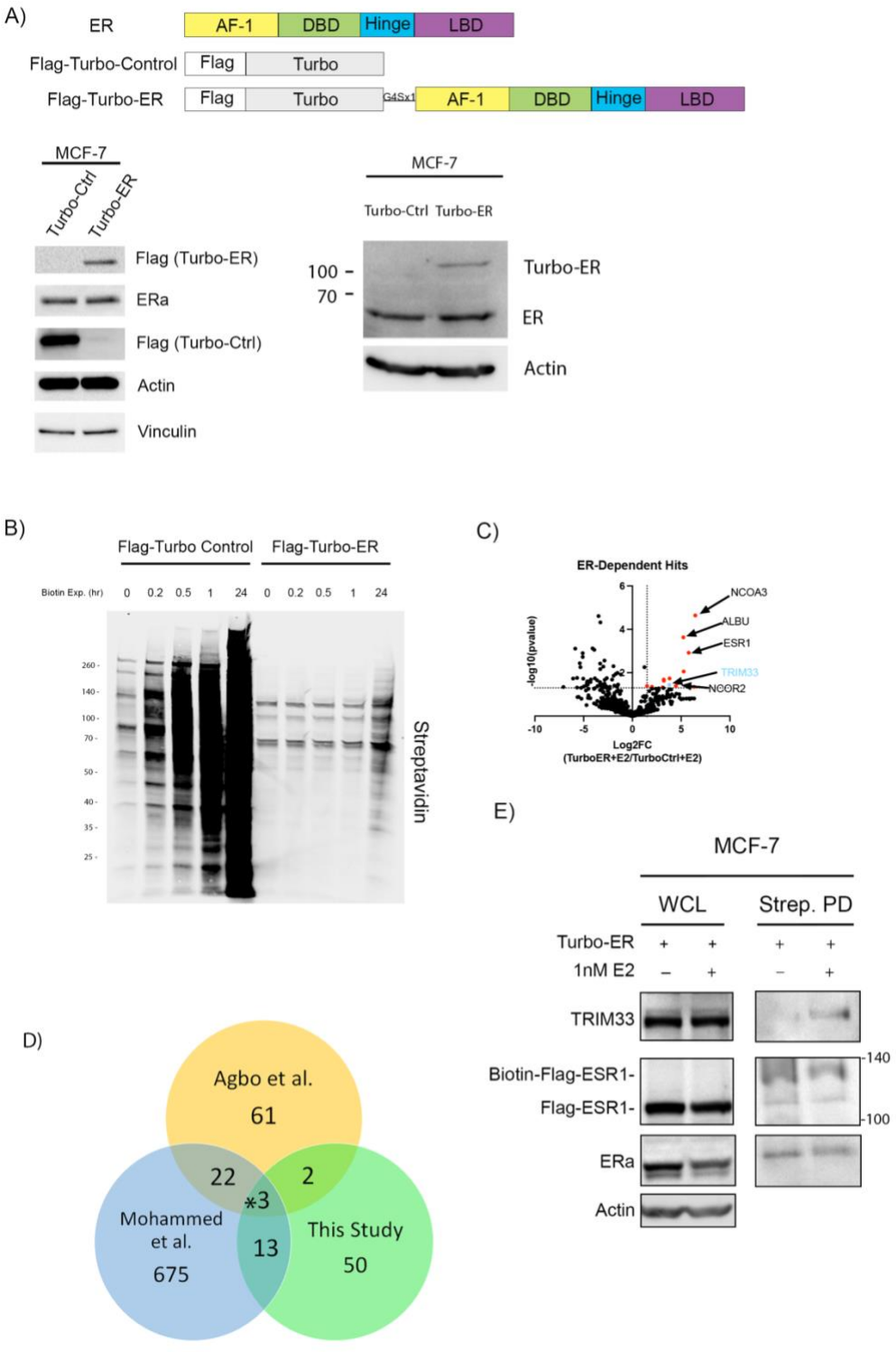

(Legend on Next Page)

Figure 3.3. Estrogen Induced Proximity Labeling by ER. A) Construct maps identifying wildtype ER, Flag-Turbo-Ctrl, and Flag-Turbo-ER. MCF-7 cell lines stably transduced with Turbo-Ctrl or Turbo-ER. Immunoblot confirmation of construct expression and levels of overall expression of ER **B)** MCF-7 cells stably transduced with (Flag-Turbo-Ctrl) or (Flag-Turbo-ER) treated with 100uM biotin over time course of 0-24 hrs and immunoblotted for streptavidin. **C)** Volcano plot of significant (red) E2 dependent TurboER hits. Blue dot indicates TRIM33. **D)** Venn diagram overlapping identified interactors from two ER interactomes profiling experiments compared to findings from this study. (*) indicates TRIM33 as one of common overlap targets. **E)** MCF-7 cells expressing (Flag-Turbo-ER) treated with 1nM E2 for 24hrs and subjected to Strep-Tactin® Sepharose® bead pulldown. TRIM33 pulldown under E2 conditions validated by immunoblot. Strep.PD- Strep-Tactin® Sepharose® bead pulldown. WCL- whole cell lysate. In (C), Lauren C. and Brooke B. processed samples for LC-MS/MS, and Arminja K. analyzed LC-MS/MS data.

Table 3.4 Significant E2-induced Interactors of ER.

Gene Name	-log10(pvalue)	Gene Name	-log10(pvalue)
NCOA3	4.641	SAFB	1.472
PC	1.349	GSPT2	2.282
ESR1	2.923	ILF3	1.391
CD9	2.058	KIF5C	4.322
ALB	3.635	IDH1	2.169
NCOR2	1.525	ERP44	1.511
TFAP2A	1.392	NDUFA10	1.415
ETFB	1.735	KIF5A	2.425
TRIM33	1.443	NUP153	1.565
KDM1A	1.63	KIF5B	4.613
TLE4	1.686	PGD	1.385
MCCC2	1.327	PRCC	1.654
FUBP3	1.353	RAB27A	1.742
SMARCD2	1.391	CRIP2	3.058
KMT2D	2.256	SELENBP1	3.123
CBX3	1.917	AHSA1	1.685
SNRPB	1.451	CAPZA2	1.572
SNRPN	1.451	FHL1	1.6
RAI1	1.992	RXRG	1.451
SNRPD3	1.357	CAPZA1	1.601
SNRPD2	1.943	L1RE1	1.507
SYNCRIP	1.407	ATP5MF	1.41
HNRNPAB	1.862	MYL12A	1.365
CCT4	2.301	RXRB	1.728
TJP1	1.683	CCT7	2.902
EEF1D	1.354	CALU	2.728
PIP4K2C	1.752	SEPTIN2	1.304
NIBAN2	1.346	GRB2	2.259
G3BP1	1.365	PAK3	2.437
CSRP1	1.311	RAB27B	1.761
UBAP2L	1.433	MYL12B	1.315
U2SURP	1.674	SERBP1	3.111
SP100	1.491	TAGLN3	1.73
HMGB1P1	2.563	PCNP	1.341

A)

Figure 3.4 Molecular Functions of ER Interactomes A) Statistically Significant molecular functions by MSigDB of genes identified in this study, Agbo et al. 2022, and Mohammed et al. 2013. For Mohammed et al. 2013, 500 genes were used for generation of list.

3.3.3 TRIM33 Possesses ER Regulatory Capabilities

Due to TRIM33 interacting with ER in an estrogen-dependent manner, we aimed to determine TRIM33 effects on ER function in an estrogen-replete setting. We first measured the levels of TRIM33 across ER+ cell lines (Fig. 3.5A). MCF-7 cells showed the highest level of expression and as a result were used for the generation of stable shRNA knockdown models (Fig. 3.6A). Conversely, T47D cells possessed one of the lowest levels of TRIM33 expression, prompting their use for a TRIM33 overexpression model (Fig. 3.5A).

To determine the effects of TRIM33 on estrogen/ER signaling, we generated cells with stable shRNA knockdown and constitutive overexpression of TRIM33. TRIM33 knockdown led to a reduction in the intensity of E2-driven transcript induction as measured by downstream E2/ER-inducible genes (Fig. 3.5B). These results indicate that TRIM33 plays a role in the regulation of E2 signaling. Interestingly, TRIM33 overexpression does not promote elevated levels of induction of the E2/ER signaling pathway (Fig. 3.5C). Among the genes assayed, TRIM33 overexpression did not lead to an increased induction of downstream targets when treated with E2 with the exception of *PR* in the T47D cell line. TRIM33 overexpression may be causing a saturation of E2 signaling. To determine the effects of TRIM33 on the global transcriptome, we performed RNA-seq analysis on MCF-7 shCtrl and MCF-7 sh#6 knockdown cells treated with +/- E2 treatment (Fig. 3.11A). A broad overview of RNA-seq data shows that samples clusters on the basis of E2 treatment. To determine more specific perturbations caused by TRIM33 knockdown, down-regulated and up-regulated

genes were subjected to Hallmark Pathway analysis (Fig 3.5D). Pathways that were enriched in down-regulated genes include pathways relating to DNA repair, G2M checkpoint, and E2F targets, pathways previously associated with TRIM33[99,121–124]. Of the upregulated genes both late and early estrogen response pathways were observed to be altered upon TRIM33 knockdown. This coincides with results from RT-qPCR data showing elevated levels of transcripts upon TRIM33 knockdown when supplemented with E2. Further investigation is warranted into the mechanism by which transcript levels are increased at baseline and how they also coincide with a decrease in the overall fold change induced by E2 supplementation. These results suggest a role of TRIM33 affecting E2-driven signaling.

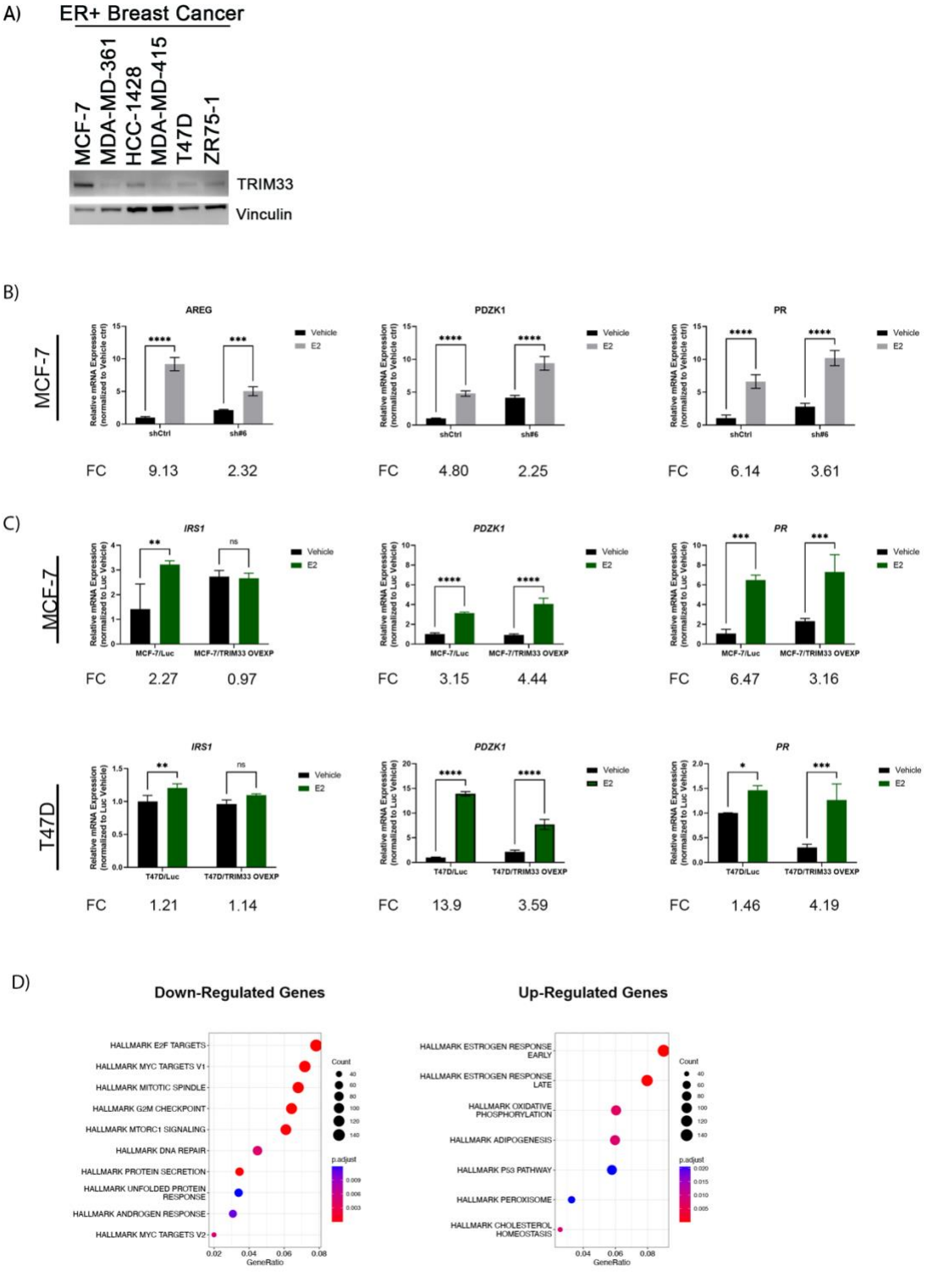

(Figure legend next page)

Figure 3.5. TRIM33 Regulates ER Signaling. A) Immunoblot probing for TRIM33 expression across ER+ breast cancer cell lines. **B)** RT-qPCR of ERα target genes in MCF-7: shCtrl and sh#6 treated with +/- 1nM of E2 for 24 hrs. **C)** RT-qPCR of ERα target genes in MCF-7 and T47D: Luc and TRIM33 OVEXP treated with +/- 1nM E2 for 24hrs. **D)** Hallmark pathway analysis of down-regulated and up-regulated genes in E2 conditions between MCF-7: shCtrl and sh #6 Data shown in **B/C** are mean of triplicate ± SD. *****$p \leq$ 0.05, **$p \leq$ 0.01, *** $p \leq$ 0.001, ****$p \leq$ 0.0001 by Bonferroni multiple comparison-adjusted post-hoc test. Alexa W. contributed to preliminary data. Hallmark pathway analysis done by Barbara K.

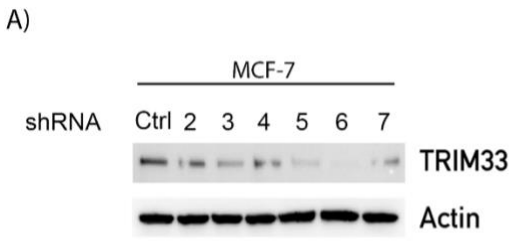

Figure 3.6. Generation of TRIM33 shRNA Knockdown Cell Lines. A) MCF-7 cell lines stably transduced with shRNA targeting TRIM33 or shCtrl. Immunoblot for validation of knockdown.

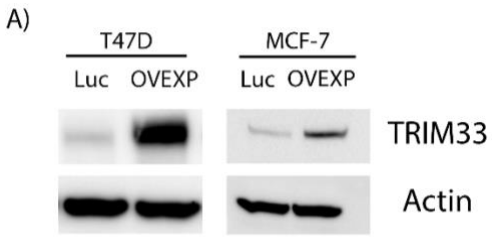

Figure 3.7. Generation of TRIM33 OVEXP Cell Lines. A) MCF-7 and T47D cell lines stably transduced with Luc or TRIM33 OVEXP. Immunoblot confirmation of construct expression.

3.3.4 TRIM33 Stabilizes ER Protein Levels

To better understand the observed results of TRIM33 knockdown resulting in decreased ER transcriptional activity in response to E2, we aimed to determine the effects of knockdown on ER stability. Through cycloheximide pulse-chase assays, we determined that TRIM33 knockdown leads to decreased ER protein levels at baseline (no E2) conditions (Fig. 3.8A). Upon administration of E2, TRIM33-knockdown cells exhibited a reduction in the stability of ER over the course of 8 h. Conversely, TRIM33 overexpression led to an increase in protein levels of ER over time upon the addition of E2 at 5 hrs in comparison to T47D Luc cells (Fig. 3.8B).

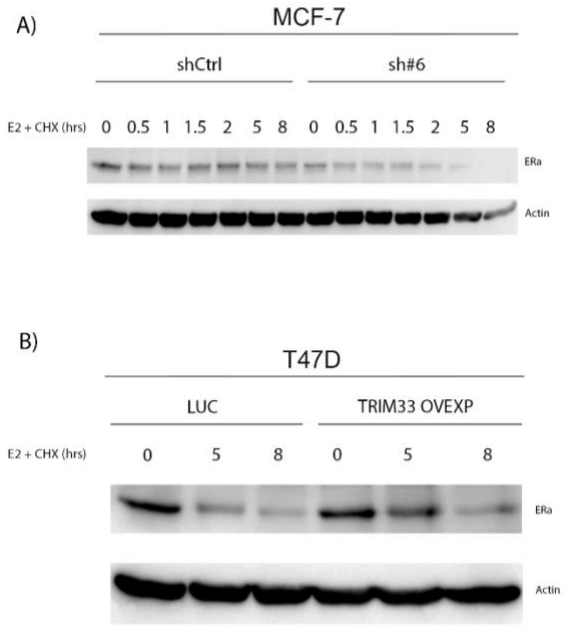

Figure 3.8. TRIM33 Stabilizes ER Levels. A) MCF-7/shCtrl and MCF-7/sh#6 cells were HD for 4 days and treated with 1nM E2 and 100uM cycloheximide over 8 hrs. ERα levels were measured by immunoblot. **B)** T47D Luc and T47D/TRIM33 OVEXP cells were HD for 4 days and treated with 1nM E2 and 100uM cycloheximide over 8 hrs. ER levels were measured by immunoblot. Immunoblot in (A) was done by Huijuan Y.

3.3.5 TRIM33 Regulates E2-Driven Cell Growth

TRIM33 has been established to have differing roles as a tumor suppressor or oncogene in breast cancer[100,101]. In an effort to elucidate the role of TRIM33 in our ER+ models, we subjected cells to E2 treatment either in conditions of TRIM33 knockdown or overexpression. Despite knockdown of TRIM33, cells remained growth-responsive to estrogen stimulation (Fig. 3.9A, Fig. 3.10A). However, in examining the fold change in growth induced by E2, we observed a significant decrease as a consequence of TRIM33 knockdown. TRIM33 overexpression showed a cell-dependent effect on growth (Fig. 3.9B). MCF-7 cells overexpressing TRIM33 remained sensitive to E2 stimulating effects. However, there was no significant difference observed at low doses of estrogen, and only at higher doses of estrogen did we observe a growth promoting effect. Conversely, T47D/TRIM33 OVEXP cells were growth stimulated by estrogen, but overall showed a growth inhibitory effect when compared to T47D/Luc control cells. These results indicate that TRIM33 promotes the growth of MCF-7 cells in an estrogen dependent manner. MCF-7 cells possessed the highest level of TRIM33 expression at baseline, while T47D exhibited some of the lowest level of expression (Fig 3.5A). We believe that the cell dependent response to TRIM33 overexpression lies in MCF-7 cell's ability to better tolerate TRIM33 overexpression due to their elevated levels of TRIM33 that is not able to be tolerated by T47D cells. Additionally, the transcriptional activity of ER has been observed to be affected by protein turnover[58]. This effect could be occurring in our model and would also explain the saturation of transcript levels upon E2

supplementation in the context of TRIM33 overexpression causing increased ER protein levels (Fig 3.5C).

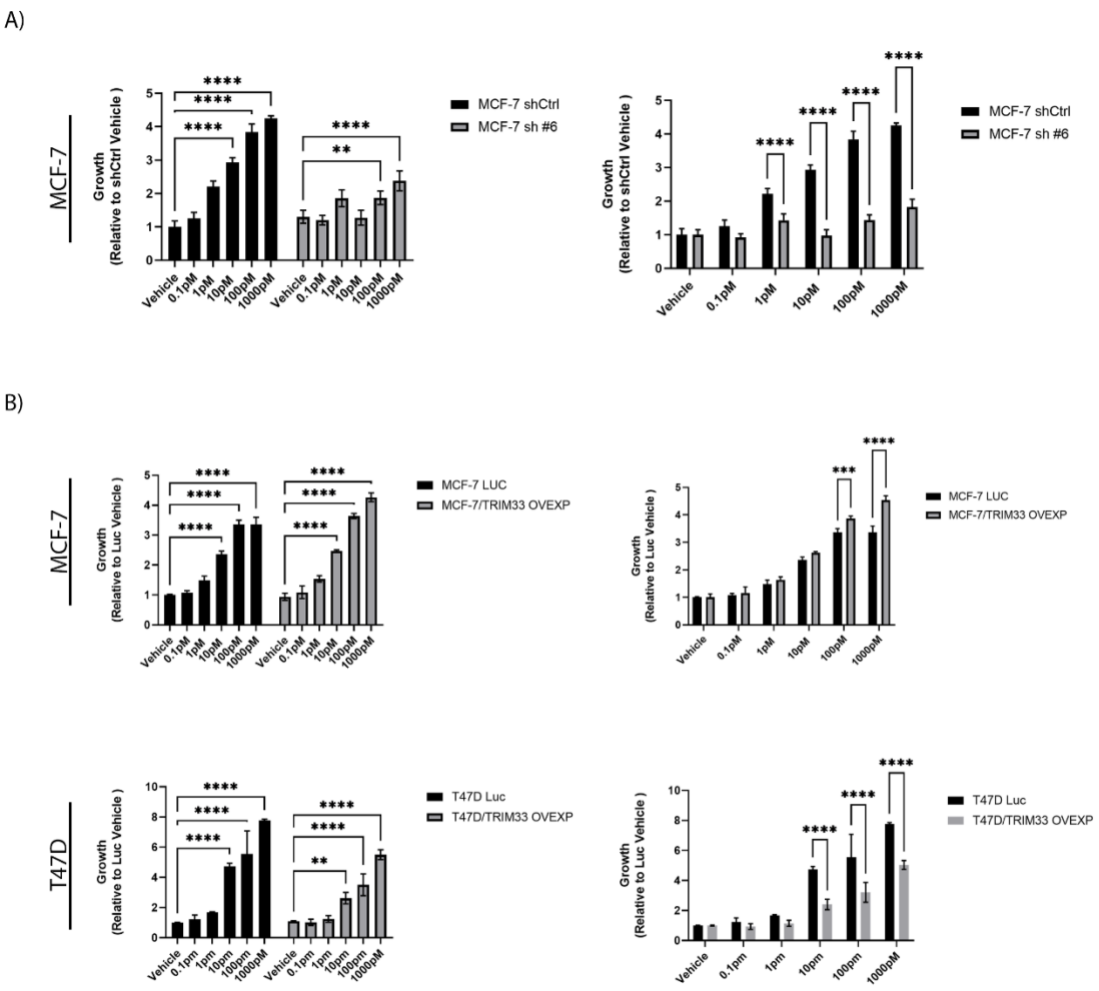

Figure 3.9. TRIM33 Regulates E2-Driven Cell Growth. A/B Cells were HD for 4 days prior to E2 treatment. Cells were treated for 7 days before fixation. **A)** MCF-7 shCtrl and sh#6. **B)** MCF-7: Luc and TRIM33 OVEXP and T47D: Luc and TRIM33 OVEXP. Data shown are mean of triplicate $\pm$ SD. ***p*$\leq$ 0.05, **$p\leq$ 0.01, *** $p\leq$ 0.001, ****$p\leq$ 0.0001 by Bonferroni multiple comparison-adjusted post-hoc test.

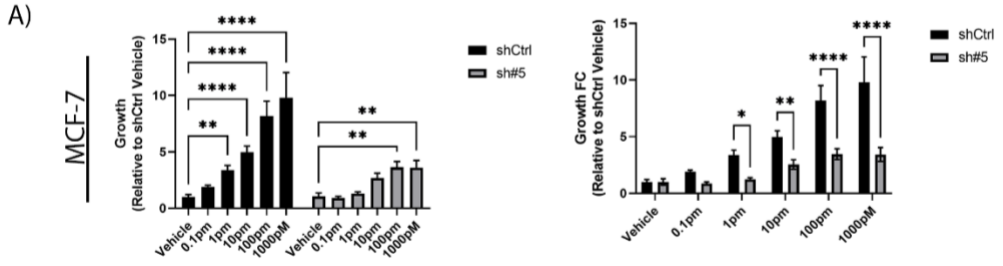

Figure 3.10. TRIM33 Knockdown Inhibits E2-Stimulated Growth. A) Cells were HD for 4 days prior to E2 treatment. Cells were treated for 7 days before fixation. **A)** MCF-7 shCtrl and sh#5. Data shown are mean of triplicate ± SD. *$p \leq 0.05$, **$p \leq 0.01$, *** $p \leq 0.001$, ****$p \leq 0.0001$ by Bonferroni multiple comparison-adjusted post-hoc test.

3.4 Discussion

ER+ breast cancer is canonically driven by the mitogenic effects of estrogens. In an effort to identify co-regulators that can modulate ER transcriptional activation, we developed a Turbo-ER construct for the purposes of generating an estrogen dependent ER interactome. From our screen, we identified the E3 ubiquitin ligase TRIM33 as an interactor of ER in an E2-dependent manner. This was validated by both LC-MS/MS and immunoblot, with immunoblot showing a significant difference in the interaction of TRIM33 with ER in response to E2. Comparing our ER-interacting hits to those of two previously reported screens, TRIM33 was identified to be common across all interactomes[115,119].

TRIM33 (TIF1γ) is a member of the transcriptional intermediary 1 (TIF1) family of proteins involved in chromatin binding. Across several cancer types TRIM33 has been shown to have a varied distinction as either a tumor suppressor or oncogene[96,121,125–127]. These examples show the context-dependent function of TRIM33 across different cancer types. In the case of breast cancer, we are met with conflicting results as to the classification of TRIM33 as a tumor suppressor or oncogene[100,101]. In this study, we aimed to determine TRIM33's role in the context of ER+ breast cancer.

Herein, we have identified that TRIM33 plays a role in the regulation of E2 driven signaling as evidenced by a reduction in E2 induced signaling upon

TRIM33 knockdown and reduced E2 driven growth. However, overexpression of TRIM33 did not lead to an increase in estrogen induced signaling, signifying that TRIM33 overexpression can elicit a saturation to estrogen dependent signaling, providing no further growth advantage. Additionally, ER function is regulated by protein turnover and inhibition of the proteasome pathway negatively impacts the transcriptional activation by ER[58]. By promoting the stabilization of ER by increased levels of TRIM33, we may be modeling this effect and thereby affecting the transcriptional activation of ER upon E2 supplementation.

As a result of dampened estrogen induced signaling, TRIM33 knockdown cells remained growth responsive to estrogen but ultimately lead to a significant decrease in estrogen driven growth rate, showing that TRIM33 is necessary for estrogen induced cell growth. Additionally, TRIM33 effects on cell growth appear to be cell line dependent. MCF-7 cells overexpressing TRIM33 were not granted a superior advantage to growth, indicating that TRIM33 only affects growth in the context of knockdown. While T47D cells were observed to have a growth inhibitory effect when TRIM33 was overexpressed. This could be explained by the fact that T47D parental cells possessed very low levels of TRIM33, and by causing increased expression of TRIM33, we have affected cell viability. This requires further investigation as to the levels of apoptosis that arise in response to increased TRIM33.

In investigating the potential mechanism by which TRIM33 could be affecting estrogen signaling and subsequently cell growth, we observed that TRIM33 functions to stabilize protein levels specifically when under estrogen conditions. In TRIM33 being an E3 ligase, our work has shown that TRIM33 has an overall stabilizing effect of ERα. Further work will be to investigate the mechanism by which TRIM33 protects ER from protein degradation. TRIM33 has been found to have protein stabilizing effects on the androgen receptor in prostate cancer, another hormone dependent model, by preventing Skp-2 mediated protein degradation[99]. We believe that TRIM33 is behaving in a similar manner acting to protect ER from ubiquitin led protein degradation.

Extending our findings to potential explanations for mechanisms of endocrine resistance, it has been observed that elevated levels of ER can promote resistance to estrogen deprivation[128]. Our findings raise the question of whether TRIM33 is involved in the upregulation of ER levels in this estrogen deprived population and whether increased levels of TRIM33 could be used as a marker for the development of resistance to extended periods of hormone deprivation.

A)

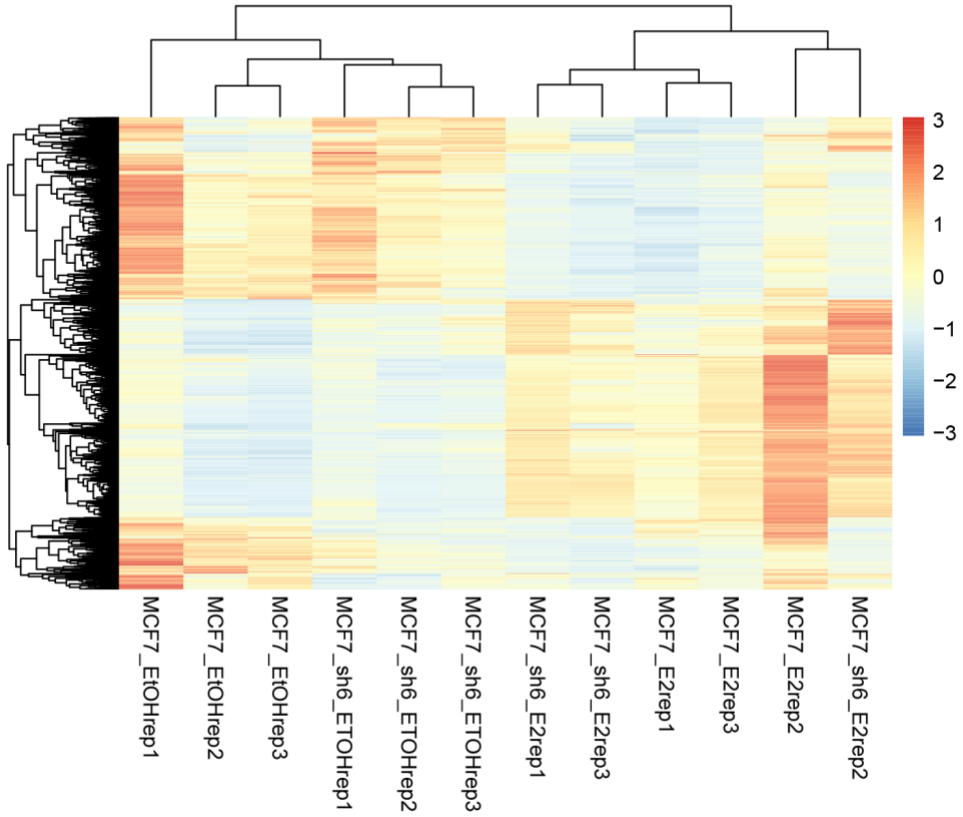

Figure 3.11 Global Transcriptional Changes in TRIM33 Knockdown Cells. A) MCF-7: shCtrl and sh#6 cells treated +/- 1 nm E2 were subjected to transcriptome analysis. Top 10% of normalized expression counts of genese that were significantly differentially expressed ($q \geq 0.05$, $|\log_2 FC| > 0.7$).

(Analysis and Figure done by Barbara K.)

CHAPTER 4: INVESTIGATING MECHANISMS OF RESISTANCE TO PI3K INHIBITORS

Work described in this chapter is unpublished and was done as a follow up to a study by Hosford, et al 2017[129].

4.1 Introduction

PI3K is involved in a myriad of processes including cell proliferation, migration, metabolism, and growth. PI3K enzymes exist in three classes. Herein, class IA PI3Ks will be discussed. PI3Ks are activated via G protein-coupled receptors (e.g., Ras) and receptor tyrosine kinases. PI3K consists of a catalytic subunit and a regulatory subunit. The p110 catalytic subunit exists in several isoforms (α, β, γ, and δ). Isoforms γ and δ are restricted to immune cell populations, while isoforms α and β are universally expressed. Activity of PI3K is modulated by the regulatory subunit. Upon activation, the catalytic components are responsible for the conversion of phosphatidylinositol 4,5-bisphosphate (PIP2) to the effector phosphatidylinositol 3,4,5-trisphosphate (PIP3). The PIP3 second messenger allows for the recruitment of pleckstrin homology (PH)-domain-containing proteins to the plasma membrane, including AKT and phosphoinositide-dependent protein kinase 1 (PDK1)[130,131]. Acting in opposition to PI3K, phosphatase and tensin homolog (PTEN) functions as a tumor suppressor by dephosphorylating PIP3 to yield PIP2.

AKT is a major downstream target of PI3K signaling. Upon activation, AKT is phosphorylated at Thr308 and Ser473 by PDK1 and mammalian target of rapamycin 2 (mTORC2), respectively[132,133]. AKT can further modulate signaling by promoting the downstream activation of mammalian target of rapamycin 1 (mTORC1), a key player in processes related to metabolism, cell growth and proliferation. An important contribution of mTORC1 is negative feedback on the

PI3K pathway[134,135]. For this reason, treatment with therapeutics targeting mTORC1 could result in PI3K pathway activation, compromising the efficacy of therapeutic strategies[136,137].

In ER+ breast cancer, alterations to the PI3K pathway occur in 70% of tumors. Alterations in the pathway occur in the genes encoding catalytic subunits (*PI3KCA*-p110α and *PI3KCB*-p110β), a regulatory subunit (*PIK3R1*-p85α), PTEN, and receptor tyrosine kinases like HER2 (human epidermal growth factor receptor 2), with some of these alterations being known to suppress therapeutic response to endocrine treatment[78,138–145]. Within luminal breast cancer, the incidences of *PIK3CA* mutations range from 32 to 49% and *PTEN* mutations/loss range from 13 to 24%[80]. Due to the high prevalence of these mutations in breast cancer, efforts are being implemented to treat patients using isoform targeting drugs. In the case of PTEN loss of function, p110β has been observed to be essential for tumors[146]. Preclinical data with *PIK3CA* mutations (activating p110α) showed an increased sensitivity to targeting with the p110α-selective inhibitor alpelisib (BYL-719)[147]. This promising response led to the stratification of patients with *PI3KCA* mutations to be treated with combined alpelisib and the selective estrogen receptor downregulator fulvestrant in the SOLAR-1 trial, which showed an increase in progression-free survival by 11 months compared to fulvestant/placebo and ultimately led to FDA approval in 2019[87,148]. Preclinical work in PTEN-deficient models validated dependency on p110β and warranted targeting of the beta isoform in this subpopulation[149,150]. However, recent work

established that in ER+ PTEN-deficient tumors, targeting the alpha and beta isoforms provides the most robust treatment strategy to induce tumor regression and maintain a suppressed proliferative state in preclinical models[129].

The PI3K pathway exists as a major hub of activity and as such its activity can further modulate other signaling pathways including ER. Phosphorylation of ER at Ser167 by AKT or p70S6K induces transcriptional activation of ER[79,151]. Conversely, ER can lead to the activation of PI3K by the transcription of genes whose products are receptor tyrosine kinases and ligands[152]. In the treatment of breast cancer, aromatase inhibitor treatment was observed to reduce AKT activation as evidenced by reduced phospho-AKT-S473 and phospho-mTOR-S2448[143,153]. Due to this existing crosstalk, it is advantageous to provide combination endocrine and PI3K-targeting therapies to properly inhibit the growth promoting effects of each pathway.

Previous work in the lab showed that in PTEN-deficient, ER+ breast cancer, short-term treatment of tumors resulted in apoptosis and tumor regression while long-term treatment elicited a cytostatic response[129]. In this study, it was observed that tumors from mice treated with the combination of GSK2636771 (p110β inhibitor) and BYL-719 (p110α inhibitor) for 10 wks showed recovery of PI3K pathway activity (as measured by AKT phosphorylation) despite continued suppression of mTORC1 signaling. From these observations, we

conducted a phosphoproteomic investigation to identify potential kinases responsible for reactivation of the PI3K pathway.

4.2 Materials and Methods

4.2.1 Cell Culture

T47D, ZR75-1, MDA-MB-415, CAMA-1 cells were obtained from the American Type Culture Collection (ATCC). ZR75-1/FR, MDA-MB-415/FR cells were established from parental lines. *PI3KCA* mutant cell lines: MCF-7/FR (MJE) were obtained from Matthew Ellis (Washington Univ., St. Louis, MO). Cells were maintained in DMEM (Dulbecco's modification of Eagle's Medium with 4.5 g/L glucose, L-glutamine & Sodium pyruvate) (Cellgro, Corning) supplemented with 10% fetal bovine serum (FBS). FR (fulvestrant resistant) cells were maintained in 1uM fulvestrant. To generate fulvestrant resistant cell lines: cells were cultured for a minimum of 4 months in the presence of the respective drug. *PI3KCA* mutants (MCF-7/FR and T47D/FR) were dosed at 1 uM (BYL-719 or GDC-0941) for a minimum of four months.

4.2.2 Drugs

Pictilisib (GDC-0941, pan-isoform inhibitor), AZD1390 (ATM inhibitor), and alpelisib (BYL-719, p110α inhibitor) were purchased from Selleck Chemical. Fulvestrant (selective estrogen receptor downregulator) was purchased from Tocris Biosciences. For *in vitro* experiments, cells were dosed at 1uM (BYL-719 & GDC-0941 & Fulvestrant) & 10 nM AZD1390.

4.2.3 Immunoblotting

Immunoblotting procedure carried out as detailed in Chapter 2. Membranes were probed for ERα (1:1000, Sc-8002, Santa Cruz), phospho-AKT-S473 (1:1000, 4060, Cell Signaling Technology), β-actin (1:5000, 3700, Cell Signaling Technology), vinculin (1:5000, 13901, Cell Signaling Technology), phsopho-AKT-T308 (1:1000, 13038/4056, Cell Signaling Technology), pS6 240/244 (1:1000, 5364, Cell Signaling Technology).

4.2.4 Mouse Studies

Mice were implanted orthotopically with ZR75-1/FR cells and s.c. with a 17β-estradiol (1 mg) pellet. Mice were treated with a backbone of weekly fulvestrant 5 mg/dose s.c. Tumors were allowed to grow until 400 mm^3. Mice were then enrolled in treatment groups of vehicle or GDC-0941 (100mg/kg/d p.o.). Tumors were harvested on Day 0 (n=3), Day 3 at 4 h post-last dose (=3), and Day 56 at 4 h post-last dose (n=3). Tumors were processed as in 4.2.6 for phosphoproteomic analysis.

4.2.5 Immunohistochemistry

Samples used for immunohistochemistry were taken from Hosford et al. 2017[129]. Time points of 0 wk, 0.5 wk, and 10 wks treated with combination

GSK2636771 (30 mg/kg/d, p.o.), BYL719 (25 mg/kg/d, p.o.), and fulvestrant (5 mg/wk s.c.; clinical formulation; gift from Astrazeneca). Samples were formalin-fixed paraffin embedded (FFPE) blocks were prepared by Norris Cotton Cancer Center Pathology Shared Resource and were cut into 5-micron sections and placed on slides. The Norris Cotton Cancer Center Pathology Shared Resource carried out IHC staining against phoshpho-CHK2-T68 and pKAP1 S824. Proportions of positively stained cells were quantified in 3 representative 200x magnification microscopic images from each tumor using HALOVelocity software (Indica Labs).

4.2.6 Processing of Tumors for Phosphoproteomic Analysis

Samples resuspended in of ice-cold lysis buffer [8 M urea, 25 mM Tris-HCl pH 8.6, 150 mM NaCl, containing phosphatase inhibitors (2.5 mM beta-glycerophosphate, 1 mM sodium fluoride, 1 mM sodium orthovanadate, 1 mM sodium molybdate) and protease inhibitors (1 mini-Complete EDTA-free tablet per 10 ml lysis buffer; Roche Life Sciences), and lysed by sonication (three times for 15 s each with intermittent cooling on ice)[154]. Lysates were subjected to centrifugation (15,000g for 30 min at 4 °C). Supernatants were transferred to a new tube, and the protein concentration was determined using a BCA assay (Pierce/ThermoFisher Scientific), DTT was then added to the lysates to a final concentration of 5 mM to reduce disulfide bond, and DTT-lysate was incubated for 30 min at 55 °C. Lysates were then cooled to room temperate, and 15 mM

iodoacetamide (room temperature) was added to achieve alkylation. After a 45-min room temperature incubation in the dark, alkylation was quenched by the addition of 500 mM DTT (1:100 dilution). After sixfold dilution with 25 mM Tris-HCl pH 8, the samples were incubated overnight at 37 °C with 1:100 (w/w) trypsin. The next day, the trypsin digest was stopped by the addition of 0.25% TFA (final v/v). Precipitated lipids were removed by centrifugation (3500g for 15 min at room temperature), and the peptides in the supernatant were desalted over an Oasis HLB 60 mg plate (Waters).

Phosphopeptide enrichment was achieved using a Fe-NTA phosphopeptide enrichment kit (Thermo Fisher) according to instructions provided by the manufacture and desalted over an Oasis HLB 60 mg plate (Waters). Phosphopeptides were resuspended in 133 mM HEPES (SIGMA) pH 8.5, and TMT reagent (ThermoFisher Scientific) stored in 100% acetonitrile (ACN) (Burdick & Jackson) was added, vortexed to mix reagent and peptides. After 1 h at room temperature, an aliquot was withdrawn to check for labeling efficiency while the remaining reaction was stored at –80 °C. Once labeling efficiency was confirmed to be at least 95%, each reaction was quenched by the addition of ammonium bicarbonate to a final concentration of 50 mM for 10 min, mixed, diluted with 0.1% TFA in water, and desalted. The desalted multiplex was dried by vacuum centrifugation and separated by offline Pentafluorophenyl (PFP)-based reversed-phase HPLC fractionation performed as previously described[155]. TMT-labeled phosphopeptides samples were analyzed on an Orbitrap Fusion

mass spectrometer (ThermoScientific) equipped with an Easy-nLC 1000 (ThermoScientific). Phosphopeptide intensities were adjusted based on total TMT reporter ion intensity in each channel and log2 transformed. Probability of phosphorylation site localization was determined by PhosphoRS[156]. p-Values were calculated using a two-tailed Student's t test assuming unequal variance.

4.2.7 Phosphoproteomic Data Analysis

ZR75-1/FR cells treated with vehicle or GDC-0941 (100mg/kg/d p.o.). Tumors were harvested on Day 0 (n=3), Day 3 at 4 h post-last dose (=3), and Day 56 at 4 h post-last dose (n=3). Differential peptide abundance (DPA) – between PI3Ki resistant (56day treated, proliferating) and control (untreated, proliferating) ZR751/FR PDX tumors – was determined from independent t-test and log2 fold change values. Phosphopeptides with adjusted p-value <0.05 and absolute log2FC >1.5 were considered significant.

Differential peptide abundance – between PI3Ki resistant (56d treated) and short term (3 day treated) ZR751/FR PDX tumors – was determined from independent t-test and log2 fold change values. Phosphopeptides with adjusted p-value <0.05 and absolute log2FC >1.5 were considered significant.

The Normalized Enrichment Score (NES) reflects the degree to which genes in S are overrepresented at the top or bottom of the ranked-ordered list; only use for representing complete FC dataset unique to 56 v control comparisons.

To obtain a single enrichment score for each time point while appropriately accounting for biological variance across replicate measurements, we applied a one sample moderated t test to replicates of each time point, and used the signed, log-transformed p values as input to PTM-SEA.

To obtain a single enrichment score for each time point while appropriately accounting for biological variance across replicate measurements, we applied a one sample moderated t test to replicates of each time point, and used the signed,log-transformed p values as input to PTM-SEA.
This appropriately accounted for the variance observed across replicates captured in a p value. The resulting vector of p values was log-transformed and multiplied by the sign of the average log2 reporter ion ratio:
$S \in \{site\}: ps = -10\log10(pvalue)\,sign(\log(foldchange))$

To combine the triplicate measurements in each time point into a single readout as input for PTM-SEA, we employed a moderated one-sample t test using the limma R-package. This appropriately accounted for the variance observed across replicates captured in a p value. The resulting vector of p values was log-transformed and multiplied by the sign of the average log2 reporter ion ratio:$S \in \{site\}: ps = -10\log10(pvalue)\,sign(\log(foldchange))$.

For the generation of top predicted kinases, phoshphopeptides that were upregulated in 56 d (tumors resistant to PI3K inhibitor) were subjected to analysis by the program Networkin[157].

4.3 Results

4.3.1 Phosphoproteomic Analysis Identifies Top Kinases Upregulated in Resistant Tumors

Previous findings in the lab identified continued activation of the PI3K pathway following 10 wks of combination treatment with PI3K inhibitors (BYL-719 and GSK2636771)[129] as evidenced by elevated p-AKT T308 and pAKT S473. Experiments were done in the setting of fulvestrant resistance to accurately evaluate the effects of combination PI3K and ER inhibition and avoid confounding effects of fulvestrant treatment alone in sensitive parental cells[129]. From these findings, we deduced that kinases could be involved in this maintained pathway activation. To begin investigating this pathway alteration, *in vivo* experiments were carried out to establish ZR75-1/fulvestrant resistant tumors secondarily resistant to the pan-isoform PI3K inhibitor (GDC-0941) (Figure 4.1). Tumors were harvested from mice at 0 d, 3 d, and 56 d. These tumors were analyzed by phosphoproteomic analysis as mentioned in 4.2.6. As mentioned above, special attention was directed to resistant tumors to identify unique phoshphopeptides (Figure 4.2) that would be subjected to pathway enrichment analysis (Figure 4.3A) and kinase prediction (Figure 4.3B). Using the Top predicted kinases with a Networkin score greater than 10 were mapped back to their substrate associated phosphorylation site (Figure 4.4).

McCabe et al. 2015 found in colorectal and prostate cancer models that targeting ataxia telangiectasia mutated (ATM) in *PTEN*-null models leads to

synthetic lethality[158] that was observed across multiple cancer cell subtypes including breast cancer. ZR75-1/FR tumors used in this study are *PTEN*-deficient. Based off the findings of McCabe et al. 2015 and our phosphoproteomic analysis, ATM was selected as a potential kinase to further investigate for its role in the development of resistance to PI3K inhibition.

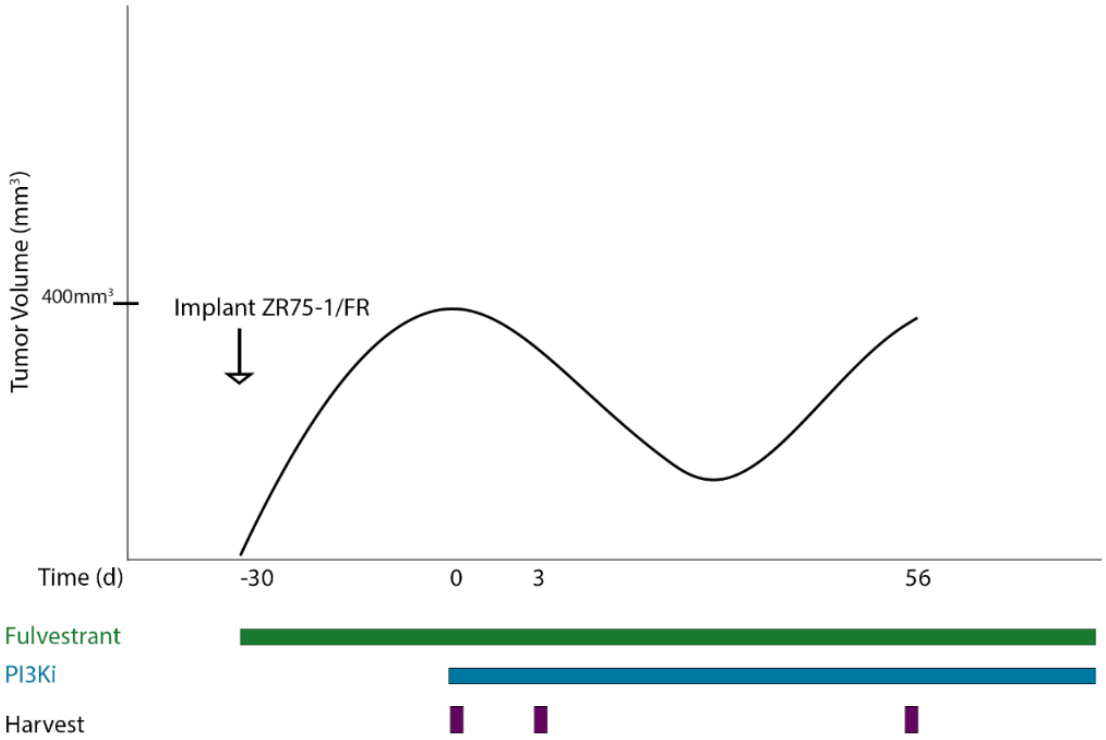

Figure 4.1 Schematic of Mouse Model of Generation of PI3K Inhibitor Resistance

ZR75-1 fulvestrant-resistant cells implanted into mammary fat pad of NSG mice. Mice were on a continuous backbone of 17β-estradiol pellet and fulvestrant. GDC-0941 dosing began when tumors reached 400 mm^3. Tumors were harvested at specified time points. Growth curve is an illustration of approximate tumor growth pattern. (Mouse experiment performed by Nicole Traphagen, Ph.D.)

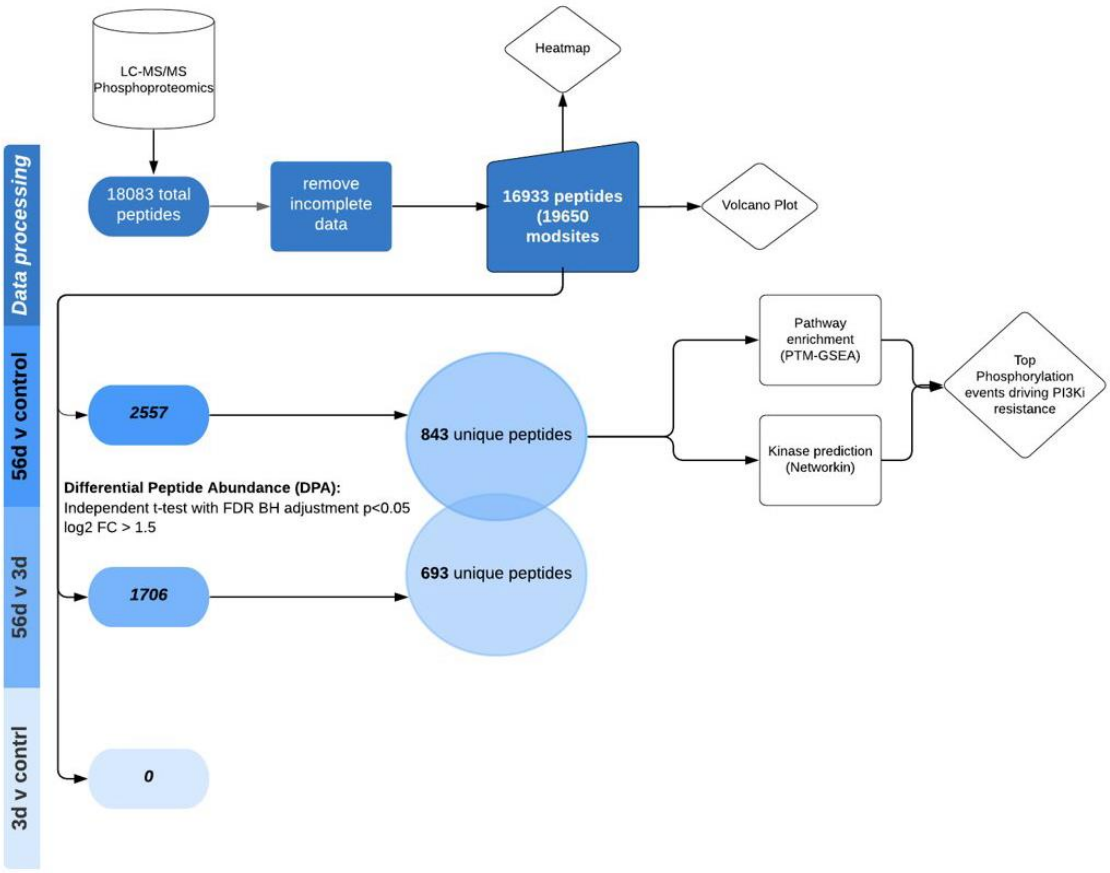

Figure 4.2 Diagram of Pipeline for Analysis of Phosphoproteomic Dataset. ZR75-1 fulvestrant resistant tumors with varied duration of treatment with GDC-0941 were analyzed by LC-MS/MS. Depicted is the pipeline for processing of phoshphopeptides altered during treatment. (Phosphoproteomic analysis done by Kettenbach lab and data processing by Jaqueline Griffin Ph.D.)

A)

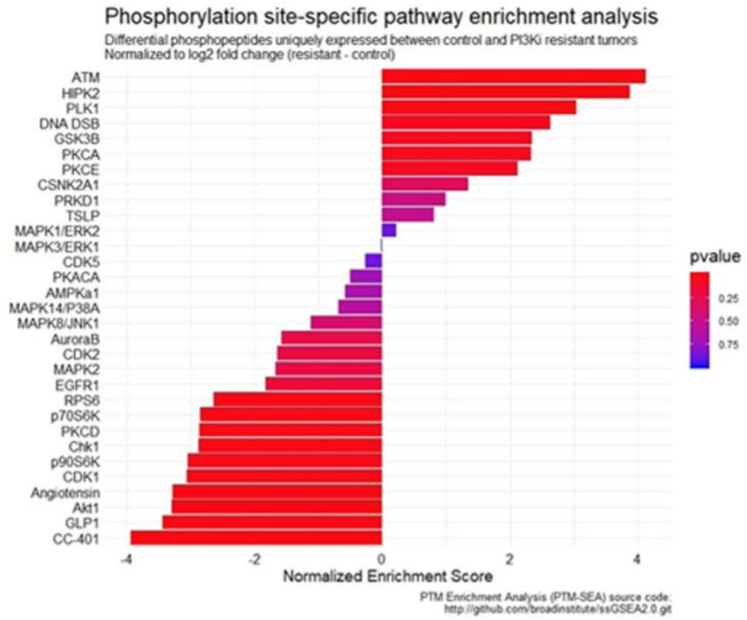
Phosphorylation site-specific pathway enrichment analysis
Differential phosphopeptides uniquely expressed between control and PI3Ki resistant tumors
Normalized to log2 fold change (resistant - control)
ATM
HIPK2
PLK1
DNA DSB
GSK3B
PKCA
PKCE
CSNK2A1
PRKD1
TSLP
MAPK1/ERK2
MAPK3/ERK1
CDK5
PKACA
AMPKa1
MAPK14/P38A
MAPK8/JNK1
AuroraB
CDK2
MAPK2
EGFR1
RPS6
p70S6K
PKCD
Chk1
p90S6K
CDK1
Angiotensin
Akt1
GLP1
CC-401
-4
-2
0
2
4
Normalized Enrichment Score
pvalue
0.25
0.50
0.75
PTM Enrichment Analysis (PTM-SEA) source code:
http://github.com/broadinstitute/ssGSEA2.0.git

B)

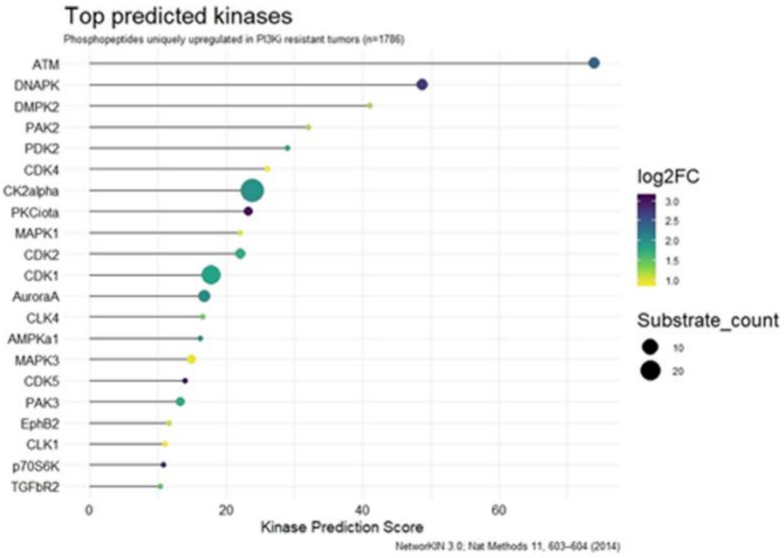
Top predicted kinases
Phosphopeptides uniquely upregulated in PI3Ki resistant tumors (n=1786)
ATM
DNAPK
DMPK2
PAK2
PDK2
CDK4
CK2alpha
PKCiota
MAPK1
CDK2
CDK1
AuroraA
CLK4
AMPKa1
MAPK3
CDK5
PAK3
EphB2
CLK1
p70S6K
TGFbR2
0
20
40
60
Kinase Prediction Score
NetworKIN 3.0; Nat Methods 11, 603–604 (2014)
log2FC
3.0
2.5
2.0
1.5
1.0
Substrate_count
10
20

Figure 4.3 Identification of Pathways and Kinases involved in PI3K Inhibitor Resistance. A) Differential phoshphopeptides identified between control and 56 d (resistant) tumors. **B)** Networkin software used to analyze unique phoshphopeptides that were found to be upregulated in 56 d (resistant) tumors. (Analysis done by Jacqueline Griffin, Ph.D.)

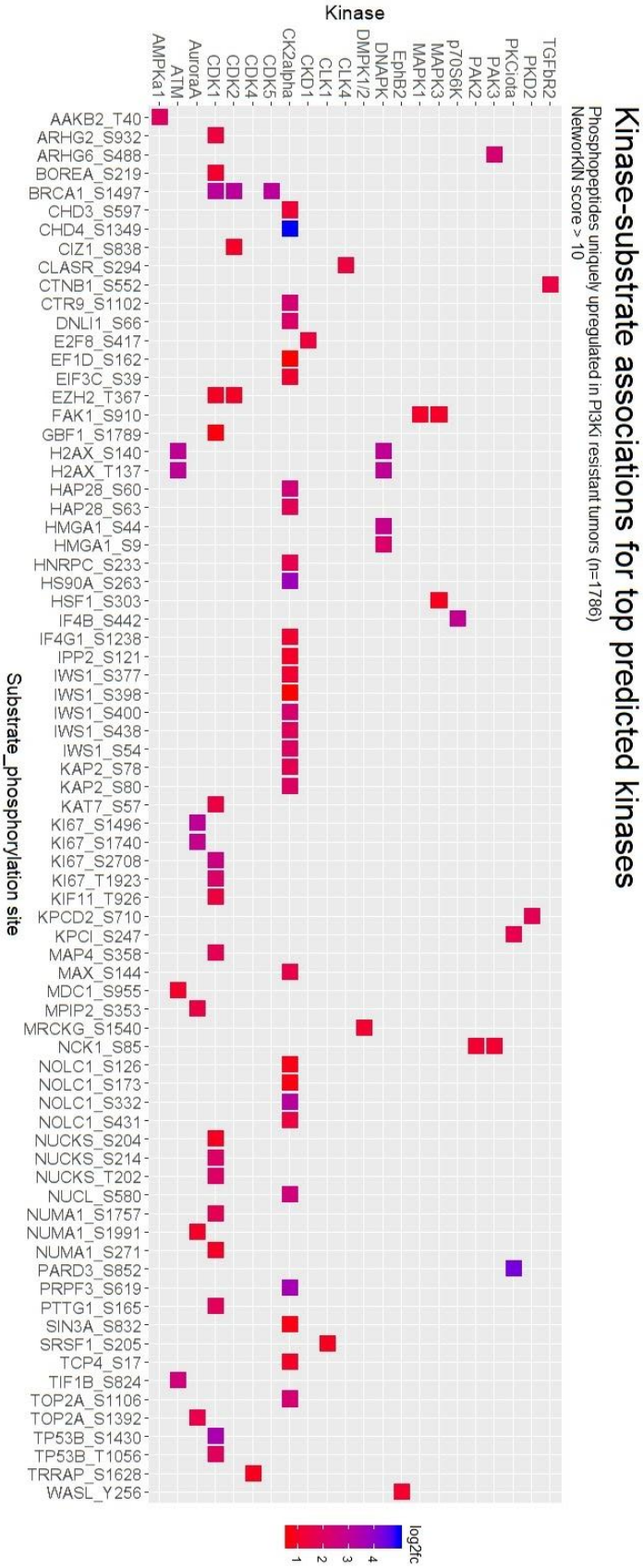
Kinase-substrate associations for top predicted kinases
Phosphopeptides uniquely upregulated in PI3Ki resistant tumors (n=1786)
NetworKIN score > 10
Kinase
TGFbR2
PKD2
PKCiota
PAK3
PAK2
p70S6K
MAPK3
MAPK1
EphB2
DNAPK
DMPK1/2
CLK4
CLK1
CKD1
CK2alpha
CDK5
CDK4
CDK2
CDK1
AuroraA
ATM
AMPKa1
Substrate_phosphorylation site
AAKB2_T40
ARHG2_S932
ARHG6_S488
BOREA_S219
BRCA1_S1497
CHD3_S597
CHD4_S1349
CIZ1_S838
CLASR_S294
CTNB1_S552
CTR9_S1102
DNLI1_S66
E2F8_S417
EF1D_S162
EIF3C_S39
EZH2_T367
FAK1_S910
GBF1_S1789
H2AX_S140
H2AX_T137
HAP28_S60
HAP28_S63
HMGA1_S44
HMGA1_S9
HNRPC_S233
HS90A_S263
HSF1_S303
IF4B_S442
IF4G1_S1238
IPP2_S121
IWS1_S377
IWS1_S398
IWS1_S400
IWS1_S438
IWS1_S54
KAP2_S78
KAP2_S80
KAT7_S57
KI67_S1496
KI67_S1740
KI67_S2708
KI67_T1923
KIF11_T926
KPCD2_S710
KPCI_S247
MAP4_S358
MAX_S144
MDC1_S955
MPIP2_S353
MRCKG_S1540
NCK1_S85
NOLC1_S126
NOLC1_S173
NOLC1_S332
NOLC1_S431
NUCKS_S204
NUCKS_S214
NUCKS_T202
NUCL_S580
NUMA1_S1757
NUMA1_S1991
NUMA1_S271
PARD3_S852
PRPF3_S619
PTTG1_S165
SIN3A_S832
SRSF1_S205
TCP4_S17
TIF1B_S824
TOP2A_S1106
TOP2A_S1392
TP53B_S1430
TP53B_T1056
TRRAP_S1628
WASL_Y256
log2fc
1
2
3
4

Figure 4.4. Mapping of Phosphorylation Sites to Top Predicted Kinases. Kinases having a Networkin score of greater than 10 were mapped back to upregulated phoshphopeptides that were unique to tumors resistant to PI3K inhibitor treatment. (Analysis done by Jacqueline Griffin, Ph.D.)

4.3.2 Generation of PI3K Inhibitor-Resistant PIK3CA-Mutant ER+ Breast Cancer Cell Lines

Alpelisib was FDA approved in combination with fulvestrant in *PIK3CA* mutant ER+ advanced breast cancer[87,148]. To model a PI3K inhibitor-resistant setting, we established PI3K inhibitor-resistant cell lines in *PIK3CA* mutants (Figure 4.5). *PIK3CA* mutants were chosen to determine if results observed from phosphoproteomic analyses in a *PTEN*-deficient model could be extended to models with other forms of PI3K pathway activation and resistance to other PI3K inhibitors. MCF-7/FR/BR and T47D/FR/BR cells resistant to the p110α-selective PI3K inhibitor BYL-719 (alpelisib) showed a growth advantage over MCF-7/FR and T47D/FR cells with a singular resistance to fulvestrant when treated with BYL-719 (Figure 4.5A). MCF-7/FR/GR and T47D/FR/GR cells resistant to GDC-0941 also showed a growth advantage over their MCF-7/FR and T47D/FR GDC-0941-naïve counterparts in the presence of drug (Figure 4.5B).

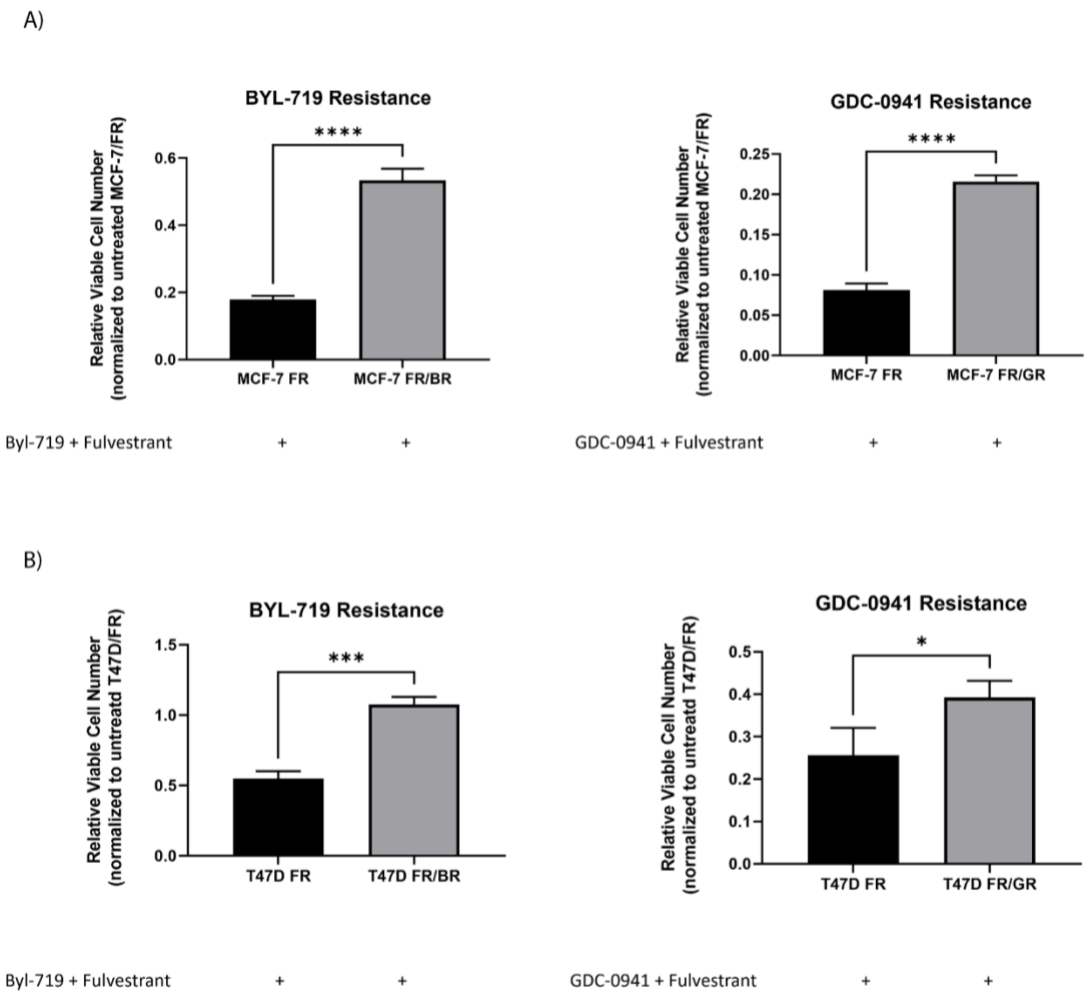

Figure 4.5. Generation of PI3K Inhibitor-Resistant *PIK3CA*-mutant ER+ Breast Cancer Cell Lines. A) MCF-7/FR, MCF-7/FR/BR, and MCF-7/FR/GR and **B)** T47D/FR, T47D/FR/BR, and T47D/FR/GR (*PIK3CA*) cell lines were plated in triplicate and administered combination treatment of 1uM fulvestrant and 1uM (BYL-719 or GDC-0941) for 7 d. Cells were fixed and analyzed by SRB assay. Data was normalized to untreated MCF-7/FR or T47D/FR in a cell line dependent

manner. Data shown are mean of triplicate ± SD. *$p \leq 0.05$, **$p \leq 0.01$, *** $p \leq 0.001$, ****$p \leq 0.0001$ by Bonferroni multiple comparison-adjusted post-hoc test.

4.3.3 ATM Inhibition Inhibits Growth of PI3K Inhibitor-Resistant PIK3CA-Mutant ER+ Breast Cancer Cell Lines

To begin investigating the role of ATM in PI3K inhibitor resistance, we utilized our newly-generated drug-resistant *PIK3CA* cell lines to assess the effects of ATM inhibition on cell growth. Our findings indicate that BYL-719 treatment inhibits growth in the fulvestrant-resistant setting and, more importantly, in the PI3K inhibitor-resistant setting (MCF-7/FR/BR and T47D/FR/BR) (Figure 4.6 A/B). GDC-0941 treatment shows a significant growth inhibitory effect only in the context of PI3K resistance (Figure 4.6 A/B). These findings show that MCF-7/FR/GR and T47D/FR/GR cells resistant to GDC-0941 show an increased sensitivity to ATM inhibitor treatment.

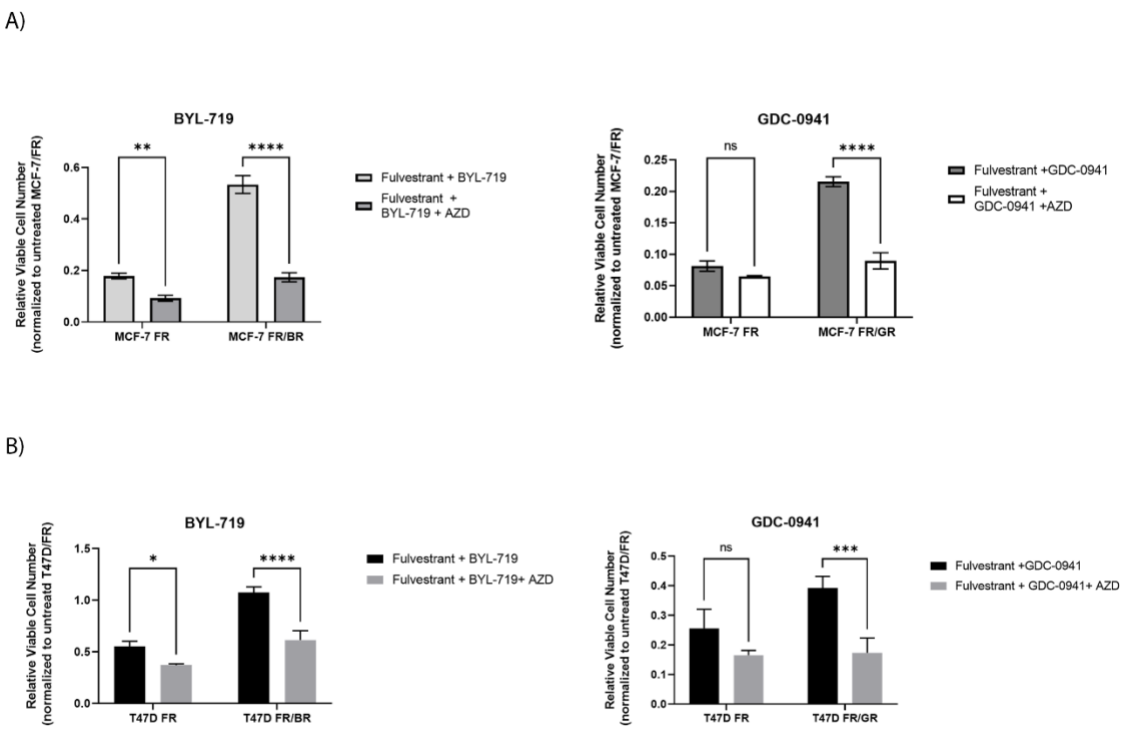

Figure 4.6. ATM Inhibition Inhibits Growth of PI3K Inhibitor-Resistant Cell Lines. A) MCF-7/FR, MCF-7/FR/BR, and MCF-7/FR/GR and **B)** T47D/FR, T47D/FR/BR, and T47D/FR/GR (*PIK3CA*) cell lines were plated in triplicate and administered combination treatment of 1uM fulvestrant, 1uM (BYL-719 or GDC-0941), and +/- 10nM of AZD1390 for 7 days. Cells were fixed and analyzed by SRB assay. Data was normalized to untreated MCF-7/FR or T47D/FR in a cell dependent manner. Data shown are mean of triplicate $\pm$ SD. *$p \leq 0.05$, **$p \leq 0.01$, *** $p \leq 0.001$, ****$p \leq 0.0001$ by Bonferroni multiple comparison-adjusted post-hoc test.

4.3.4 Investigation of Markers of ATM Activation in PI3K Inhibitor-Resistant Tumors

To validate *in vivo* phosphoproteomic findings on ATM activation, we needed to sample tumors treated with long-term PI3K inhibition. Tumors used for phosphoproteomic analysis were not available for analysis by immunohistochemistry. As a result, banked ZR75-1/FR FFPE tumor sections from Hosford et al. 2017 treated with combination fulvestrant, GSK2636771 (p110β targeting), and BYL719 (p110α targeting) for 0 wk, 0.5 wk, or 10 wks were used for further analysis. Hosford et al. 2017 observed that these samples maintained PI3K activation via phosphorylated AKT (T308 and S473) following 10 wks of treatment, leading us to believe that kinase activity could be causing this continued pathway activation. These tumor sections were stained for phoshpho-KAP1-S824 (Figure 4.7 A), based on top predicted kinase-substrate associations, and pCHK2 T68 (Figure 4.7 B), based on raw data. A significant increase was observed for pKAP1 staining following 0.5 wk of treatment compared to baseline. However, no significant changes were observed in the long-term-treated setting in either pKAP1 or pCHK2 staining compared to baseline.

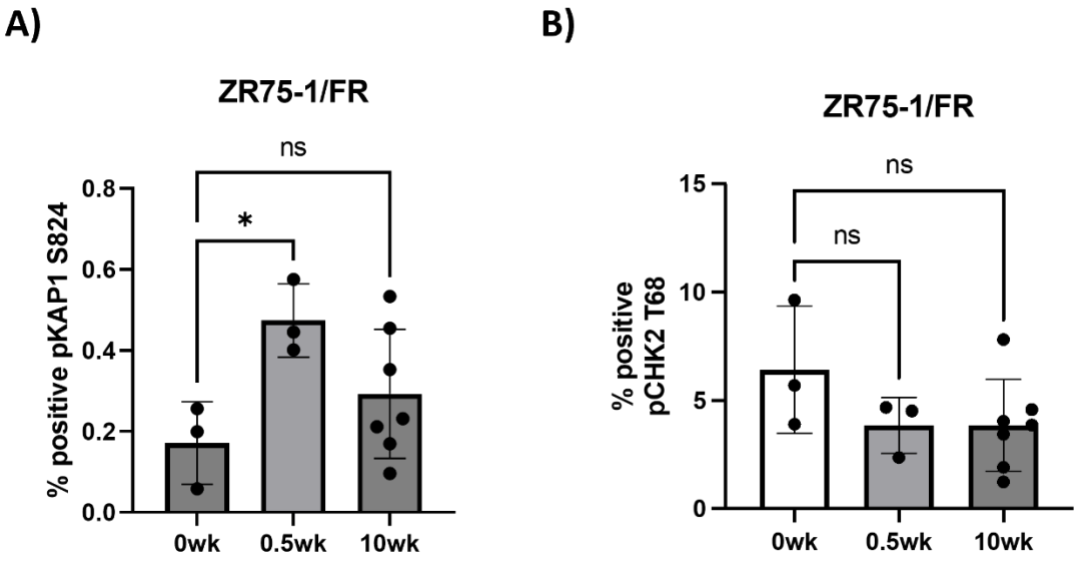

Figure 4.7. Investigation of ATM Activation in PI3K Inhibitor-Resistant Tumors. A/B) ZR75-1/FR tumors samples collected from Hosford et al. 2017. Tumor samples were treated with combination GSK2636771 and BYL-719 and harvested after 0wk, 0.5wk, or 10wk of treatment, and tissue formalin-fixed and paraffin embedded. IHC was performed on tumor samples probing for **A)** pKAP1 S824 or **B)** pCHK2 T68. Data shown are mean of representative images ± SD. *$p \leq 0.05$ by Bonferroni multiple comparison-adjusted post-hoc test. **IHC staining done by Norris Cotton Cancer Center Pathology Shared Resource.**

4.4 Discussion

The PI3K pathway is genetically altered in ~70% of ER+ breast cancers. Common alterations in luminal breast cancer consist of *PIK3CA* mutations, accounting for 32-49% of cases, and *PTEN* deficiency, accounting for 13-24% of cases[80]. Isoform-targeting drugs have been implemented for the treatment of ER+ breast cancer patients. *PIK3CA*-mutant patients had increased clinical benefit when treated with the p110α-selective inhibitor alpelisib as evidenced in the SOLAR-1 trial[87,147,148]. Additionally, *PTEN*-deficient models are sensitive to p110β targeting[149,150], with a sustained long-term response occurring following p110a/b dual targeting[129].

Due to the crosstalk that exists between the PI3K and ER pathways, this provides the continue rationale for dual targeting. However, a caveat to any successful treatment in patients remains the development of resistance. Previous work in the lab identified the onset of such resistance to long-term treatment with combination fulvestrant and PI3K inhibitors[129]. In an effort to address potential mechanisms of resistance, we carried out a phosphoproteomic analysis on long-term PI3K inhibitor-treated tumors. From these results, we identified ATM as a potential target for its involvement in resistance development. From preliminary findings, we see that BYL-719 resistant cells are sensitive to ATM inhibition, and in the setting of resistance to the pan-isoform target (GDC-0941), we see a more robust growth-inhibitory effect. This effect has only been observed in the context

of *PIK3CA* mutants. We are in the process of generating *PTEN*-deficient PI3K inhibitor-resistant cell lines. We have chosen to test both mutations to determine if the results from the phosphoproteomic analysis can be extended across PI3K pathway alterations, or if results are drug- or mutation-dependent. Currently, the relatively increased sensitivity in GDC-0941-resistant cell lines (MCF-7/FR/GR and T47D/FR/GR) as compared to fulvestrant resistant lines (MCF/FR and T47D/FR) indicates that these results might be a consequence of pan-inhibitor treatment. Results from *PTEN*-deficient models would provide a better understanding of the drug- or mutation-dependent sensitivity.

Results from IHC have proven inconclusive with the results established by phosphoproteomic analysis. Phosphoproteomic analysis required the use of entire tumor specimens, preventing the possibility of conducting IHC validation. As a potential alternative to this problem, we performed IHC on banked tumor samples from a previous *in vivo* study utilizing two separate PI3K inhibitors targeting the α and β isoforms[129]. A potential explanation for the lack of elevated levels of pKAP1 S824 and pCHK2 T68 in 10 wks treated tumor samples could be tied to the proliferation status of the tumors at time of harvest. Tumors harvested for use in the phosphoproteomic analysis were in a growth phase, while banked tumor samples were harvested while in a growth inhibited state evidenced by low levels of KI67[129]. To have the best possible chance of recapitulating findings associated with phosphoproteomic analysis, we will be repeating the experiment detailed in Figure 4.1. Attempts were made to establish an additional PTEN-

deficient PDX tumor model (HCI-003) however mice implanted with tumors developed complications and were ultimately sacrificed. Additionally, we will add an AZD1390 treatment arm to validate initial findings and investigate the use of AZD1390 a potential therapeutic.

Chapter 5: Apoptotic Priming in Triple-negative Breast and Ovarian Cancers

Work described in this chapter is unpublished and was done as a follow-up study to work published by Shee et al 2020[159]. This work was conducted as a rotation project.

5.1 Introduction

According to the American Cancer Society, breast and ovarian cancers are the second and fifth leading cause of cancer related deaths in women. As of 2018, the expected new cases of breast and ovarian cancer in females is 266,120 and 22,240 respectively with the number of expected deaths from breast to be 40,920 and ovarian to be 14,070[160]. Within the branch of breast cancer, there are several specific subsets determined by the presence of specific pathological markers: Progesterone receptor [PR], estrogen receptor [ER], and human epidermal growth factor 2 receptor [HER2][161]. Of these various subtypes, triple negative breast cancer is a particularly difficult form to treat due to the absence of all three characteristic pathological markers. Similar to triple-negative breast cancer, ovarian cancer lacks targetable markers and does not present with specific symptoms and as a result, diagnosis often occurs when the tumor has progressed to advanced stages[162]. The absence of specific markers in both cancer types has made tumor-targeted treatment more difficult. However, these cancer subtypes are not without treatment options.

Standard methods of treatment include administration of anthracyclines and chemotherapies that target DNA replication and microtubule function [163,164,165]. However, these treatment options do not provide specific targeting to the individual tumor. In certain circumstances, the potential for targeted therapies does exist. For example, the mutations in the tumor suppressors BRCA1 and

BRCA2, most known for their role in damage response through DNA repair process activation, increase the risk of developing breast and ovarian cancer; however, treatment of BRCA1 and BRCA2 mutant tumors with Poly(ADP-ribose) polymerase (PARP) inhibitors shows increased vulnerability[166,167]. This mechanism works by trapping PARP onto DNA leading to replication fork stalling and ultimately collapse causing double strand breaks. PARP inhibitor treatment of HR deficient BRCA mutated patients provides an interesting avenue for synthetic lethality[168]. Other methods to treat triple negative breast cancer include combination of PARP inhibitor with PI3Kα-specific inhibitor alpelisib, showing efficacy in patients without BRCA mutations, but further sensitization in BRCA-mutant tumors is currently in phase 1b clinical trials [169].

In an effort to continue the investigation of targetable vulnerabilities, work in the lab focused on examining tumor-targeted therapies in the treatment of triple negative breast cancer and ovarian cancer. Prior analysis of these two cancers' gene expression profiles and mined drug sensitivity data revealed two distinct transcriptionally-identifiable subgroups across both cancer types: mesenchymal-like (M-like) and basal-like (B-like); additional findings showed that when heat shock protein 90 (Hsp90) chaperones were inhibited in mesenchymal-like cells an observable sensitization was observed [159]. As a consequence of inhibition of Hsp90, pro-apoptotic BH3-only proteins Bim and PUMA of the Bcl-2 family of proteins were found to be upregulated [159]. Based off of these previous findings, this ushered in the desire to determine if other Bcl-2 family protein levels

and/or activation could be used as predictive markers for potential therapeutic applications of Bcl-2 family inhibitors, stratifying on the basis of mesenchymal-like and basal-like in different cell lines of triple negative breast and ovarian cancer.

Apoptosis plays a fundamental role in development. The implementation of apoptosis is tightly regulated and when this regulation is disrupted this can result in disastrous effects, one of which includes preserving cells carrying mutations, allowing them to invade and metastasize to other tissues [170]. Evasion of apoptosis can be facilitated by alterations to Bcl-2 family proteins, specifically the pro-survival proteins: Bcl-2, Bcl-xL, or Mcl-1 [171]. In this project, we aim to focus on the key players, Bcl-2 family proteins, of the stress pathway or 'intrinsic' pathway which converges on the activation of caspase-9, leading to downstream activation of additional caspases termed 'effector caspases' that cause cleavage of proteins eliciting cellular death [170].

The Bcl-2 family can be divided into three distinct groups: stress sensing BH3 proteins (Bik, Bad, Bid, Bim, Bmf, Hrk, Noxa, and Puma), proteins that cause mitochondrial outer membrane permeabilization (MOMP) by oligomerization (Bax and Bak), and the pro-survival proteins which prevent BH3 proteins from activating Bak and Bax (Bcl2-A1, Bcl-2, Bcl-xL, Bcl-w and Mcl-1) [166,172]. Dysregulation of these proteins have been shown to lead to the development of resistance with high Bcl-2 being linked to decreased sensitivity to

taxanes[173] and Adriamycin[174], and amplification of Mcl-1 was observed in TNBC samples refractory to chemotherapy[175].

In this project, we will investigate the effects of various pro-survival inhibitors and Hsp90 inhibition on mesenchymal-like and basal-like triple negative breast and ovarian cancer in the hopes of determining a subtype specific therapeutic target by assessing sensitivity to respective inhibitors.

5.2 Materials and Methods

5.2.1 Drugs

ABT-737: Bcl-2, Bcl-xL, Bcl-w, ABT-199: Bcl-2, A-1155463: Bcl-xL, and S63845: Mcl-1 were purchased from APExBIO. Hsp90 inhibitor were purchased from Astex Therapeutics, Ltd.

5.2.2 Sulforhodamine B (SRB) Growth Assay

2,000 cells/well were plated in 96-well plates for each cell line in triplicate and treated with a dose range (0-2 μm) of each drug. For chronic drug exposure, cells were treated with each drug for 5-7 d, then assayed. For acute drug exposure, cells were treated with drug for 24 hrs, followed by drug washout and continued culture for another 5 d before assay. Combination treatment with Hsp90 inhibition was modeled under conditions of chronic or acute treatment as listed above.

5.2.3 *Immunoblotting*

Immunoblotting procedure carried out as detailed in Chapter 2. Antibodies used are as follows: Bim C3C45 (Cell Signaling), Bak D4E4 (Cell Signaling), Bax 2774 (Cell Signaling), Mcl-1 4572 (Cell Signaling), PUMA (D30C10) (Cell Signaling), Bcl-2 (Human Specific) 2872 (Cell Signaling), Bcl-xL (54H6) (Cell Signaling), NOXA (D8L7U) (Cell Signaling), Bad (11E3) (Cell Signaling), Bid 2002 (Cell Signaling), Beta-Actin (8H10D10) (Cell Signaling).

5.3 Results & Discussion

5.3.1 Single agent targeting of anti-apoptotic members of the Bcl-2 protein family fails to induce a subtype specific sensitivity

To test the effects of a panel of Bcl-2 family inhibitors on ovarian cancer cell lines, cells were treated with respective inhibitors either chronically or acutely. Treatment with the Bcl-xL inhibitor A-1155463 showed inhibitory effects on growth in the majority of cell lines both when treated acutely and chronically (Figure 5.1A/B). Treatment with the Mcl-1 inhibitor, S63845, resulted in moderate inhibition of growth across cell lines, although not as dramatic as treatment with A-1155463 (Figure 5.1A/B). Treatment with ABT-199 and ABT-737 resulted in a pattern of inhibition with the highest and lowest doses causing inhibition, while intermediate doses seemed to allow for growth to occur in both the chronic and acute treatments that was not specific to either mesenchymal-like or basal-like cells (Figure 5.1A/B). Ovarian cancer cell lines when treated with Bcl-2 family targeting drugs did not yield a subtype specific response.

To determine downstream effects to Bcl-2 protein levels in response to drug inhibition, ovarian cancer cells were exposed to Bcl-2 targeting drugs for 24 hrs. Mesenchymal-like cells were preferentially used for preliminary studies. Mcl-1 inhibitor treatment led to an increase in Mcl-1 and the stress sensing protein Bid in dose dependent manner (Figure 5.2A). ABT-737 had minimal effect in tested cell

lines showing increased levels of Bid in EFO21 (Basal-like) and a slight increase in Mcl-1 in SKOV3 cells at the highest tested dose (Figure 5.2). ABT-199 altered protein levels to favor apoptosis by increasing Bim and Bax and showing a trend of decreasing Bcl-2 in EFO27 lines and a decrease of Mcl-1 and increased levels of Bid (Figure 5.2). Previous literature showed that single agent Mcl-1 inhibition of solid tumors were insensitive to treatment [176]. In support of this, promising results were seen when S63845 was used in combination with agents priming cells for apoptosis or chemotherapy and HER2 targeting drugs. Of the treatments tested, ABT-199 led to the most noticeable alterations to Bcl-2 family proteins. However, between cell lines tested there was not a consistent response in altered Bcl-2 proteins, indicating a potential cell line specific response to treatment. The limitation of these findings is that ovarian lines were tested and were skewed towards mesenchymal-like lines. Additionally, treatment was only administered over 24 hrs and is possibly not enough time to adequately see a shift of Bcl-2 family proteins in response to treatment.

As a parallel to these experiments, triple negative breast cancer cell lines were also treated to determine if inhibition of Bcl-2 family proteins resulted in a subtype specific response. This work was done by Natasha Mariano as part of her rotation project. ABT-737 showed a reduction in growth when treated at doses of 0.25uM in the chronic setting that were not observed during acute treatment (Figure 5.3 A/B). ABT-199 and A115463 drugs showed similar trends failing to induce death over the range of doses (Figure 5.3 A/B). Following previously

reported results in triple negative breast cancer[171], S63845 showed a consistent decrease in cell number both in the acute and chronic setting, suggesting Mcl-1 targeting is a more sensitive target in triple negative breast cancer lines (Figure 5.3 A/B). In two of the four drugs tested, Cal120, a mesenchymal-like cell line, showed an increased sensitivity even at low doses when treated with A1155463 and ABT-737, suggesting the importance of targeting Bcl-xL in this cell line. As with ovarian cancer cell lines, single arm treatment did not lead to an overall cell-type specific targeting across cell lines tested.

Across both cancer types, the drug treatments that lead to the most growth inhibition affected Bcl-2 family member, Bcl-xL although these growth inhibitory effects were not consistent across cancer types. We speculate that single arm treatment could be ineffective due to compensatory activation of pro-survival factors when treating with single protein targeting inhibitors. A potential avenue to pursue in the future would be to assess the level of expression of anti-apoptotic proteins in these cancer cell lines to determine a potential explanation for treatment response observed. High Bcl-2 levels have been implicated in priming cells to be more sensitive to ABT-737 treatment [177]. Additionally, amplification of Mcl-1 levels in triple negative breast cancer have been identified in patients resistant to chemotherapy treatment[175].

5.3.2 Dual agent targeting of Hsp90 and Bcl-2 anti-apoptotic proteins fails to induce a subtype specific sensitivity to treatment

After observing the lack of robust effects with single agent treatment, we next wanted to determine how combination treatment with an Hsp90 inhibitor would affect the targeting of Bcl-2 family members. Preliminary work in the lab showed Hsp90 inhibition to have a greater sensitivity in mesenchymal-like cancer populations, showing elevated levels of cleaved PARP and expression of pro-apoptotic proteins (Bim and PUMA)[159]. Cells were cultured either alone or in combination with 0.1uM Hsp90 inhibitor. For ease of display, results were separated by Bcl-2 inhibitor. Acute treatment with A1155463 single agent treatment showed minimal to no treatment response, while combination treatment reduced viable cell number greater than single treatment with Hsp90 treatment (Figure 5.4 A). Intermediate doses in SKOV3 (mesenchymal-like) cells showed increased sensitivity to combination treatment. Acute treatment with ABT-199 showed a mix of results, showing increased sensitivity to combination treatment in OVCAR4 cells with no effect in SKOV3 or EF021 cells (Figure 5.5A). Chronic treatment with ABT-199 also failed to show enhanced sensitivity with combination treatment in breast cancer basal-like lines (Figure 5.5B). Treatment with ABT-737 showed enhanced sensitivity with combination treatment in SKOV3 mesenchymal-like cells (Figure 5.6A). S63845 treatment in the acute setting showed a greater sensitivity in breast cancer basal-like cell lines, while mesenchymal-like cells regardless of cancer failed to show increased sensitivity to drug treatment (Figure 5.7A). Chronic

treatments with S63845 did not show greater sensitivity to treatment than Hsp90 inhibition alone (Figure 3.7B). In this preliminary data, acute treatment with ABT-737 and A1155463 were the only conditions that showed sensitivity in a subtype specific manner. S63845 showed greater sensitivity in the acute setting, but in the basal-like subtype.

Overall, these results indicate that there is a timing and drug-dependent response when treating basal-like or mesenchymal-like cell lines. A future avenue of investigation could examine the effects of timing of drug administration. More specifically the order in which drug is administered. Due to increased expression of Bim and PUMA proteins following Hsp90 inhibition[159], I propose preliminary treatment with Hsp90 inhibitors followed by treatment with Bcl-2 family targeting treatments. This treatment modality could potentially take advantage of these primed cells and lead to increased levels of apoptosis upon administration of secondary drug treatment.

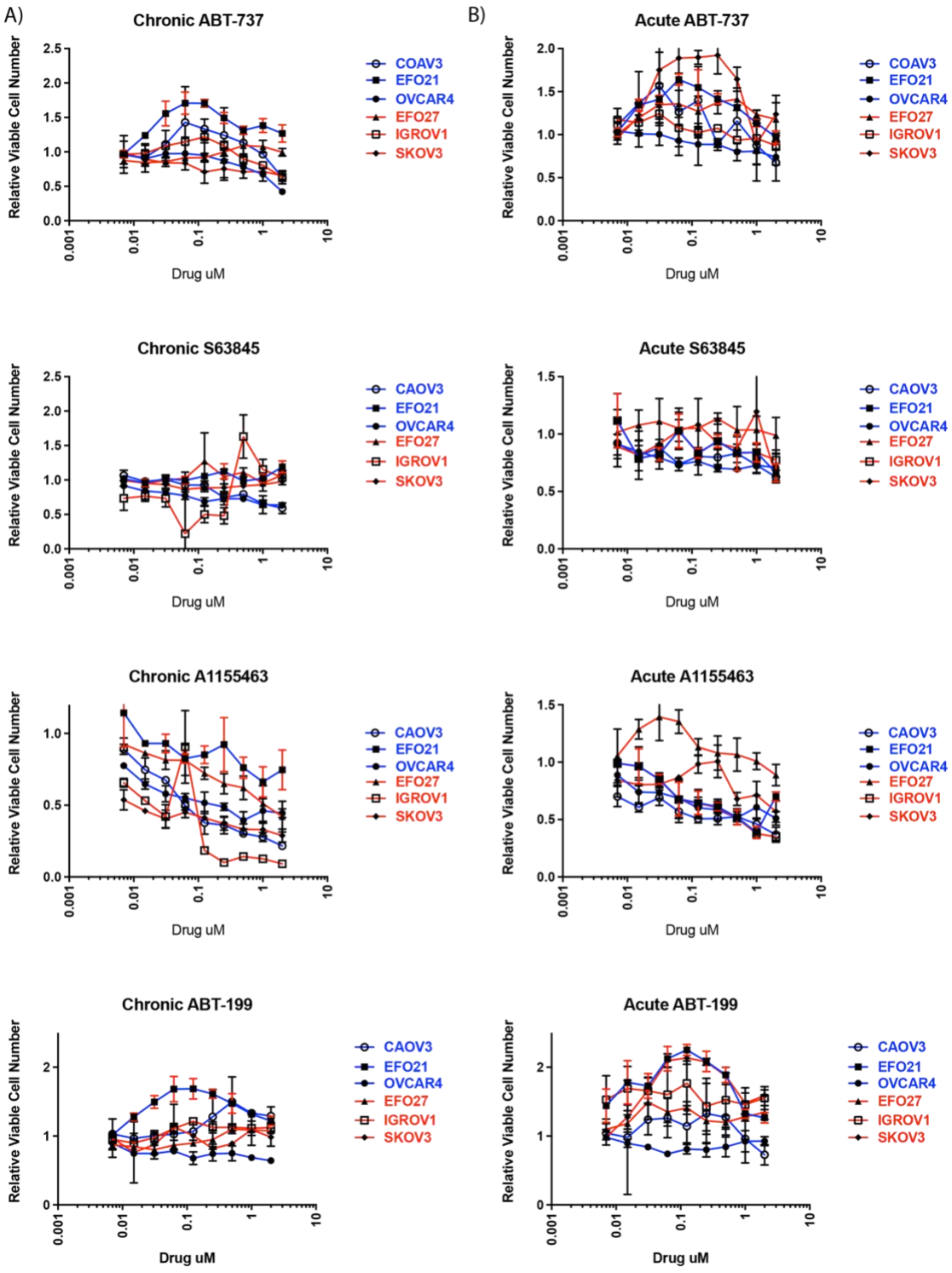
A)
Chronic ABT-737
Relative Viable Cell Number
Drug uM
COAV3
EFO21
OVCAR4
EFO27
IGROV1
SKOV3
B)
Acute ABT-737
Chronic S63845
CAOV3
Acute S63845
Chronic A1155463
Acute A1155463
Chronic ABT-199
Acute ABT-199

Figure 5.1. Ovarian Cancer Treatment Response to BH3 Mimetics. (A/B) Respective cell lines treated with A-1155463 (Bcl-xL), ABT-199 (Bcl-2), ABT-737 (Bcl-2, Bcl-xL, Bcl-w), S63845 (Mcl-1). Relative viable cell number determined through SRB assay. Mesenchymal (red) and Basal-like (blue). Data are shown as a mean of triplicates + SD.

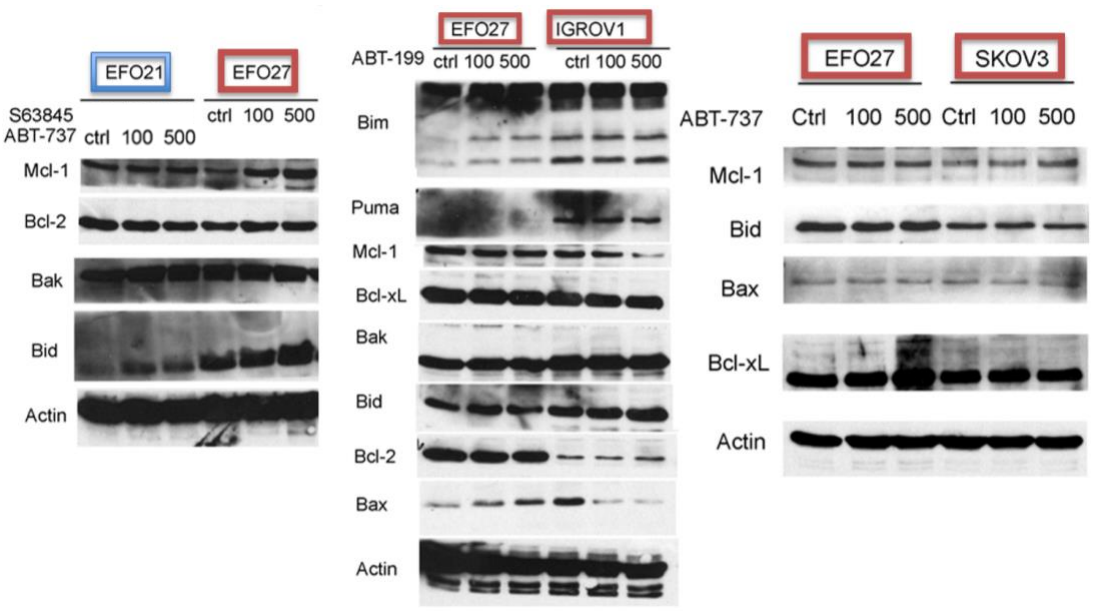

Figure 5.2 BCL-2 Family Proteins in Ovarian Cancer following Acute Inhibitor Treatment. Immunoblot for Bcl-2 family proteins in Mesenchymal (red) and Basal-like (blue) cell lines following 24 hr drug exposure (100uM or 500uM) to Bcl-2 targeting proteins.

A)

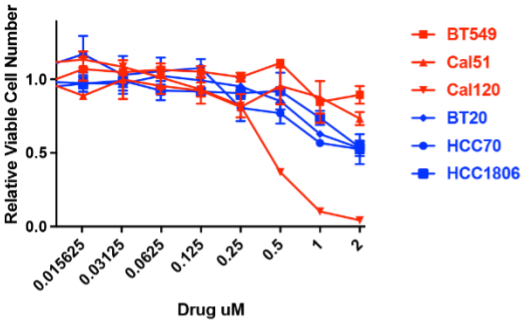
Chronic ABT-737 Treatment
Relative Viable Cell Number
1.0
0.5
0.0
0.015625
0.03125
0.0625
0.125
0.25
0.5
1
2
Drug uM
BT549
Cal51
Cal120
BT20
HCC70
HCC1806

B)

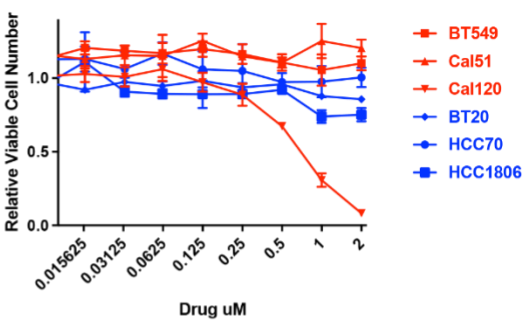
Acute ABT-737 Treatment
Relative Viable Cell Number
1.0
0.5
0.0
0.015625
0.03125
0.0625
0.125
0.25
0.5
1
2
Drug uM
BT549
Cal51
Cal120
BT20
HCC70
HCC1806

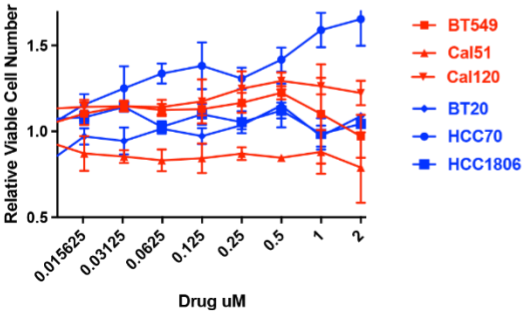
Chronic ABT-199 Treatment
Relative Viable Cell Number
1.5
1.0
0.5
0.015625
0.03125
0.0625
0.125
0.25
0.5
1
2
Drug uM
BT549
Cal51
Cal120
BT20
HCC70
HCC1806

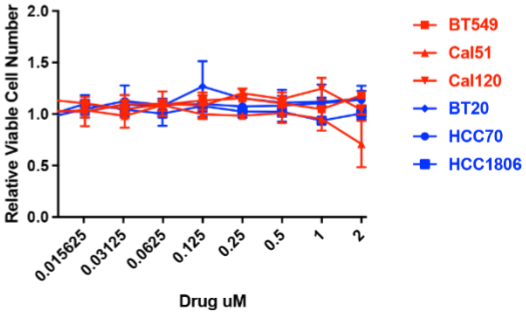
Acute ABT-199 Treatment
Relative Viable Cell Number
2.0
1.5
1.0
0.5
0.0
0.015625
0.03125
0.0625
0.125
0.25
0.5
1
2
Drug uM
BT549
Cal51
Cal120
BT20
HCC70
HCC1806

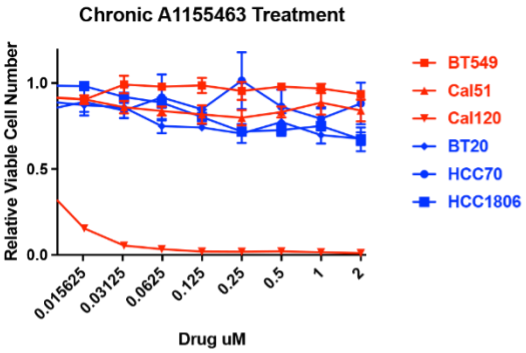
Chronic A1155463 Treatment
Relative Viable Cell Number
1.0
0.5
0.0
0.015625
0.03125
0.0625
0.125
0.25
0.5
1
2
Drug uM
BT549
Cal51
Cal120
BT20
HCC70
HCC1806

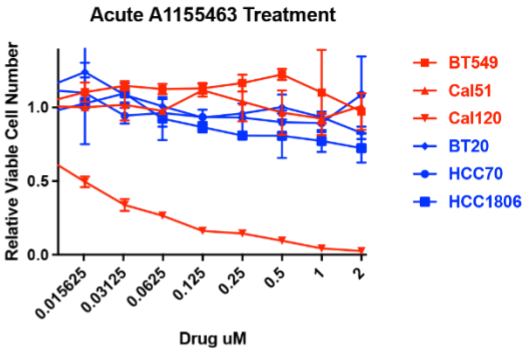
Acute A1155463 Treatment
Relative Viable Cell Number
1.0
0.5
0.0
0.015625
0.03125
0.0625
0.125
0.25
0.5
1
2
Drug uM
BT549
Cal51
Cal120
BT20
HCC70
HCC1806

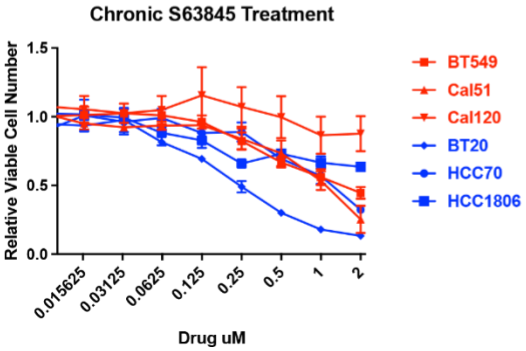
Chronic S63845 Treatment
Relative Viable Cell Number
1.5
1.0
0.5
0.0
0.015625
0.03125
0.0625
0.125
0.25
0.5
1
2
Drug uM
BT549
Cal51
Cal120
BT20
HCC70
HCC1806

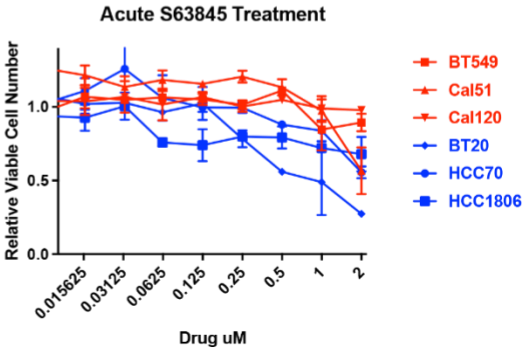
Acute S63845 Treatment
Relative Viable Cell Number
1.0
0.5
0.0
0.015625
0.03125
0.0625
0.125
0.25
0.5
1
2
Drug uM
BT549
Cal51
Cal120
BT20
HCC70
HCC1806

Figure 5.3. Triple Negative Breast Cancer Treatment Response to BH3 Mimetics. (Data generated by Natasha Mariano). (A/B) Chronic and Acute treatment of respective Triple Negative Breast Cancer cell lines treated with A-1155463 (Bcl-xL), ABT-199 (Bcl-2), ABT-737 (Bcl-2, Bcl-xL, Bcl-2), S63845 (Mcl-1). Relative viable cell number determined through SRB assay. Mesenchymal (red) and Basal-like (blue). Data are shown as a mean of triplicates + SD.

A)

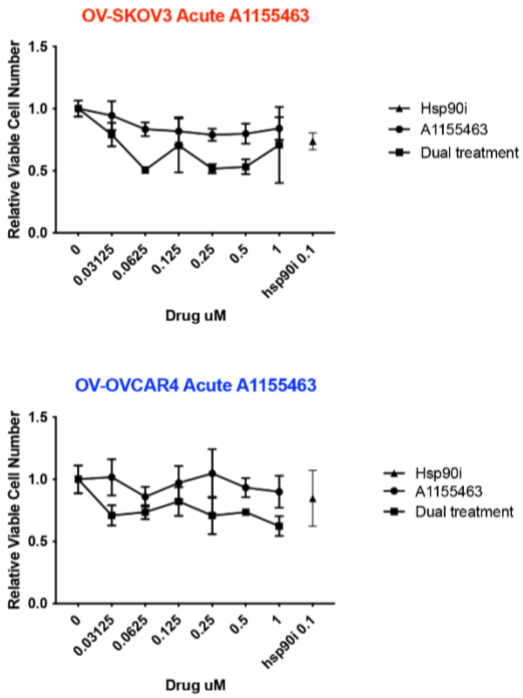

Figure 5.4 Cell Viability following Bcl-xL Inhibition. (A) Respective ovarian cancer cell lines treated with A-1155463 (Bcl-xL) and Hsp90 inhibition either alone or in combination. Relative viable cell number determined through SRB assay. Mesenchymal (red) and Basal-like (blue). Data are shown as a mean of triplicates + SD.

A)

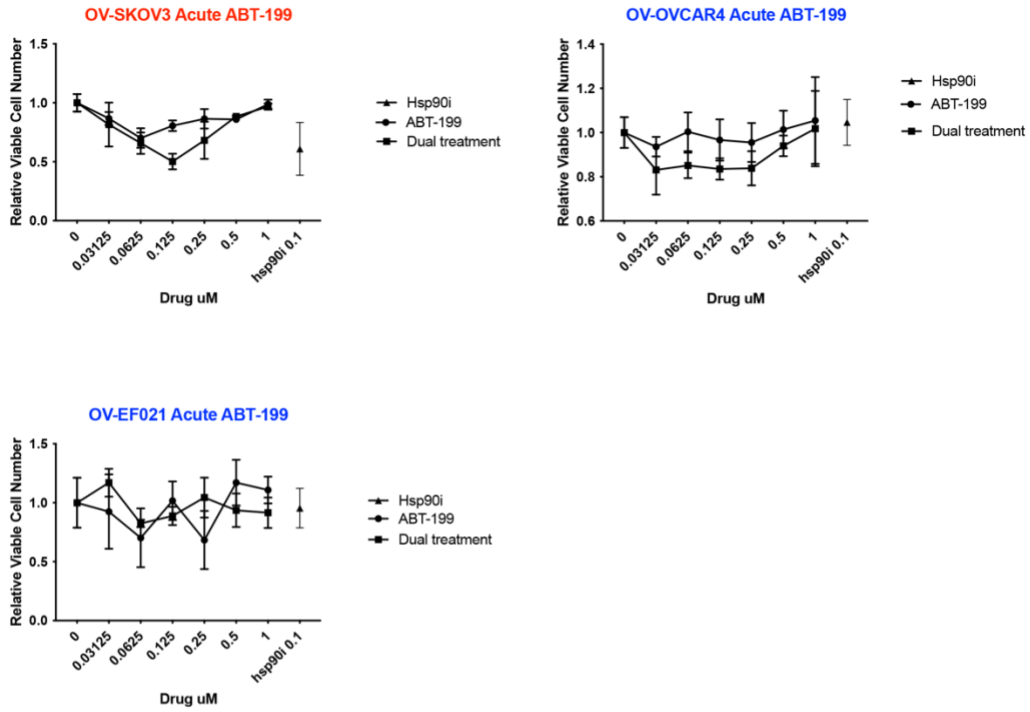
OV-SKOV3 Acute ABT-199
Relative Viable Cell Number
1.5
1.0
0.5
0.0
0
0.03125
0.0625
0.125
0.25
0.5
1
hsp90i 0.1
Drug uM
Hsp90i
ABT-199
Dual treatment
OV-OVCAR4 Acute ABT-199
Relative Viable Cell Number
1.4
1.2
1.0
0.8
0.6
Drug uM
Hsp90i
ABT-199
Dual treatment
OV-EF021 Acute ABT-199
Relative Viable Cell Number
Drug uM
Hsp90i
ABT-199
Dual treatment

B)

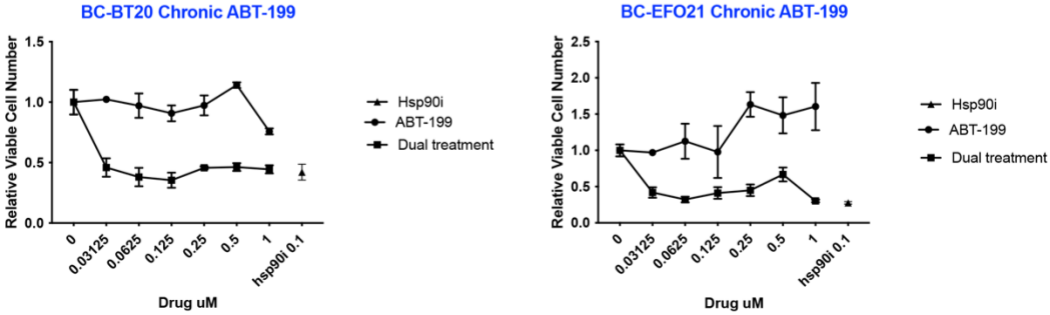
BC-BT20 Chronic ABT-199
Relative Viable Cell Number
1.5
1.0
0.5
0.0
0
0.03125
0.0625
0.125
0.25
0.5
1
hsp90i 0.1
Drug uM
Hsp90i
ABT-199
Dual treatment
BC-EFO21 Chronic ABT-199
Relative Viable Cell Number
2.5
2.0
1.5
1.0
0.5
0.0
Drug uM
Hsp90i
ABT-199
Dual treatment

Figure 5.5 Cell Viability following Bcl-2 Inhibition. (A) Acute treatment of ovarian cancer or **(B)** Chronic treatment of triple negative breast cancer cell lines treated with ABT-199 (Bcl-2) and Hsp90 inhibition either alone or in combination. Relative viable cell number determined through SRB assay. Mesenchymal (red) and Basal-like (blue). Data are shown as a mean of triplicates + SD.

A)

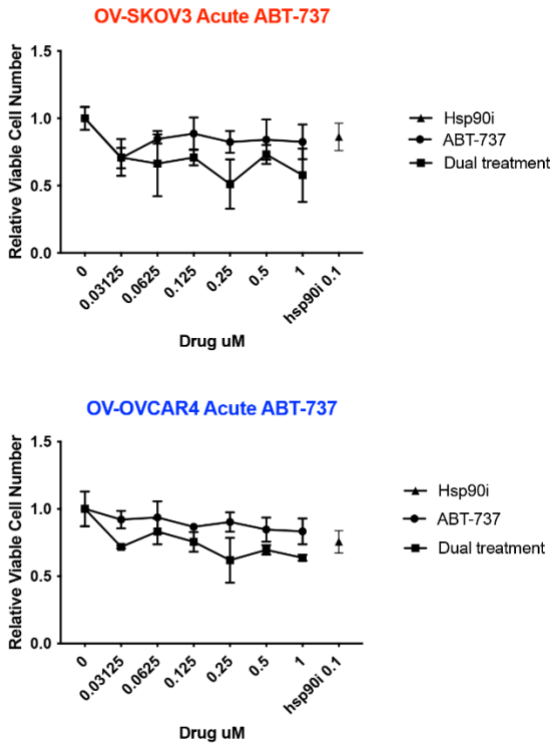

Figure 5.6 Cell Viability following pan Bcl-2, Bcl-xL, Bcl-w Inhibition. (A) Acute treatment of respective ovarian cell lines treated with ABT-737 (pan Bcl-2, Bcl-xL, Bcl-w) and Hsp90 inhibition either alone or in combination. Relative viable cell number determined through SRB assay. Mesenchymal (red) and Basal-like (blue). Data are shown as a mean of triplicates + SD.

A)

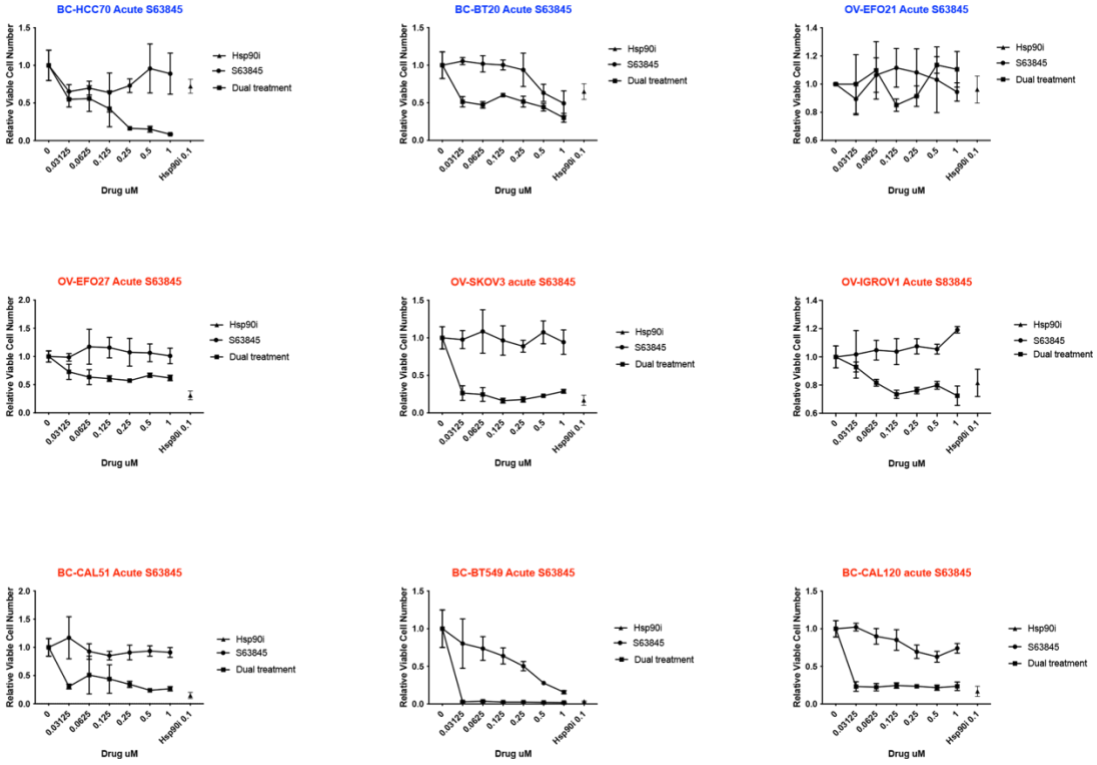
BC-HCC70 Acute S63845
BC-BT20 Acute S63845
OV-EFO21 Acute S63845
OV-EFO27 Acute S63845
OV-SKOV3 acute S63845
OV-IGROV1 Acute S83845
BC-CAL51 Acute S63845
BC-BT549 Acute S63845
BC-CAL120 acute S63845
Relative Viable Cell Number
Drug uM
Hsp90i
S63845
Dual treatment

B)

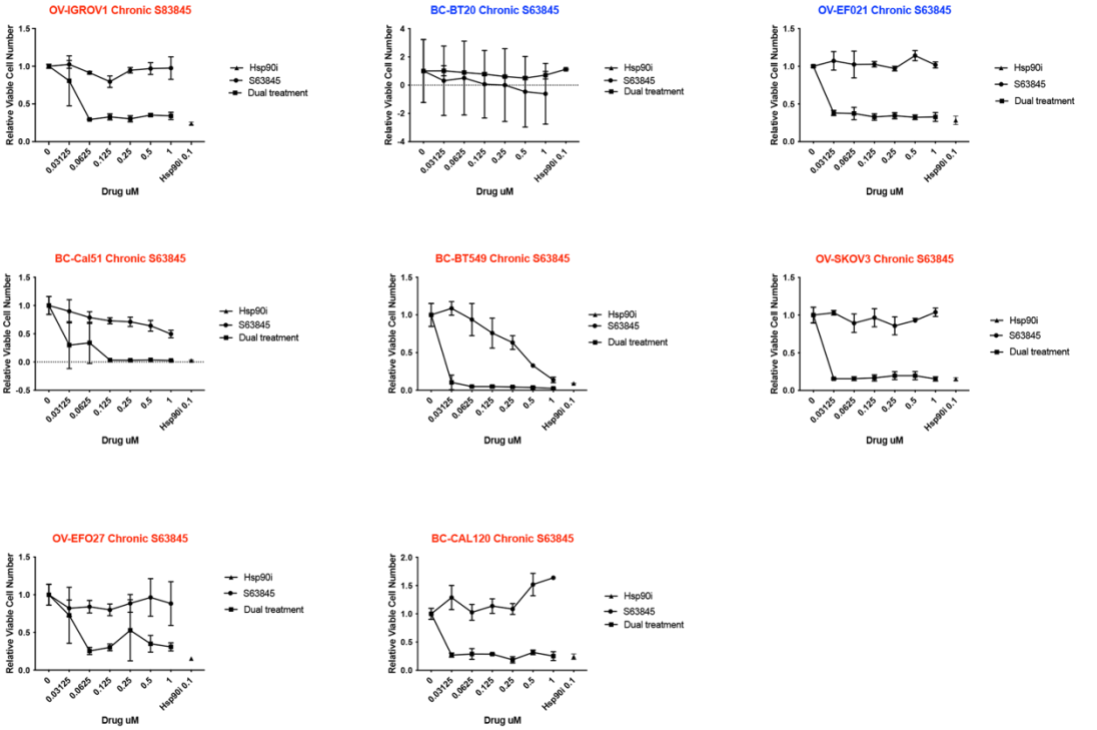
OV-IGROV1 Chronic S83845
BC-BT20 Chronic S63845
OV-EF021 Chronic S63845
BC-Cal51 Chronic S63845
BC-BT549 Chronic S63845
OV-SKOV3 Chronic S63845
OV-EFO27 Chronic S63845
BC-CAL120 Chronic S63845
Relative Viable Cell Number
Drug uM
Hsp90i
S63845
Dual treatment

Figure 5.7. Cell Viability following Mcl-1 Inhibition. (A) Acute or **(B)** chronic treatment of respective ovarian and triple negative breast cancer cell lines treated with S63845 (Mcl-1) and Hsp90 inhibition either alone or in combination. Relative viable cell number determined through SRB assay. Mesenchymal (red) and Basal-like (blue). Data are shown as a mean of triplicates + SD.

Chapter 6: The Roles of CDK4/6 inhibitors in dormancy in ER+ breast Cancer

Work described in this chapter was proposed as a part of a qualifying project

Work laid out in this chapter is unpublished.

Research contributions to the data shown were done by this author.

6.1. Introduction

Breast cancer is one of the most common causes of cancer in women. In the U.S., breast cancer was expected to account for about 14% of the cancer related deaths in 2018 [160]. Upon diagnosis, patients will undergo tumor resection and biopsy to further categorize the breast cancer subtype based on the presence of specific markers for estrogen receptor (ER), progesterone receptor (PR), and human epidermal growth factor 2 receptor (HER2) [161]. Of the diagnosed breast cancer subtypes, over 70% of breast cancers are hormone receptor positive[178].

In treating ER+ breast cancer, anti-estrogen therapy is a potential option. Anti-estrogen therapies fall into three different categories: selective estrogen receptor downregulators (SERDs), selective estrogen receptor modulators (SERMs), and aromatase inhibitors (AIs). Anti-estrogens aim to prevent binding of the ligand, estrogen, to estrogen receptors, downregulate (ER), or prevent estrogen production. In the case of some anti-estrogens like aromatase inhibitors, patients can remain on adjuvant treatment for upwards of 10 years[179]. Tamoxifen adjuvant therapy can be extended to 10 years, reducing tumor recurrences[180]. Despite anti-estrogen therapy being initially effective, 1/3 of patients develop resistance to treatment and experience relapse [16,135]. Targeted treatments with inhibitors of phosphoinositide 3-kinase (PI3K) and mechanistic

target of rapamycin (mTOR) have become an additional option to treat patients who have disease progression despite anti-estrogen therapy.

Recurrence is a major issue faced by cancer patients. Recurrences can develop decades following treatment of the primary tumor, with the possibility of recurrent tumors being resistant to treatment. It is believed that these recurrences are caused by the re-awakening of dormant tumors that exist in a quiescent, non-proliferating state[181]. The interval until clinical manifestation is defined as tumor dormancy [182]. Current therapies aim to target actively proliferating tumors as well as anti-apoptotic proteins to shift the balance to favor the pro-apoptotic process. In targeting these growing tumors, there is the risk of failing to effectively target dormant tumors [183]. Some avenues that can induce growth arrest include chemotherapeutic treatment, modulation of p38/ERK activity ratios, and activation of stress pathways like that of the unfolded protein response (UPR) [184–188]. Attention must be given to how therapies can potentially affect the replication potential of tumor cells.

In considering the consequences of replication, different approaches of targeting dormant tumors have been proposed in the hopes of preventing recurrence. Such approaches include re-awakening the dormant population to target with cytotoxic therapies that affect cycling cells, potentially promoting the out-growth of even more aggressive tumors; targeting the tumor population while

dormant, circumventing the potential of residual disease; or to keep tumors dormant indefinitely, requiring indefinite treatment [189].

In targeting dormant tumors while they are in this quiescent state, the hope is that recurrence will be prevented. Dormancy is delineated by two ideologies: cellular dormancy or balanced proliferation. Cellular dormancy being lack of proliferation by cells, and balanced proliferation whereby cells are proliferating but simultaneously undergoing apoptosis [190]. One such paradoxical therapeutic option is to target tumors in this dormant state with CDK4/6 inhibitors to potentially upset this balanced proliferation, leading to a shift in apoptosis of the cell population.

CDK4/6 complexes with members of the cyclin D family to phosphorylate retinoblastoma (Rb) protein, lifting its repressive effect on E2F transcription factors, allowing for the progression through the G1-to-S-phase of the cell cycle. CDK4/6 inhibitors bind within the cleft of CDK4/6, preventing the attachment to ATP, and inhibiting the phosphorylation of Rb. In beginning to target CDKs in cancer, first-generation inhibitors acted upon a broad range of kinases leading to dose limiting toxicities[191–193]. First-generation flavopiridol, appeared to have promising results in hematological cancers[194], but no phase III studies were reported and development was ultimately discontinued. Second-generation inhibitors aimed to target CDK1/2 or have increased potency like dinaciclib were observed to be effective against a range of advanced malignancies in promoting

stable disease[195,196]. However, multiple phase II trials failed to provide treatment benefit in solid tumors[197–199]. Failure of these initial trials can be explained by: undefined patient population, unbiased cell targeting, and uncertainty of drug action[196]. CDK4/6 is a promising target due to its ability to elicit G0/G1 arrest. In the treatment of ER+ breast cancer, several CDK4/6 inhibitors have been approved for combination treatment with endocrine therapies. Based on findings from the PALOMA-1 and PALOMA-2 trials, Palbociclib was FDA-approved for use with an aromatase inhibitor in post-menopausal women as first-line therapy in advanced breast cancer[85,197]. Additionally, ribocilib and abemaciclib were FDA-approved following results from the MONALEESA-2[200,201] and MONARCH-3[202] trials, respectively.

As expected, palbociclib and ribociclib exhibit targeted inhibition of CDK 4/6; however, off-target effects of abemaciclib include CDK9 with potential casein kinase inhibition [203,204]. As the mechanism of CDK4/6 inhibitors continues to be investigated, several axes have been implicated to be activated upon CDK4/6 treatment, one of which being metabolism. However, it is believed that the mechanism of action can differ in a context specific manner [205–208]. In following up with this indication of context specific mechanisms caused by CDK4/6 inhibition, cell cycle inhibitors have yet to be employed in the dormant setting.

Previous work in the lab established an ER+ breast cancer model of clinical dormancy by prolonged estrogen withdrawal of tumors to drive tumor

regression to a non-palpable state[209]. Using this model of dormancy, previous findings in the lab showed CDK4/6 inhibitors when administered to dormant tumors, as established through prolonged estrogen deprivation, a reduction of tumor burden believed to be a consequence of cell death was observed. This project aimed to understand the mechanism of how cell cycle inhibiting drugs can elicit cytotoxic effects on growth arrested cells and how this modulation differs from mechanisms observed in the treatment of persistently cycling cells.

6.2. Materials & Methods

6.2.1 Mouse Studies

Mouse studies approved by institutional protocols. NOS/SCID/IL2Rγ-/- (NSG) were obtained from Norris Cotton Cancer Center Mouse Modeling Shared Resource. Mice received 5-mg/kg s.c. injection of ketoprofen and placed under isoflurane anesthesia. Mice were ovariectomized and bilaterally and orthotopically injected with 5 x10^6 MCF-7/Luciferase/Clover-GFP breast cancer cells. Mice were subcutaneously implanted with 1 mg beeswax 17β-estradiol pellet at the base of the neck. Tumors were measured twice weekly using calipers (volume = length x width x width/2). When tumors reached 300 mm^3, 17β-estradiol pellet was removed and tumors were allowed to regress until no longer palpable. Following ~60d of 17β-estradiol withdrawal, baseline bioluminescence was taken. Following baseline bioluminescence reading, mice were administered CDK4/6 inhibitor treatment for 10 days: vehicle control (100uL/d p.o.), Palbociclib (100mg/kg/d p.o. in 100uL), ribociclib (100mg/kgd p.o. in 100uL), abemaciclib (100mg/kg/d p.o. in 100uL). Palbociclib was reconstituted in saline. All other drugs were reconstituted in methyl cellulose. Following treatment, mice were given a 1-week drug holiday and reimplanted with a 17β-estradiol pellet. Tumors were measured twice weekly as mentioned previously.

6.2.2 Bioluminescent Imaging

For dormancy experiments, residual tumor burden was measured via bioluminescent imaging. Mice were injected i.p. with 100ul *in vivo* grade D-luciferin (Promega) in PBS and placed under isoflurane anesthesia. Following 15 min., mice were placed into the Xenogen IVIS 200 System (Perkin Elmer), serial exposures taken until saturation of signal was reached. From images, regions of interest (ROIs) were drawn around each tumor and regions without tumor burden to determine signal using LivingImage software (Perkin Elmer). Signal was measured at baseline, 24hrs post day1, 24hrs post day 5, and 24hrs post day 10. 1s exposure was used for data quantification.

6.2.3 *Flow Cytometry*

Cells were rinsed with PBS and trypsinized. Trypsin was neutralized with serum containing media. Cells were stained for Annexin/PI (Southern Biotech). Stained cells were then analyzed with MACSQuant-10 flow cytometer.

6.2.4 *Immunohistochemistry*

Immunohistochemistry procedure was carried out as described in Chapter 2. Antibodies used: KI67 (BiocareMedical), pHH3 Ser10 (Cell Signaling Technology). For TUNEL staining, Promega protocol was followed.

6.2.5 *Statistical Analysis*

IHC, TUNEL, and flow cytometry data were analyzed by ANOVA followed by Bonferroni multiple comparison-adjusted posthoc testing.

6.3 Results

6.3.1 Chronic CDK4/6 inhibitor treatment inhibits cell growth

We aimed to determine the roles of CDK4/6 in dormancy in ER+ breast cancer. To begin elucidating these roles, we aimed to determine the effects of chronic CDK4/6 inhibition on long-term breast cancer cell growth. From our results, cells appear to maintain residual cycling capabilities after prolonged culturing in hormone depleted media (Figure 6.1A). As expected, CDK4/6 inhibition by palbociclib, inhibited growth in a dose dependent manner (Figure 6.1 A). MDA-MB-415 cells showed a greater sensitivity to CDK4/6 inhibition at doses as low as 25 nM. MCF-7 experienced less sensitivity to CDK4/6 inhibition with cells maintaining a high level of relative growth even at the highest dose of 800 nM. These results indicate that there are cell type differences in sensitivity to CDK4/6 inhibition.

6.3.2 CDK4/6 inhibitor treatment does not induce cytotoxic effects in cells growth arrested by serum starvation

We next aimed to determine if CDK4/6 inhibitor treatment resulted in cytotoxic effects on growth arrested cells. To do this we cultured cells in serum free media for 4 d followed by subsequent CDK4/6 inhibition for either 24 hrs or 48 hrs. Neither 24 hr nor 48 hr treatment with CDK4/6 inhibitor resulted in a significant

increase in apoptosis (Figure 6.2 A-C). Potential explanations could be that cells were not exposed to CDK4/6 inhibitors for the appropriate amount of time.

6.3.3 CDK4/6 Inhibition does not lead to robust cytotoxic effects in long-term hormone deprived cells

We next wanted to ask if CDK4/6 inhibition could lead to cytotoxicity, specifically in cells that had been long-term hormone deprived for ~60d like that of preliminary *in vivo* findings. Following treatment with CDK4/6 inhibitors, it was observed that only abemaciclib treated cells showed marginal significance in increasing apoptosis (Figure 6.3A).

6.3.4 Treatment of dormant tumors with CDK4/6 inhibitors does not lead to a decrease in tumor burden

To validate *in vivo* findings previously observed by Riley Hampsch, Ph.D., tumors experiencing ~60d of estrogen withdrawal were subjected to CDK4/6 inhibition with concurrent bioluminescence imaging (Figure 6.4A). CDK4/6 inhibition did not induce a reduction of bioluminescence signal (Figure 6.4B/C). IHC analysis for KI67 following 3 days of treatment revealed no significant difference in proliferation between treatment groups (Figure 6.4D). However, from TUNEL staining there was an observed trend towards increased levels in the palbociclib and abemaciclib treated groups with ribociclib showing slight

significance in increased TUNEL staining (Figure 6.4E). However, the scale of this induction of TUNEL staining is rather low across all samples. Staining for phosphohistone H3 Ser10 (pHH3 Ser 10), a marker of mitosis did show a significant difference between CDK4/6 treated groups and vehicle, indicating that CDK4/6 inhibitors are lowering the mitotic count following 3 days of inhibitor treatment (Figure 6.4 F). Results confirmed previously known results that long-term hormone deprived tumors do have populations of proliferating cells. From *in vivo* results, the project was discontinued after failure to replicate preliminary data. The data enclosed here validate that CDK4/6 inhibitors work to inhibit growth of breast cancer cell lines. CDK4/6 inhibitors as a whole did not elicit cytotoxic effects in growth arrested or long-term hormone deprived cells.

6.4 Discussion

Of the women receiving treatment for breast cancer, 1/3 of patients will eventually experience recurrence. These recurrences can develop decades following initial treatment. One explanation that has been offered for the emergence of these tumors is the rekindling of cells that have been existing in a quiescent, non-proliferative state [181]. The treatment of these dormant populations poses a unique problem because the majority of therapeutics rely on the specific targeting of highly replicating cells. Proposed methods to target this subset of cells provide two opposing solutions each with its own drawback such as the re-awakening of dormant cells to be susceptible to treatments or indefinite treatment to maintain cells in their dormant niche [189].

To circumvent these potential problems, we set out to specifically eliminate dormant cells while in their arrested state. Riley Hampsch, Ph.D. generated a model of tumor dormancy[209]. In the long-term hormone deprived setting, these tumors exhibited significantly decreased proliferation rates. Preliminary work treating dormant tumors with the CDK4/6 inhibitor, palbociclib, showed a significant decrease in residual tumor burden that failed to recur following a weeklong treatment cessation, providing evidence for tumor cell elimination.

CDK4/6 kinases complex with cyclins to induce the hyperphosphorylation of retinoblastoma (RB) protein to allow for progression through the cell cycle.

Traditionally, CDK4/6 inhibitors function by blocking this hyperphosphorylation thereby halting cells in the G1 phase of the cell cycle. Preclinical data showed single agent CDK4/6, abemaciclib, in ER+ breast cancer was able to induce apoptosis in *in vitro* studies and could induce tumor regression via alterations to metabolism and induction of senescence [210]. Preliminary findings and preclinical evidence suggested plausible rationale for our study. This CDK4/6 inhibitor treatment modality would have provided further evidence for an innovative therapeutic approach using cell cycle inhibitors to treat these predominantly static tumors.

In proliferation experiments described above, we were able to observe the expected results on growth proliferation when administered CDK4/6 inhibitors. However, the cytotoxic effects seen in preliminary *in vivo* work could not be recapitulated with either *in vitro* or *in vivo* experiments. If this experiment were to be repeated, I would like to investigate using an alternative method of tumor measurement. When acquiring images, bioluminescent signal would often saturate affecting the accurate quantifications of tumor burden. I believe that by having a more consistent and reliable method of measuring tumor burden we would be able to discern differences in treatment. Such an alternative would be the use of near-infrared fluorescence labeled cells. This particular technique utilizes the Pearl® Trilogy imaging system. This system minimizes tissue auto-fluorescence which has been a weakness associated with bioluminescent quantification accuracy as a result of scattering light in the body contributing to

signal loss[211]. Additionally, bioluminescent imaging has inconsistencies with signal as a result of limitations to the depth of penetration by the system.

Secondarily, when testing cytotoxic effects *in vitro,* I would have liked to have validated that our cells were truly in a growth arrested state or a predominantly cytostatic state by a BrdU assay. We could have potentially delineated if CDK4/6 inhibitor treatment required cell population to be at a specific state in order to cause cytotoxic effects. However, follow up studies as laid out in this chapter do not provide rationale for a novel use of CDK4/6 inhibitors to treat dormant tumors. As such the CDK4/6 inhibitors, mode of action remains to be a cytostatic agent.

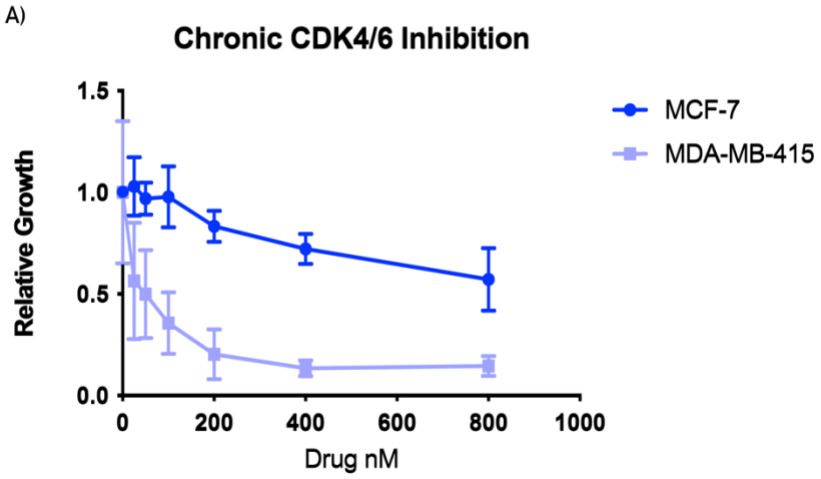

Figure 6.1 Palbociclib treatment slows growth of short-term hormone deprived ER+ breast cancer cells. (A) MCF-7 and MDA-MD-415 cells were hormone deprived for 15d followed by platting in 96 well format at 1000 cells/well with continued hormone deprivation plus palbociclib at specified doses. SRB assay was performed when cells reached 60% confluency. Data are shown as a mean of triplicates + SD.

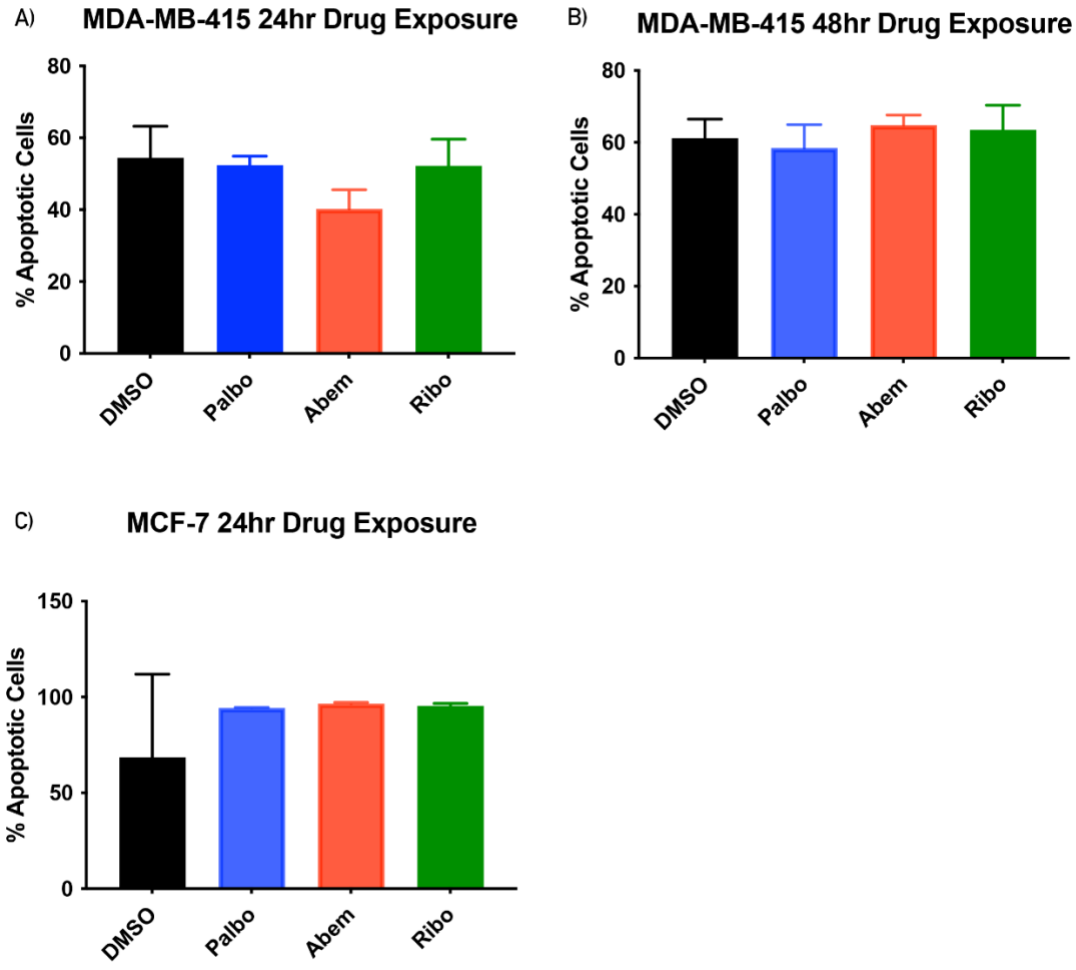

Figure 6.2 CDK4/6 inhibition fails to induce cytotoxic effects on growth arrested cells. (A/B) MDA-MD-415 and MCF-7 **(C)** cells were cultured in serum-free medium for 4 days. Cells then underwent treatment with DMSO or CDK4/6 inhibitors (Palbo-200nM, Abem-500nM, Ribo-2uM) for 24 hrs **(A/C)** or 48 hrs **(B).** Cells were subjected to annexin/PI staining and analyzed by flow cytometry. Data are shown as a mean of triplicates + SD. *$p \leq 0.05$ by Bonferroni multiple comparison-adjusted posthoc test.

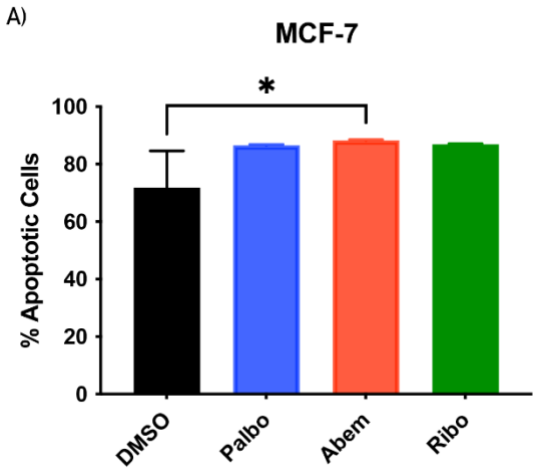

Figure 6.3 CDK4/6 inhibition fails to cause robust cell death in long term hormone deprived ER+ breast cancer cells. (A) MCF-7 cells were hormone deprived for ~60. Cells were treated for 6 days with vehicle or CDK4/6 inhibitors (Palbo-200 nM, Abem-500 nM, Ribo-2 uM). Cells were subjected to annexin/PI staining and analyzed by flow cytometry. Data are shown as a mean of triplicates + SD. *p≤ 0.05 by Bonferroni multiple comparison-adjusted posthoc test.

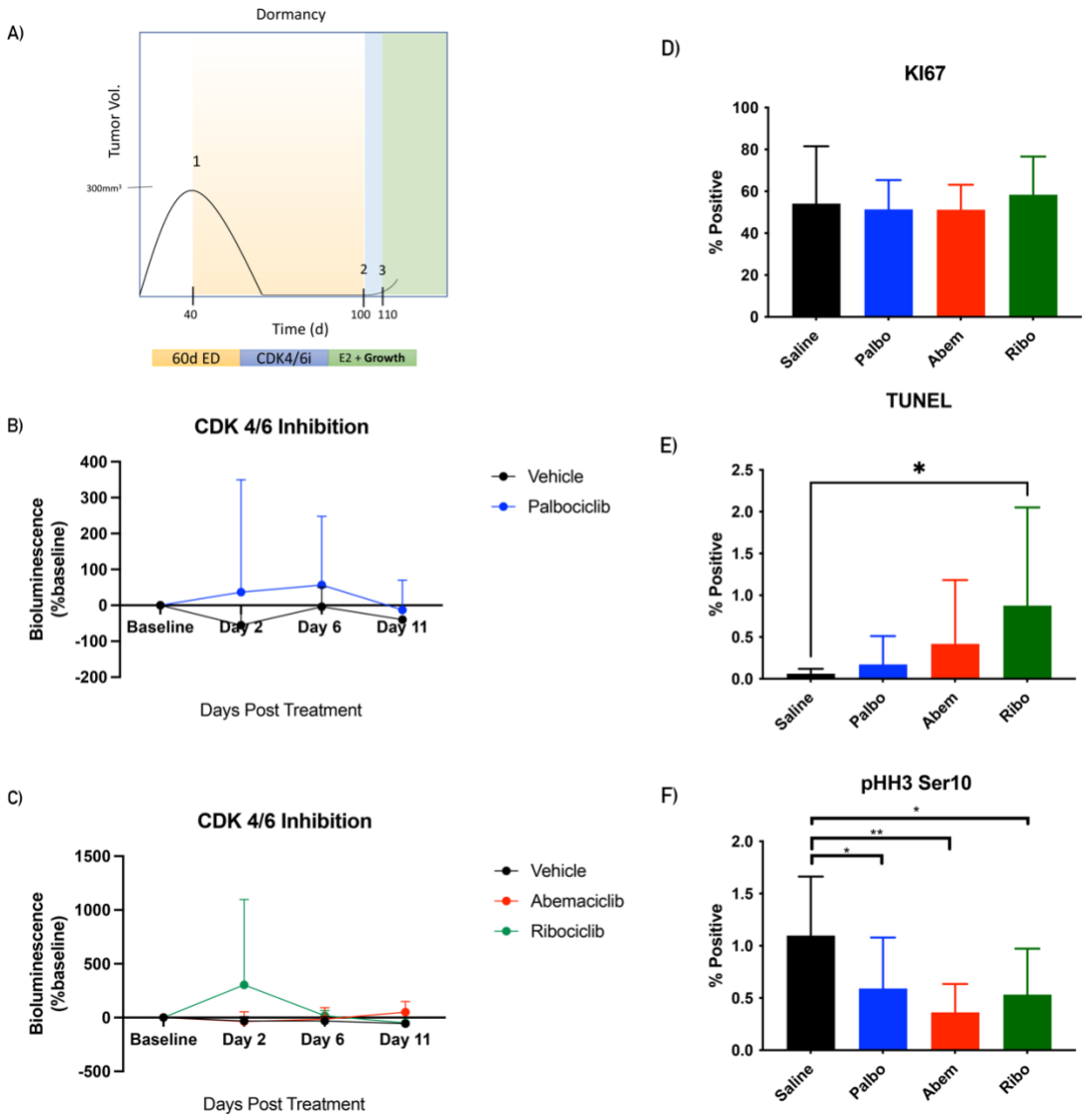

(Legend on next page)

Figure 6.4 *In vivo* CDK4/6 inhibitor treatment does not result in cytotoxic effects on dormant tumors. (A) Experimental setup to determine effects of CDK4/6 inhibitors on dormant tumors. **(B/C)** OVX mice with MCF-7/Luciferase/GFP tumors following ~60 d hormone deprivation led to tumor regression. Mice were randomized and treated for 10 days with: 100 mg/kg/d-palbociclib, ribociclib, abemaciclib or vehicle control. Residual tumor burden was measured via bioluminescence imaging. Values at 1s exposure were used to determine bioluminescence signal. **(D-F)** IHC for KI67 **(D)** TUNEL **(E)** or (pHH3 Ser10) **(F)** was done on specimens harvested 4 hrs post 3 d of treatment. Data shown are a mean of all mice + SD. *$p \leq 0.05$ by Bonferroni multiple comparison-adjusted posthoc test.

Chapter 7: Conclusions & Future Directions

7.1 Summary of Findings

A great deal of work has investigated the mechanism by which estrogens exerts growth-promoting effects; however, as we develop more sensitive assays, we are discovering novel interactors with the potential to modulate estrogen signaling. Hoping to further expound on known ER interactors, we utilized the proximity labeling technique of TurboID to generate an E2-induced interactome of ER. From our profiling, we were able to discern an interaction between ER and TRIM33 by both LC-MS/MS and pulldown/immunoblotting of biotinylated proteins. Immunoblot of biotin pulldown proteins showed associations of ER with TRIM33 under E2-treated conditions. TRIM33 was found to be necessary for E2-induced cell growth as evidenced by a growth inhibitory effect under TRIM33 knockdown conditions.

In investigating the potential mechanism by which TRIM33 knockdown inhibited growth, we observed a decrease in the levels of transcripts canonically induced by E2/ER. These results signified that TRIM33 is involved in the regulation of ER transcriptional activation. However, in cases of overexpression of TRIM33, we did not see a robust increase in growth or induction of estrogen signaling, suggesting estrogen signaling has saturated and is unable to surpass the level of induction observed in Luc cells treated with E2. Due to TRIM33

having E3 ligase capabilities, we investigated the effects of TRIM33 on ER protein stability. E3 ubiquitin ligases can promote ubiquitination chains of K11/63 that promote stability of proteins, and additionally competitively bind to different E3 ubiquitin ligases preventing interactions with alternative ubiquitin ligases that promote protein turnoever[212,213]. Previous work shown by Chen et al. 2022 follows this secondary option showing that TRIM33 is able to promote AR stability by preventing Skp2 (E3 ubiquitin ligase) mediated ubiquitination resulting in protein degradation [99]. Our findings show that TRIM33 has a stabilizing role on ER protein levels, further suggesting a critical role of TRIM33 in regulating estrogen-induced growth of breast cancer cell lines. Further investigation is warranted into TRIM33 protein-stabilizing capabilities in models of endocrine resistance.

The PI3K pathway is a crucial signaling circuit that intersects with multiple regulatory pathways within the cell playing roles in proliferation, survival, and migration. As such, this pathway is a promising target for therapeutic intervention, specifically in ER+ breast cancer. PI3K inhibitors have been shown to have promising effects in preclinical studies with alterations in *PTEN* and *PIK3CA* with *PIK3CA* mutants showing clinical benefit when treated with combination alpelisib (p110a targeting) and fulvestrant. To determine potential mechanisms of resistance to PI3K inhibitors, phosphoproteomic analysis identified ATM as a potential targetable kinase specifically in populations with *PTEN* deficiencies. Preliminary work has established *PIK3CA* mutant cell lines resistant to single

isoform (p110α-targeting BYL-719, alpelisib) and pan-isoform (GDC-0941). BYL-719-resistant lines show sensitivity to ATM inhibitor treatment. GDC-0941-resistant lines show increased sensitivity to ATM inhibition in comparison to their GDC-0941-sensitive counterparts (MCF-7/FR and T47D/FR). Further investigation is warranted to ascertain if the effects seen by phosphoproteomic analysis can be extended to resistance to other PI3K inhibitors (p110α-selective) or other PI3K pathway alterations (*PIK3CA* mutation).

7.2 Future Directions & Discussion

7.2.1. TurboID as a mechanism for ERα interactome labeling

We identified estrogen-induced interactors of ER. Previous iterations of this Turbo-ER construct took advantage of the first-generation BioID system (Fig. 3.1). While capable of profiling interactions with ER, the timeline for BioID labeling required incubation with biotin over the course of 24 h. This is a crucial limitation due to the fact that I wanted to profile early changes that occur in response to estrogen supplementation. For this reason, it was ultimately decided to proceed with TurboID seeing as it can biotinylate on the order of minutes.

In the generation of the first BioID constructs, I had to establish constructs with variable linker lengths, either G4Sx1 or G4Sx4. These were arbitrary linker lengths that were initially chosen. I decided on using G4Sx1 as the linker length for subsequent experiments with TurboID. However, this could become a potential limitation in that linker size, in this case G4Sx1, could be inhibited in its labeling radius thereby biasing interactome profiles. Conversely, the implementation of a longer linker length could also allow for higher levels of non-specific labeling. If experiments were to be repeated, I would like to compare how a slightly longer linker would affect the interactome obtained under estrogen conditions.

While I was able to perform labeling of nuclear localizing proteins in the turbo-ctrl samples, the attachment of a nuclear localizing signal (NLS) to the Turbo-ctrl could provide a more detailed account of non-specific background proteins that could subsequently be used for more stringent identification of nuclear ERα interactors.

In comparing my ER interactome with that of published ER interactomes, there were minimal interactors common to all three compared datasets. In considering the reasons for this, the differences observed may be explained by differing experimental techniques and conditions. The findings of Mohammed et al. 2013 were identified by RIME (rapid immunoprecipitation mass spectrometry of endogenous protein) and consisted of findings identified in both MCF-7 and ZR75-1 cell lines. This technique specifically identifies proteins that exist in complexes and with chromatin. The study done by Agbo et al. 2022 was done using TurboID, similarly to my experiment, but in their TurboID construct they included a nuclear localization signal. This inclusion could lead to differences in downstream analysis thereby contributing to differences in proteins being classified as significant interactors. Finally, the two other studies profiled the ER interactome under steady-state conditions, while I performed experiments under hormone-deprived conditions and subsequent treatment with E2 to capture early protein interactions. Additionally, Agbo et al. 2022, allowed for 5 h of biotin labeling, whereas my experimental settings were only 1 h which could contribute to further differences in proteins identified. When considering the difference in the

numbers of proteins identified, it is my speculation that the number of proteins that can be identified by TurboID is reduced due to linker length, and as such prevents the identification of proteins from reaching that of levels identified by RIME. I could increase the linker length to increase the number of proteins identified, however, I also run the risk of over labeling and introducing proteins that are not actual interactors of ER. From comparing my interactome findings with that of the two other studies, I identified TRIM33 as being involved in both early E2-induced interactions with ER but also steady-state interactions with ER.

7.2.2 Defining the mechanism by which TRIM33 modulates estrogen/ER signaling

We identified TRIM33 as a novel regulator of ER activity, but there remain unidentified mechanisms of regulation. Due to the chromatin-binding capabilities of TRIM33, I propose investigating the effects of TRIM33 on the cistrome of ER. TRIM33 was observed to be required for maximal binding of androgen receptor (AR) to genomic loci in prostate cancer cells[99]. If decreased binding of ER at genomic loci is observed upon TRIM33 knockdown, this would help to explain our findings of decreased ER transcriptional activity upon TRIM33 knockdown.

TRIM33's association with ER was implied through biotin labeling by Turbo-ER. Immunoprecipitation reactions for ERα failed to co-precipitate TRIM33. The lysis buffer used may have been too stringent and led to disruption of these protein-protein interactions. Future work could use a nuclear-specific

extraction buffer for immunoprecipitation. An alternative method could generate TRIM33 and ERα proteins to be labeled with fluorophores to monitor interaction through the use of Förster resonant energy transfer (FRET). However, ER may not interact directly with TRIM33, but instead interact via the generation of a complex. To profile such a complex, a secondary Turbo-TRIM33 construct could be generated to profile the estrogen-induced interactome and compare hits to our established ER interactome. Hits that overlap could then be further investigated by immunoprecipitation and probed for their interaction with both TRIM33 and ERα.

E3 ubiquitin ligases have been shown to promote the stability of their interaction proteins such examples include Casitas B-lineage lymphoma (Cbl) family proteins, specifically (CLBC) which interacts with AURKA in lung adenocarcinoma promoting both mono- and poly- K11/63 ubiquitination, allowing for protein stability [212], and the E3 ubiquitin ligase, TRIM26, competitively binds SOX2 to prevent ubiquitination by WWP2 mediated degradation in glioblastoma[213]. Due to the protective capabilities of TRIM33 seen by Chen et al. 2022, future work will identify the mechanism by which TRIM33 works to stabilize ER from degradation[99]. We believe that TRIM33 is involved in stabilizing ER levels due to the expression dependent effects of TRIM33 on ER levels as seen in cycloheximide assays, whereby knockdown shows a decrease in overall levels in both in the E2 deprived and E2 supplemented conditions. Additionally, TRIM33 overexpression in T47D cells shows increased protein levels of ER. In prostate

cancer models, TRIM33 protected AR from Skp2-mediated degradation[99]. Work was carried out to determine the effects of TRIM33 knockdown and overexpression on ER. However, there were no observable differences in the level of ubiquitinated ER (Fig. 7.1 A/B). In an effort to optimize this experiment, I believe that to observe any differences in ubiquitination, cells must be in a hormone deprived state and subsequently administered estrogen and MG132. I base this decision on the results of Fig 3.5A: following 4 days of hormone deprivation and subsequent incubation with estrogen for 5 h, we can appreciate a difference in protein turnover between 0 hr and 5 hr in the sh#6 conditions. As an alternative to the above-mentioned technique, mass spectrometry can be utilized to identify sites of ubiquitination[214] on ER. With this in mind, we can compare the sites that are ubiquitinated both in the presence and absence of TRIM33. Identification of these sites of ubiquitination can then be used to map this post-translational modification back to known E3 ligases involved in targeting ER for proteasomal degradation[50–56]. To further expound on TRIM33's role in regulating ER protein levels, I performed an MG132 assay to determine the effects of TRIM33 knockdown on the induction of the proteasome pathway. Preliminary results indicate that TRIM33 protects ER from degradation by the proteasome pathway (Fig. 7.2 A). Findings further suggest reduced overall levels of ERα protein. Potential explanations could be a reduction of *ESR1* transcripts or potentially engaging in another method of degradation. Further investigation is required to determine a possible mechanism for these results.

As shown in Fig. 3.2C and Fig. 3.6B, overexpression of TRIM33 failed to promote increased levels of ER-inducible transcripts or increased levels of cell growth. Future work will investigate the degree to which TRIM33 overexpression can lead to ER signaling saturation. In our models, we utilize a constitutively expressing TRIM33 construct. It was observed that overexpression of ER in T47D cells allowed E2 to act in a growth-inhibitory manner[128]. From our results (Fig. 3.7B) we see that TRIM33 overexpression led to an increase in ER levels. In combination with the growth inhibitory effects seen in Fig. 3.9B and Fig. 7.3A in T47D, we see that increased ER protein levels does not necessarily translate into an increase in growth and E2 driven signaling. This can be explained by the mechanism through which ER transcriptional activity is controlled. As evidenced by Lonard et al. 2000, ER activity is modulated by protein turnover[58]. Upon inhibition of protein degradation by treatment with MG132, transcriptional activation was attenuated. Using a dox-inducible model, we will establish a graded increase in TRIM33 expression to determine the expression-dependent consequences to estrogen signaling. I would like to examine how differing levels of TRIM33 affect ER stability and overall activity. I believe that in constitutively expressing TRIM33 we could be missing the potentially increased levels of downstream estrogen/ER signaling targets.

To investigate the cause of growth inhibition as it relates to TRIM33 expression levels, we will investigate perturbations to the cell cycle and the induction of apoptosis. Chen et al 2022. observed a reduction in cell growth in

response to TRIM33 knockdown that was associated with halting of cells in G1 and an overall increase in apoptosis. We hypothesize that TRIM33 is operating in a similar fashion in ER+ breast cancer.

As TRIM33 is associated with ER protein stability, I wanted to investigate the potential for TRIM33 to promote endocrine therapy resistance. In our *in vitro* models of resistance to estrogen deprivation, we see that TRIM33 protein levels show a relative increase over parental cell lines in hormone deprived conditions similar to that of parental conditions when treated with E2 (Fig. 7.4A). Following these results, I attempted to generate a stable TRIM33 knockdown MCF-7 LTED cell line, however, this proved cytotoxic to LTED cells while parental cells experienced a growth inhibitory effect. From these initial preliminary findings, I would like to further investigate TRIM33's role in the development of resistance to long-term estrogen deprivation. To investigate this, I propose the use of a dox-inducible TRIM33 plasmid using the two LTED cell lines that have shown relatively increased ER protein levels. In parallel *in vivo* studies can investigate the level of TRIM33 expression in patient-derived xenograft (PDX) models (WHIM16 and CTG-3346) both of which grow in ovariectomized (OVX) mice, recapitulating aromatase inhibitor resistance seen in patients.

Upon initial investigation as to the role of TRIM33 in survival of ER+ breast cancer patients using available Kaplan-Meier Plotter software, we did not observe any significant associations of survival on the basis of TRIM33 mRNA

levels. I hypothesize that by looking in populations specifically resistant to aromatase inhibitors, we would better be able to parse out potential associations of TRIM33 with resistance to treatment. By using a dataset sub-set to this population of patients[215], we can also examine if increased expression of TRIM33 at primary tumors is predictive of resistance to aromatase inhibition.

Additionally, for populations with increased levels of TRIM33 that lead to increased ER protein stability, TRIM33 targeting could become an option to prevent estrogen independent outgrowth. E3 ligase targeting drugs are becoming a new field of study by taking advantage of proteolysis targeting chimeras (PROTACs) technology. E3 ligases do not contain active sites and operate on protein-protein interactions[216]. This would require further investigation for generation of TRIM33 targeting therapeutics.

7.2.3 Profiling the interactome of ERα under conditions of endocrine resistance

As mentioned in Chapter 3, we generated a Turbo-ER construct. Future applications can investigate the interactome of ER under various conditions of endocrine resistance. One such example is in the setting of fulvestrant resistance. Currently, we have generated stable TurboID-expressing MCF-7 fulvestrant-resistant cell lines. Shown in Fig. 7.5A, we show the biotinylation capabilities of our stable cell lines validating the promiscuous nature of Turbo-Ctrl and the more targeted labeling present in the Turbo-ER construct. Previous papers have investigated the ER interactome in response to various endocrine

therapies[217,218], but using techniques such as tandem affinity purification (TAP). This technique is able to provide information as to the formation of protein complexes however is limited in its ability to profile transient and weak interactions. These disadvantages can be rectified by the labeling abilities of TurboID.

The development of resistance to fulvestrant has a myriad of potential mechanisms such as dysregulation of cell cycle regulators[219], activation of the ErbB family[220], and activation of the NF-κB pathway[221]. The above-mentioned are but a few of the examples of possible mechanisms of resistance. By profiling interactions that are altered between sensitive and treatment resistant conditions, we can identify potentially novel interactions that could promote outgrowth while on fulvestrant treatment.

A potential limitation to this experimental set-up could be that treatment of fulvestrant sensitive cells could result in the downregulation of not only ER but Turbo-ER, thereby skewing the available construct needed for protein interaction labeling. Additionally, ER levels would need to be determined to validate that exogenous expression of ER in MCF-7 cells still enables cells to be sensitive to fulvestrant treatment and does not inadvertently help in the development of fulvestrant resistance. This could be circumvented by validating targets in parental cells to determine their role in the development of resistance.

Tamoxifen, a selective estrogen receptor modulator, operates by competitively binding to ER. When bound to ER, tamoxifen promotes a conformational change different from ER when bound to estrogen that dictates associations with corepressors rather than coavtivators[222–224]. We have seen before that alterations to the levels of these coregulators can have drastic effects on the successful response to endocrine treatment, such examples include the overexpression of Oct-4 and HOXB7, and the expression MDC1 in invasive lobular carcinoma (ILC) [72–74]. Due to this direct interaction with coregulators, I believe that this would be a promising setting to further investigate the interactome of ER to identify not only novel interactors, but novel regulators involved in the response to tamoxifen treatment.

7.2.4 Investigating PI3K inhibitor resistance

Previous work in the lab identified combined inhibition of α/β isoforms of p110 were needed for sustained response of PTEN-deficient, ER+ breast cancer[129]. We have been investigating unique phoshphopeptides enriched in PI3K inhibitor resistant tumors. From our dataset, we have identified ATM to be activated in the resistant setting. Tumors on which phosphoproteomics was performed was done on PTEN-deficient tumors treated with the pan-isoform inhibitor GDC-0941. A limitation of this investigation is that all tumor specimens were utilized for phosphoproteomic analysis. As mentioned in Chapter 4, IHC of selected targets have failed to recapitulate preliminary phosphoproteomic data which can potentially be explained by the inhibited proliferation in the stained

tumor sections. A future direction would be to reestablish resistant tumors for validation of identified targets by immunohistochemistry.

Secondarily, we can perform phosphoproteomic analysis of BYL-719 sensitive and resistant cell lines (*PIK3CA* mutant) to further expound on whether unique phoshphopeptides enriched in this resistant setting model those found when treating PTEN-deficient tumors, providing information as to whether these phosphopeptide signatures are generalizable to treatment with PI3K inhibition or to determine if we can subset a phosphopeptide signature on the basis of PI3K pathway alteration.

Preliminary findings in *PIK3CA* mutant cells Figure 4.6 show growth inhibition to ATM inhibition both in the fulvestrant resistant and combination (fulvestrant/BYL-719) resistant setting. However, combination (fulvestrant/GDC-0941) resistant show preferential growth inhibition when treated with ATM inhibitor over fulvestrant resistant cells. Future work will look at the mechanism by which ATM is affecting growth inhibition. We will examine the level of apoptosis that is being induced by ATM inhibition. Due to PI3K's involvement in DNA proliferation and cell cycle regulation, this pathway plays a major role in maintaining genomic stability[225]. As such inhibition can play a role promoting replication stress and cell death[226] we will investigate the level of γH2AX staining occurring in cells in response to prolonged PI3K inhibitor treatment and subsequent ATM inhibition. Findings here could explain potential mechanisms of

resistance in patients as well as provide additional avenues for targeted treatment.

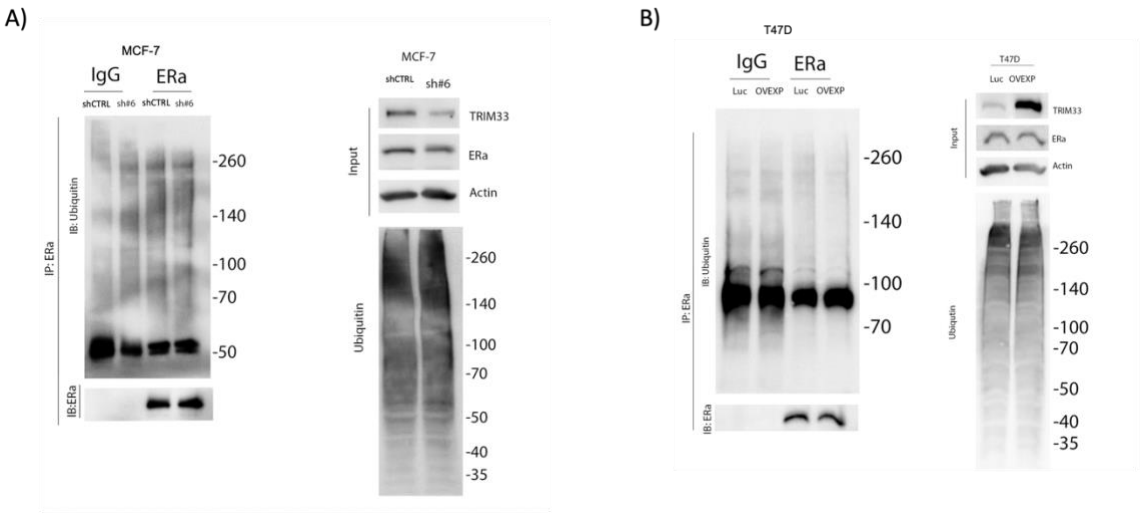

Figure 7.1 Ubiquitination Assays did not distinguish differences in ER ubiquitination. A) MCF-7 shCtrl vs sh#6 **B)** T47D Luc vs TRIM33 OVEXP cell lines treated with 10 uM MG132 for 4 hrs. Immunoprecipitation for ER protein was performed and endogenous levels of ubiquitin were probed.

A)

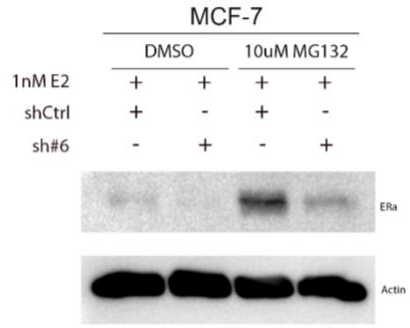

Figure 7.2 TRIM33 Protects ER from degradation by the proteasome. A) MCF-7 shCtrl and MCF-7 sh#6 cells hormone deprived for 4 days and treated 10 uM MG132 for 1.5 hr followed by treatment with 1 nM E2 and 10 uM MG132 for 5 hrs.

A)

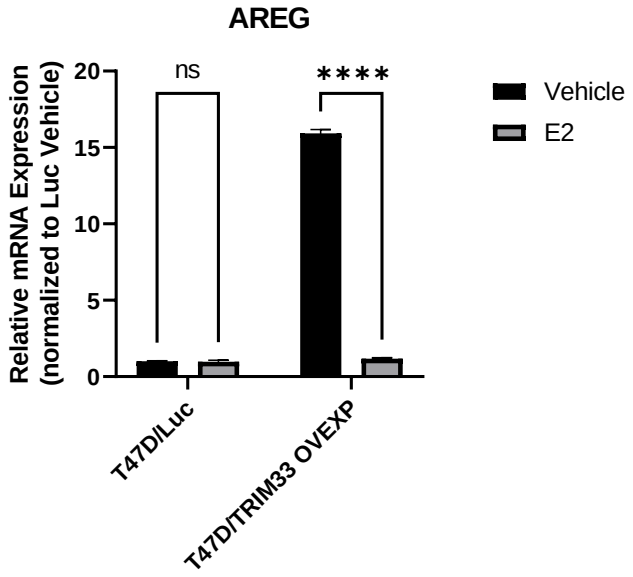

Figure 7.3 TRIM33 OVEXP causes increased baseline signaling. A) T47D Luc vs T47D TRIM33 OVEXP cells hormone deprived for 4 days and treated +/- 1nM E2 for 24hrs. Data shown are mean of triplicate ± SD. *$p \leq 0.05$, **$p \leq 0.01$, *** $p \leq 0.001$, ****$p \leq 0.0001$ by Bonferroni multiple comparison-adjusted post-hoc test.

A)

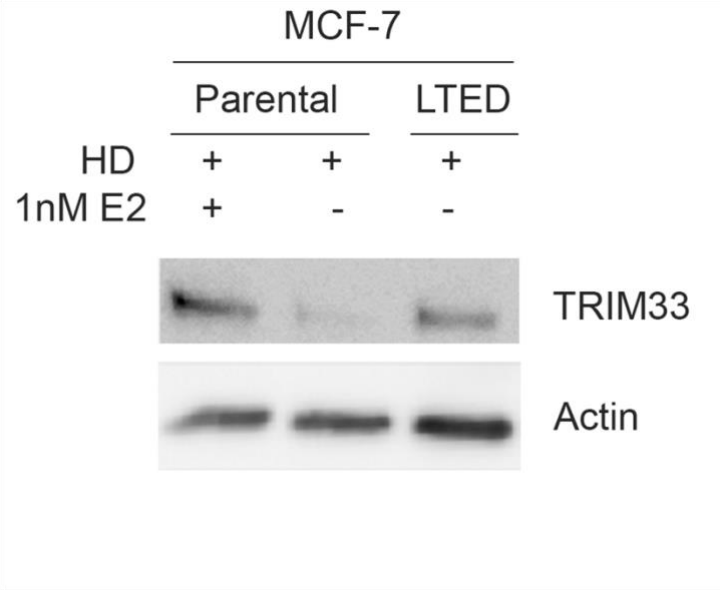

Figure 7.4. MCF-7 LTED cells show elevated levels of TRIM33 in hormone deprived conditions. A) MCF-7 parental vs MCF-7 LTED cells. MCF-7 parental cells cultured in hormone deprived media for 3-4 days and subsequently treated with 1 nM E2 for 3 days.

A)

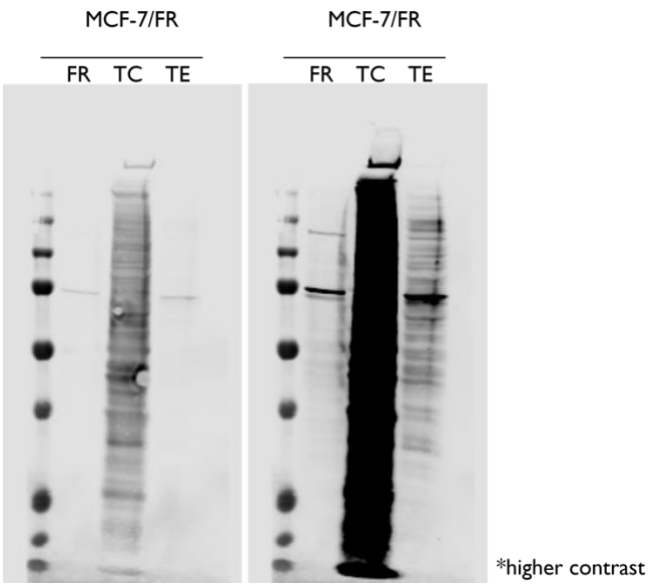

Figure 7.5. Biotinylation profile of MCF-7/FR TurboID cells. A) MCF-7/FR parental vs MCF-7/FR Turbo-Ctrl (TC) vs MCF-7/FR Turbo-ER (TE). Cells treated with 100 uM biotin 24 hrs.

Chapter 8: References Cited

1. Giaquinto, A. N. *et al.* Breast Cancer Statistics, 2022. *CA. Cancer J. Clin.* **72**, 524–541 (2022).
2. Berry, D. A. *et al.* Effect of screening and adjuvant therapy on mortality from breast cancer. *N. Engl. J. Med.* **353**, 1784–1792 (2005).
3. Street, W. Breast Cancer Facts & Figures 2019-2020.
4. Glass, A. G., Lacey, J. V., Jr, Carreon, J. D. & Hoover, R. N. Breast Cancer Incidence, 1980–2006: Combined Roles of Menopausal Hormone Therapy, Screening Mammography, and Estrogen Receptor Status. *JNCI J. Natl. Cancer Inst.* **99**, 1152–1161 (2007).
5. Colditz, G. A., Bohlke, K. & Berkey, C. S. Breast cancer risk accumulation starts early – Prevention must also. *Breast Cancer Res. Treat.* **145**, 567–579 (2014).
6. Anstey, E. H. *et al.* Breastfeeding and Breast Cancer Risk Reduction: Implications for Black Mothers. *Am. J. Prev. Med.* **53**, S40–S46 (2017).
7. Orrantia-Borunda, E., Anchondo-Nuñez, P., Acuña-Aguilar, L. E., Gómez-Valles, F. O. & Ramírez-Valdespino, C. A. Subtypes of Breast Cancer. in *Breast Cancer* (ed. Mayrovitz, H. N.) (Exon Publications, 2022).
8. DeSantis, C. E. *et al.* Breast cancer statistics, 2019. *CA. Cancer J. Clin.* **69**, 438–451 (2019).

9. Bourguet, W., Germain, P. & Gronemeyer, H. Nuclear receptor ligand-binding domains: three-dimensional structures, molecular interactions and pharmacological implications. *Trends Pharmacol. Sci.* **21**, 381–388 (2000).
10. Kumar, V. *et al.* Functional domains of the human estrogen receptor. *Cell* **51**, 941–951 (1987).
11. Hurtado, A., Holmes, K. A., Ross-Innes, C. S., Schmidt, D. & Carroll, J. S. FOXA1 is a key determinant of estrogen receptor function and endocrine response. *Nat. Genet.* **43**, 27–33 (2011).
12. Cirillo, L. A. *et al.* Binding of the winged-helix transcription factor HNF3 to a linker histone site on the nucleosome. *EMBO J.* **17**, 244–254 (1998).
13. Cirillo, L. A. *et al.* Opening of Compacted Chromatin by Early Developmental Transcription Factors HNF3 (FoxA) and GATA-4. *Mol. Cell* **9**, 279–289 (2002).
14. Rosenfeld, M. G. & Glass, C. K. Coregulator Codes of Transcriptional Regulation by Nuclear Receptors*. *J. Biol. Chem.* **276**, 36865–36868 (2001).
15. Puglisi, R. *et al.* Non-genomic Effects of Estrogen on Cell Homeostasis and Remodeling With Special Focus on Cardiac Ischemia/Reperfusion Injury. *Front. Endocrinol.* **10**, 733 (2019).
16. Szostakowska, M., Trębińska-Stryjewska, A., Grzybowska, E. A. & Fabisiewicz, A. Resistance to endocrine therapy in breast cancer: molecular mechanisms and future goals. *Breast Cancer Res. Treat.* **173**, 489–497 (2019).

17. Kraus, W. L. & Kadonaga, J. T. p300 and estrogen receptor cooperatively activate transcription via differential enhancement of initiation and reinitiation. *Genes Dev.* **12**, 331–342 (1998).
18. Guertin, M. J., Zhang, X., Coonrod, S. A. & Hager, G. L. Transient estrogen receptor binding and p300 redistribution support a squelching mechanism for estradiol-repressed genes. *Mol. Endocrinol. Baltim. Md* **28**, 1522–1533 (2014).
19. Lanz, R. B. *et al.* Global characterization of transcriptional impact of the SRC-3 coregulator. *Mol. Endocrinol. Baltim. Md* **24**, 859–872 (2010).
20. Johnson, A. B. & O'Malley, B. W. Steroid receptor coactivators 1, 2, and 3: critical regulators of nuclear receptor activity and steroid receptor modulator (SRM)-based cancer therapy. *Mol. Cell. Endocrinol.* **348**, 430–439 (2012).
21. DiRenzo, J. *et al.* BRG-1 is recruited to estrogen-responsive promoters and cooperates with factors involved in histone acetylation. *Mol. Cell. Biol.* **20**, 7541–7549 (2000).
22. Carascossa, S., Dudek, P., Cenni, B., Briand, P.-A. & Picard, D. CARM1 mediates the ligand-independent and tamoxifen-resistant activation of the estrogen receptor alpha by cAMP. *Genes Dev.* **24**, 708–719 (2010).
23. Wang, L. *et al.* TET2 coactivates gene expression through demethylation of enhancers. *Sci. Adv.* **4**, eaau6986 (2018).
24. Kong, S. L., Li, G., Loh, S. L., Sung, W.-K. & Liu, E. T. Cellular reprogramming by the conjoint action of ERα, FOXA1, and GATA3 to a ligand-inducible growth state. *Mol. Syst. Biol.* **7**, 526 (2011).

25. Eeckhoute, J. *et al.* Positive Cross-Regulatory Loop Ties GATA-3 to Estrogen Receptor α Expression in Breast Cancer. *Cancer Res.* **67**, 6477–6483 (2007).
26. Musgrove, E. A., Caldon, C. E., Barraclough, J., Stone, A. & Sutherland, R. L. Cyclin D as a therapeutic target in cancer. *Nat. Rev. Cancer* **11**, 558–572 (2011).
27. Doisneau-Sixou, S. F. *et al.* Estrogen and antiestrogen regulation of cell cycle progression in breast cancer cells. *Endocr. Relat. Cancer* **10**, 179–186 (2003).
28. Dong, L. *et al.* Mechanisms of Transcriptional Activation of bcl-2 Gene Expression by 17β-Estradiol in Breast Cancer Cells*. *J. Biol. Chem.* **274**, 32099–32107 (1999).
29. Bhargava, V., Kell, D. L., van de Rijn, M. & Warnke, R. A. Bcl-2 immunoreactivity in breast carcinoma correlates with hormone receptor positivity. *Am. J. Pathol.* **145**, 535–540 (1994).
30. Doglioni, C. *et al.* The prevalence of BCL-2 immunoreactivity in breast carcinomas and its clinicopathological correlates, with particular reference to oestrogen receptor status. *Virchows Arch. Int. J. Pathol.* **424**, 47–51 (1994).
31. Pike, C. J. Estrogen modulates neuronal Bcl-xL expression and beta-amyloid-induced apoptosis: relevance to Alzheimer's disease. *J. Neurochem.* **72**, 1552–1563 (1999).
32. Frasor, J. *et al.* Profiling of Estrogen Up- and Down-Regulated Gene Expression in Human Breast Cancer Cells: Insights into Gene Networks and Pathways Underlying Estrogenic Control of Proliferation and Cell Phenotype. *Endocrinology* **144**, 4562–4574 (2003).
33. Göttlicher, M., Heck, S. & Herrlich, P. Transcriptional cross-talk, the second mode of steroid hormone receptor action. *J. Mol. Med. Berl. Ger.* **76**, 480–489 (1998).

34. Hayashi, S. & Yamaguchi, Y. Estrogen signaling pathway and hormonal therapy. *Breast Cancer* **15**, 256–261 (2008).

35. *Advances in Protein Chemistry and Structural Biology*. (Academic Press, 2014).

36. Björnström, L. & Sjöberg, M. Mechanisms of Estrogen Receptor Signaling: Convergence of Genomic and Nongenomic Actions on Target Genes. *Mol. Endocrinol.* **19**, 833–842 (2005).

37. Le Romancer, M. *et al.* Cracking the estrogen receptor's posttranslational code in breast tumors. *Endocr. Rev.* **32**, 597–622 (2011).

38. Le Goff, P., Montano, M. M., Schodin, D. J. & Katzenellenbogen, B. S. Phosphorylation of the human estrogen receptor. Identification of hormone-regulated sites and examination of their influence on transcriptional activity. *J. Biol. Chem.* **269**, 4458–4466 (1994).

39. Kato, S. *et al.* Activation of the estrogen receptor through phosphorylation by mitogen-activated protein kinase. *Science* **270**, 1491–1494 (1995).

40. Joel, P. B., Traish, A. M. & Lannigan, D. A. Estradiol-induced phosphorylation of serine 118 in the estrogen receptor is independent of p42/p44 mitogen-activated protein kinase. *J. Biol. Chem.* **273**, 13317–13323 (1998).

41. Chen, D. *et al.* Activation of estrogen receptor alpha by S118 phosphorylation involves a ligand-dependent interaction with TFIIH and participation of CDK7. *Mol. Cell* **6**, 127–137 (2000).

42. Chen, D. *et al.* Phosphorylation of human estrogen receptor alpha at serine 118 by two distinct signal transduction pathways revealed by phosphorylation-specific antisera. *Oncogene* **21**, 4921–4931 (2002).
43. Harrod, A. *et al.* Genomic modelling of the ESR1 Y537S mutation for evaluating function and new therapeutic approaches for metastatic breast cancer. *Oncogene* **36**, 2286–2296 (2017).
44. Bunone, G., Briand, P. A., Miksicek, R. J. & Picard, D. Activation of the unliganded estrogen receptor by EGF involves the MAP kinase pathway and direct phosphorylation. *EMBO J.* **15**, 2174–2183 (1996).
45. Lupien, M. *et al.* Growth factor stimulation induces a distinct ERα cistrome underlying breast cancer endocrine resistance. *Genes Dev.* **24**, 2219–2227 (2010).
46. Magnani, L. *et al.* The pioneer factor PBX1 is a novel driver of metastatic progression in ERα-positive breast cancer. *Oncotarget* **6**, 21878–21891 (2015).
47. Kerdivel, G., Flouriot, G. & Pakdel, F. Chapter Four - Modulation of Estrogen Receptor Alpha Activity and Expression During Breast Cancer Progression. in *Vitamins & Hormones* (ed. Litwack, G.) vol. 93 135–160 (Academic Press, 2013).
48. Helzer, K. T., Hooper, C., Miyamoto, S. & Alarid, E. T. Ubiquitylation of Nuclear Receptors: New Linkages and Therapeutic Implications. *J. Mol. Endocrinol.* **54**, R151 (2015).
49. Zhou, W. & Slingerland, J. M. Links between oestrogen receptor activation and proteolysis: relevance to hormone-regulated cancer therapy. *Nat. Rev. Cancer* **14**, 26–38 (2014).

50. Fan, M., Park, A. & Nephew, K. P. CHIP (carboxyl terminus of Hsc70-interacting protein) promotes basal and geldanamycin-induced degradation of estrogen receptor-alpha. *Mol. Endocrinol. Baltim. Md* **19**, 2901–2914 (2005).

51. Sun, J., Zhou, W., Kaliappan, K., Nawaz, Z. & Slingerland, J. M. ERα Phosphorylation at Y537 by Src Triggers E6-AP-ERα Binding, ERα Ubiquitylation, Promoter Occupancy, and Target Gene Expression. *Mol. Endocrinol.* **26**, 1567–1577 (2012).

52. Eakin, C. M., MacCoss, M. J., Finney, G. L. & Klevit, R. E. Estrogen receptor α is a putative substrate for the BRCA1 ubiquitin ligase. *Proc. Natl. Acad. Sci. U. S. A.* **104**, 5794–5799 (2007).

53. Hashizume, R. *et al.* The RING heterodimer BRCA1-BARD1 is a ubiquitin ligase inactivated by a breast cancer-derived mutation. *J. Biol. Chem.* **276**, 14537–14540 (2001).

54. Bhatt, S., Xiao, Z., Meng, Z. & Katzenellenbogen, B. S. Phosphorylation by p38 Mitogen-Activated Protein Kinase Promotes Estrogen Receptor α Turnover and Functional Activity via the SCFSkp2 Proteasomal Complex. *Mol. Cell. Biol.* **32**, 1928–1943 (2012).

55. Saji, S. *et al.* MDM2 enhances the function of estrogen receptor alpha in human breast cancer cells. *Biochem. Biophys. Res. Commun.* **281**, 259–265 (2001).

56. IIZUKA, M., SUSA, T., TAMAMORI-ADACHI, M., OKINAGA, H. & OKAZAKI, T. Intrinsic ubiquitin E3 ligase activity of histone acetyltransferase Hbo1 for estrogen receptor α. *Proc. Jpn. Acad. Ser. B Phys. Biol. Sci.* **93**, 498–510 (2017).

57. Reid, G. *et al.* Cyclic, Proteasome-Mediated Turnover of Unliganded and Liganded ERα on Responsive Promoters Is an Integral Feature of Estrogen Signaling. *Mol. Cell* **11**, 695–707 (2003).

58. Lonard, D. M., Nawaz, Z., Smith, C. L. & O'Malley, B. W. The 26S Proteasome Is Required for Estrogen Receptor-α and Coactivator Turnover and for Efficient Estrogen Receptor-α Transactivation. *Mol. Cell* **5**, 939–948 (2000).

59. Shang, Y., Hu, X., DiRenzo, J., Lazar, M. A. & Brown, M. Cofactor Dynamics and Sufficiency in Estrogen Receptor–Regulated Transcription. *Cell* **103**, 843–852 (2000).

60. Miller, T. W. Endocrine Resistance: What Do We Know? *Am. Soc. Clin. Oncol. Educ. Book* (2013) doi:10.14694/EdBook_AM.2013.33.e37.

61. Gutierrez, M. C. *et al.* Molecular Changes in Tamoxifen-Resistant Breast Cancer: Relationship Between Estrogen Receptor, HER-2, and p38 Mitogen-Activated Protein Kinase. *J. Clin. Oncol.* **23**, 2469–2476 (2005).

62. Ottaviano, Y. L. *et al.* Methylation of the estrogen receptor gene CpG island marks loss of estrogen receptor expression in human breast cancer cells. *Cancer Res.* **54**, 2552–2555 (1994).

63. Toy, W. *et al.* ESR1 ligand-binding domain mutations in hormone-resistant breast cancer. *Nat. Genet.* **45**, 1439–1445 (2013).

64. Toy, W. *et al.* Activating ESR1 mutations differentially impact the efficacy of ER antagonists. *Cancer Discov.* **7**, 277–287 (2017).

65. Li, L. *et al.* Therapeutic role of recurrent ESR1-CCDC170 gene fusions in breast cancer endocrine resistance. *Breast Cancer Res.* **22**, 84 (2020).

66. Veeraraghavan, J. *et al.* Recurrent ESR1-CCDC170 rearrangements in an aggressive subset of oestrogen receptor-positive breast cancers. *Nat. Commun.* **5**, 4577 (2014).

67. Li, S. *et al.* Endocrine-Therapy-Resistant ESR1 Variants Revealed by Genomic Characterization of Breast-Cancer-Derived Xenografts. *Cell Rep.* **4**, 10.1016/j.celrep.2013.08.022 (2013).

68. Jensen, E. V. *et al.* A two-step mechanism for the interaction of estradiol with rat uterus. *Proc. Natl. Acad. Sci. U. S. A.* **59**, 632–638 (1968).

69. Welboren, W.-J., Sweep, F. C. G. J., Span, P. N. & Stunnenberg, H. G. Genomic actions of estrogen receptor alpha: what are the targets and how are they regulated? *Endocr. Relat. Cancer* **16**, 1073–1089 (2009).

70. Oñate, S. A., Tsai, S. Y., Tsai, M. J. & O'Malley, B. W. Sequence and characterization of a coactivator for the steroid hormone receptor superfamily. *Science* **270**, 1354–1357 (1995).

71. Anzick, S. L. *et al.* AIB1, a Steroid Receptor Coactivator Amplified in Breast and Ovarian Cancer. *Science* **277**, 965–968 (1997).

72. Jin, K. *et al.* HOXB7 Is an ERα Cofactor in the Activation of HER2 and Multiple ER Target Genes Leading to Endocrine Resistance. *Cancer Discov.* **5**, 944–959 (2015).

73. Sottnik, J. L. *et al.* Mediator of DNA damage checkpoint 1 (MDC1) is a novel estrogen receptor co-regulator in invasive lobular carcinoma of the breast. *Mol. Cancer Res. MCR* **19**, 1270–1282 (2021).

74. Bhatt, S., Stender, J. D., Joshi, S., Wu, G. & Katzenellenbogen, B. S. OCT-4: a novel estrogen receptor-α collaborator that promotes tamoxifen resistance in breast cancer cells. *Oncogene* **35**, 5722–5734 (2016).

75. Frogne, T. *et al.* Activation of ErbB3, EGFR and Erk is essential for growth of human breast cancer cell lines with acquired resistance to fulvestrant. *Breast Cancer Res. Treat.* **114**, 263–275 (2009).

76. Turner, N. *et al.* FGFR1 amplification drives endocrine therapy resistance and is a therapeutic target in breast cancer. *Cancer Res.* **70**, 2085–2094 (2010).

77. Fox, E. M. *et al.* A kinome-wide screen identifies the Insulin/IGF-1 receptor pathway as a mechanism of escape from hormone dependence in breast cancer. *Cancer Res.* **71**, 6773–6784 (2011).

78. Ellis, M. J. *et al.* Estrogen-independent proliferation is present in estrogen-receptor HER2-positive primary breast cancer after neoadjuvant letrozole. *J. Clin. Oncol. Off. J. Am. Soc. Clin. Oncol.* **24**, 3019–3025 (2006).

79. Campbell, R. A. *et al.* Phosphatidylinositol 3-Kinase/AKT-mediated Activation of Estrogen Receptor α: A NEW MODEL FOR ANTI-ESTROGEN RESISTANCE*. *J. Biol. Chem.* **276**, 9817–9824 (2001).

80. Comprehensive molecular portraits of human breast tumors. *Nature* **490**, 61–70 (2012).

81. Shou, J. *et al.* Mechanisms of tamoxifen resistance: increased estrogen receptor-HER2/neu cross-talk in ER/HER2-positive breast cancer. *J. Natl. Cancer Inst.* **96**, 926–935 (2004).

82. Chang, M. Tamoxifen Resistance in Breast Cancer. *Biomol. Ther.* **20**, 256–267 (2012).

83. Bosco, E. E. *et al.* The retinoblastoma tumor suppressor modifies the therapeutic response of breast cancer. *J. Clin. Invest.* **117**, 218–228 (2007).

84. Baselga, J. *et al.* Everolimus in Postmenopausal Hormone-Receptor–Positive Advanced Breast Cancer. *N. Engl. J. Med.* **366**, 520–529 (2012).

85. Finn, R. S. *et al.* Palbociclib and Letrozole in Advanced Breast Cancer. *N. Engl. J. Med.* **375**, 1925–1936 (2016).

86. Turner, N. C. *et al.* Overall Survival with Palbociclib and Fulvestrant in Advanced Breast Cancer. *N. Engl. J. Med.* **379**, 1926–1936 (2018).

87. Narayan, P. *et al.* FDA Approval Summary: Alpelisib plus fulvestrant for patients with HR-positive, HER2-negative, PIK3CA-mutated, advanced or metastatic breast cancer. *Clin. Cancer Res. Off. J. Am. Assoc. Cancer Res.* **27**, 1842–1849 (2021).

88. Siegel, R. L., Miller, K. D., Wagle, N. S. & Jemal, A. Cancer statistics, 2023. *CA. Cancer J. Clin.* **73**, 17–48 (2023).

89. Mak, H. Y., Hoare, S., Henttu, P. M. A. & Parker, M. G. Molecular Determinants of the Estrogen Receptor-Coactivator Interface. *Mol. Cell. Biol.* **19**, 3895–3903 (1999).

90. Early Breast Cancer Trialists' Collaborative Group (EBCTCG). Relevance of breast cancer hormone receptors and other factors to the efficacy of adjuvant tamoxifen: patient-level meta-analysis of randomised trials. *Lancet* **378**, 771–784 (2011).

91. Gingras, A.-C., Abe, K. T. & Raught, B. Getting to know the neighborhood: using proximity-dependent biotinylation to characterize protein complexes and map organelles. *Curr. Opin. Chem. Biol.* **48**, 44–54 (2019).

92. Branon, T. C. *et al.* Efficient proximity labeling in living cells and organisms with TurboID. *Nat. Biotechnol.* **36**, 880–887 (2018).

93. Roux, K. J., Kim, D. I., Burke, B. & May, D. G. BioID: A Screen for Protein-Protein Interactions. *Curr. Protoc. Protein Sci.* **91**, 19.23.1-19.23.15 (2018).

94. Kanzler, C. R., Donohue, M., Dowdle, M. E. & Sheets, M. D. TurboID functions as an efficient biotin ligase for BioID applications in Xenopus embryos. *Dev. Biol.* **492**, 133–138 (2022).

95. Kim, D. I. *et al.* An improved smaller biotin ligase for BioID proximity labeling. *Mol. Biol. Cell* **27**, 1188–1196 (2016).

96. Ding, Z. *et al.* Reduced expression of transcriptional intermediary factor 1 gamma promotes metastasis and indicates poor prognosis of hepatocellular carcinoma. *Hepatol. Baltim. Md* **60**, 1620–1636 (2014).

97. Vincent, D. F. *et al.* Inactivation of TIF1gamma cooperates with Kras to induce cystic tumors of the pancreas. *PLoS Genet.* **5**, e1000575 (2009).

98. Wang, L. *et al.* Repression of TIF1γ by SOX2 promotes TGF-β-induced epithelial-mesenchymal transition in non-small-cell lung cancer. *Oncogene* **35**, 867–877 (2016).

99. Chen, M. *et al.* TRIM33 drives prostate tumor growth by stabilizing androgen receptor from Skp2-mediated degradation. *EMBO Rep.* **23**, e53468 (2022).

100. Xue, J. *et al.* Sustained activation of SMAD3/SMAD4 by FOXM1 promotes TGF-β–dependent cancer metastasis. https://www.jci.org/articles/view/71104/pdf (2014) doi:10.1172/JCI71104.

101. Kassem, L. *et al.* TIF1γ interferes with TGFβ1/SMAD4 signaling to promote poor outcome in operable breast cancer patients. *BMC Cancer* **15**, 453 (2015).

102. Martin, M. Cutadapt removes adapter sequences from high-throughput sequencing reads. *EMBnet.journal* **17**, 10–12 (2011).

103. Dobin, A. *et al.* STAR: ultrafast universal RNA-seq aligner. *Bioinformatics* **29**, 15–21 (2013).

104. Li, H. *et al.* The Sequence Alignment/Map format and SAMtools. *Bioinformatics* **25**, 2078–2079 (2009).

105. Plasilova, M. L. *et al.* Features of triple-negative breast cancer. *Medicine (Baltimore)* **95**, e4614 (2016).

106. Love, M. I., Huber, W. & Anders, S. Moderated estimation of fold change and dispersion for RNA-seq data with DESeq2. *Genome Biol.* **15**, 550 (2014).

107. Eng, J. K., Jahan, T. A. & Hoopmann, M. R. Comet: an open-source MS/MS sequence database search tool. *Proteomics* **13**, 22–24 (2013).

108. Elias, J. E. & Gygi, S. P. Target-decoy search strategy for increased confidence in large-scale protein identifications by mass spectrometry. *Nat. Methods* **4**, 207–214 (2007).

109. Valot, B., Langella, O., Nano, E. & Zivy, M. MassChroQ: a versatile tool for mass spectrometry quantification. *Proteomics* **11**, 3572–3577 (2011).

110. Schwanhäusser, B. *et al.* Global quantification of mammalian gene expression control. *Nature* **473**, 337–342 (2011).

111. Tyanova, S. *et al.* The Perseus computational platform for comprehensive analysis of (prote)omics data. *Nat. Methods* **13**, 731–740 (2016).

112. Mak, H. Y., Hoare, S., Henttu, P. M. A. & Parker, M. G. Molecular Determinants of the Estrogen Receptor-Coactivator Interface. *Mol. Cell. Biol.* **19**, 3895–3903 (1999).

113. Htun, H., Holth, L. T., Walker, D., Davie, J. R. & Hager, G. L. Direct Visualization of the Human Estrogen Receptor α Reveals a Role for Ligand in the Nuclear Distribution of the Receptor. *Mol. Biol. Cell* **10**, 471 (1999).

114. Kocanova, S., Mazaheri, M., Caze-Subra, S. & Bystricky, K. Ligands specify estrogen receptor alpha nuclear localization and degradation. *BMC Cell Biol.* **11**, 98 (2010).

115. Agbo, L., Blanchet, S. A., Kougnassoukou Tchara, P.-E., Fradet-Turcotte, A. & Lambert, J.-P. Comprehensive Interactome Mapping of Nuclear Receptors Using Proximity Biotinylation. *Methods Mol. Biol. Clifton NJ* **2456**, 223–240 (2022).

116. Chen, X., Zaro, J. L. & Shen, W.-C. Fusion protein linkers: property, design and functionality. *Adv. Drug Deliv. Rev.* **65**, 1357–1369 (2013).

117. Kim, D. I. *et al.* Probing nuclear pore complex architecture with proximity-dependent biotinylation. *Proc. Natl. Acad. Sci.* **111**, E2453–E2461 (2014).

118. Strep-Tactin® for reversible binding of biotinylated or Strep-tagged proteins. *IBA Lifesciences* https://www.iba-lifesciences.com/bioid.

119. Mohammed, H. *et al.* Endogenous purification reveals GREB1 as a key Estrogen Receptor regulatory factor. *Cell Rep.* **3**, 342–9 (2013).

120. Subramanian, A. *et al.* Gene set enrichment analysis: A knowledge-based approach for interpreting genome-wide expression profiles. *Proc. Natl. Acad. Sci.* **102**, 15545–15550 (2005).

121. Pommier, R. M. *et al.* TIF1γ Suppresses Tumor Progression by Regulating Mitotic Checkpoints and Chromosomal Stability. *Cancer Res.* **75**, 4335–4350 (2015).

122. Kulkarni, A. *et al.* Tripartite Motif-containing 33 (TRIM33) protein functions in the poly(ADP-ribose) polymerase (PARP)-dependent DNA damage response through interaction with Amplified in Liver Cancer 1 (ALC1) protein. *J. Biol. Chem.* **288**, 32357–32369 (2013).

123. McAvera, R. M. & Crawford, L. J. TIF1 Proteins in Genome Stability and Cancer. *Cancers* **12**, 2094 (2020).

124. Oza, J. *et al.* A Novel Role of Chromodomain Protein CBX8 in DNA Damage Response. *J. Biol. Chem.* **291**, 22881–22893 (2016).

125. Wang, E. *et al.* The transcriptional cofactor TRIM33 prevents apoptosis in B lymphoblastic leukemia by deactivating a single enhancer. *eLife* **4**, e06377.

126. Aucagne, R. *et al.* Transcription intermediary factor 1γ is a tumor suppressor in mouse and human chronic myelomonocytic leukemia. *J. Clin. Invest.* **121**, 2361–2370 (2011).

127. Jain, S. *et al.* Association of overexpression of TIF1γ with colorectal carcinogenesis and advanced colorectal adenocarcinoma. *World J. Gastroenterol.* **17**, 3994–4000 (2011).

128. Traphagen, N. A. *et al.* High estrogen receptor alpha activation confers resistance to estrogen deprivation and is required for therapeutic response to estrogen in breast cancer. *Oncogene* **40**, 3408–3421 (2021).

129. Hosford, S. R. *et al.* Combined inhibition of both p110α and p110β isoforms of phosphatidylinositol 3-kinase is required for sustained therapeutic effect in PTEN-deficient, ER+ breast cancer. *Clin. Cancer Res. Off. J. Am. Assoc. Cancer Res.* **23**, 2795–2805 (2017).

130. Miricescu, D. *et al.* PI3K/AKT/mTOR Signaling Pathway in Breast Cancer: From Molecular Landscape to Clinical Aspects. *Int. J. Mol. Sci.* **22**, 173 (2020).

131. Fruman, D. A. *et al.* The PI3K pathway in human disease. *Cell* **170**, 605–635 (2017).

132. Szymonowicz, K., Oeck, S., Malewicz, N. M. & Jendrossek, V. New Insights into Protein Kinase B/Akt Signaling: Role of Localized Akt Activation and Compartment-Specific Target Proteins for the Cellular Radiation Response. *Cancers* **10**, 78 (2018).

133. Revathidevi, S. & Munirajan, A. K. Akt in cancer: Mediator and more. *Semin. Cancer Biol.* **59**, 80–91 (2019).

134. Saxton, R. A. & Sabatini, D. M. mTOR Signaling in Growth, Metabolism, and Disease. *Cell* **168**, 960–976 (2017).

135. Carracedo, A. *et al.* Inhibition of mTORC1 leads to MAPK pathway activation through a PI3K-dependent feedback loop in human cancer. *J. Clin. Invest.* **118**, 3065–3074 (2008).

136. O'Reilly, K. E. *et al.* mTOR Inhibition Induces Upstream Receptor Tyrosine Kinase Signaling and Activates Akt. *Cancer Res.* **66**, 1500–1508 (2006).

137. Miller, T. W. *et al.* Inhibition of mTOR is required for optimal antitumor effect of HER2 inhibitors against HER2-overexpressing cancer cells. *Clin. Cancer Res. Off. J. Am. Assoc. Cancer Res.* **15**, 7266–7276 (2009).

138. Pérez-Tenorio, G. *et al.* PIK3CA mutations and PTEN loss correlate with similar prognostic factors and are not mutually exclusive in breast cancer. *Clin. Cancer Res. Off. J. Am. Assoc. Cancer Res.* **13**, 3577–3584 (2007).

139. Saal, L. H. *et al.* Poor prognosis in carcinoma is associated with a gene expression signature of aberrant PTEN tumor suppressor pathway activity. *Proc. Natl. Acad. Sci. U. S. A.* **104**, 7564–7569 (2007).

140. Shoman, N. *et al.* Reduced PTEN expression predicts relapse in patients with breast carcinoma treated by tamoxifen. *Mod. Pathol.* **18**, 250–259 (2005).

141. Crowder, R. J. *et al.* PIK3CA and PIK3CB inhibition produce synthetic lethality when combined with estrogen deprivation in estrogen receptor positive breast cancer. *Cancer Res.* **69**, 3955–3962 (2009).

142. Arpino, G. *et al.* HER-2 amplification, HER-1 expression, and tamoxifen response in estrogen receptor-positive metastatic breast cancer: a southwest oncology group study. *Clin. Cancer Res. Off. J. Am. Assoc. Cancer Res.* **10**, 5670–5676 (2004).

143. Baselga, J. *et al.* Phase II randomized study of neoadjuvant everolimus plus letrozole compared with placebo plus letrozole in patients with estrogen receptor-

positive breast cancer. *J. Clin. Oncol. Off. J. Am. Soc. Clin. Oncol.* **27**, 2630–2637 (2009).

144. Ellis, M. J. *et al.* Phosphatidyl-inositol-3-kinase alpha catalytic subunit mutation and response to neoadjuvant endocrine therapy for estrogen receptor positive breast cancer. *Breast Cancer Res. Treat.* **119**, 379–390 (2010).

145. Gonzalez-Angulo, A. M. *et al.* PI3K Pathway Mutations and PTEN Levels in Primary and Metastatic Breast Cancer. *Mol. Cancer Ther.* **10**, 1093–1101 (2011).

146. Schmit, F. *et al.* PI3K isoform dependence of PTEN-deficient tumors can be altered by the genetic context. *Proc. Natl. Acad. Sci. U. S. A.* **111**, 6395–6400 (2014).

147. Fritsch, C. *et al.* Characterization of the novel and specific PI3Kα inhibitor NVP-BYL719 and development of the patient stratification strategy for clinical trials. *Mol. Cancer Ther.* **13**, 1117–1129 (2014).

148. André, F. *et al.* Alpelisib for PIK3CA-Mutated, Hormone Receptor–Positive Advanced Breast Cancer. *N. Engl. J. Med.* **380**, 1929–1940 (2019).

149. Edgar, K. A. *et al.* Isoform-specific phosphoinositide 3-kinase inhibitors exert distinct effects in solid tumors. *Cancer Res.* **70**, 1164–1172 (2010).

150. Ni, J. *et al.* Functional characterization of an isoform-selective inhibitor of PI3K-p110β as a potential anti-cancer agent. *Cancer Discov.* **2**, 425–433 (2012).

151. Yamnik, R. L. *et al.* S6 kinase 1 regulates estrogen receptor alpha in control of breast cancer cell proliferation. *J. Biol. Chem.* **284**, 6361–6369 (2009).

152. Miller, T. W., Balko, J. M. & Arteaga, C. L. Phosphatidylinositol 3-Kinase and Antiestrogen Resistance in Breast Cancer. *J. Clin. Oncol.* **29**, 4452–4461 (2011).

153. Generali, D. *et al.* Down-regulation of phosphatidylinositol 3'-kinase/AKT/molecular target of rapamycin metabolic pathway by primary letrozole-based therapy in human breast cancer. *Clin. Cancer Res. Off. J. Am. Assoc. Cancer Res.* **14**, 2673–2680 (2008).

154. Rusin, S. F., Schlosser, K. A., Adamo, M. E. & Kettenbach, A. N. Quantitative phosphoproteomics reveals new roles for the protein phosphatase PP6 in mitotic cells. *Sci. Signal.* **8**, rs12 (2015).

155. Grassetti, A. V., Hards, R. & Gerber, S. A. Offline pentafluorophenyl (PFP)-RP prefractionation as an alternative to high-pH RP for comprehensive LC-MS/MS proteomics and phosphoproteomics. *Anal. Bioanal. Chem.* **409**, 4615–4625 (2017).

156. Taus, T. *et al.* Universal and Confident Phosphorylation Site Localization Using phosphoRS. *J. Proteome Res.* **10**, 5354–5362 (2011).

157. KinomeXplorer: an integrated platform for kinome biology studies | Nature Methods. https://www.nature.com/articles/nmeth.2968.

158. McCabe, N. *et al.* Mechanistic Rationale to Target PTEN-Deficient Tumor Cells with Inhibitors of the DNA Damage Response Kinase ATM. *Cancer Res.* **75**, 2159–2165 (2015).

159. Shee, K. *et al.* A Transcriptionally Definable Subgroup of Triple-Negative Breast and Ovarian Cancer Samples Shows Sensitivity to HSP90 Inhibition. *Clin. Cancer Res. Off. J. Am. Assoc. Cancer Res.* **26**, 159–170 (2020).

160. Siegel, R. L., Miller, K. D. & Jemal, A. Cancer statistics, 2018. *CA. Cancer J. Clin.* **68**, 7–30 (2018).

161. Prat, A. & Perou, C. M. Deconstructing the molecular portraits of breast cancer. *Mol. Oncol.* **5**, 5–23 (2011).

162. Colombo, N. *et al.* Ovarian cancer. *Crit. Rev. Oncol. Hematol.* **60**, 159–179 (2006).

163. Cardoso, F. *et al.* Locally recurrent or metastatic breast cancer: ESMO Clinical Practice Guidelines for diagnosis, treatment and follow-up. *Ann. Oncol. Off. J. Eur. Soc. Med. Oncol.* **23 Suppl 7**, vii11-19 (2012).

164. Ledermann, J. A. *et al.* Newly diagnosed and relapsed epithelial ovarian carcinoma: ESMO Clinical Practice Guidelines for diagnosis, treatment and follow-up. *Ann. Oncol. Off. J. Eur. Soc. Med. Oncol.* **24 Suppl 6**, vi24-32 (2013).

165. Yin, L., Duan, J.-J., Bian, X.-W. & Yu, S. Triple-negative breast cancer molecular subtyping and treatment progress. *Breast Cancer Res. BCR* **22**, 61 (2020).

166. Dziadkowiec, K. N., Gąsiorowska, E., Nowak-Markwitz, E. & Jankowska, A. PARP inhibitors: review of mechanisms of action and BRCA1/2 mutation targeting. *Przeglad Menopauzalny Menopause Rev.* **15**, 215–219 (2016).

167. Farmer, H. *et al.* Targeting the DNA repair defect in BRCA mutant cells as a therapeutic strategy. *Nature* **434**, 917–921 (2005).

168. Iglehart, J. D. & Silver, D. P. Synthetic Lethality — A New Direction in Cancer-Drug Development. *N. Engl. J. Med.* **361**, 189–191 (2009).

169. Batalini, F. *et al.* Phase 1b Clinical Trial with Alpelisib plus Olaparib for Patients with Advanced Triple-Negative Breast Cancer. *Clin. Cancer Res. Off. J. Am. Assoc. Cancer Res.* **28**, 1493–1499 (2022).

170. Adams, J. M. & Cory, S. The Bcl-2 apoptotic switch in cancer development and therapy. *Oncogene* **26**, 1324–1337 (2007).

171. Merino, D. *et al.* Synergistic action of the MCL-1 inhibitor S63845 with current therapies in preclinical models of triple-negative and HER2-amplified breast cancer. *Sci. Transl. Med.* **9**, eaam7049 (2017).

172. Williams, M. M. & Cook, R. S. Bcl-2 family proteins in breast development and cancer: could Mcl-1 targeting overcome therapeutic resistance? *Oncotarget* **6**, 3519–3530 (2015).

173. Real, P. J. *et al.* Resistance to chemotherapy via Stat3-dependent overexpression of Bcl-2 in metastatic breast cancer cells. *Oncogene* **21**, 7611–7618 (2002).

174. Teixeira, C., Reed, J. C. & Pratt, M. A. Estrogen promotes chemotherapeutic drug resistance by a mechanism involving Bcl-2 proto-oncogene expression in human breast cancer cells. *Cancer Res.* **55**, 3902–3907 (1995).

175. Balko, J. M. *et al.* Molecular profiling of the residual disease of triple-negative breast cancers after neoadjuvant chemotherapy identifies actionable therapeutic targets. *Cancer Discov.* **4**, 232–245 (2014).

176. Kotschy, A. *et al.* The MCL1 inhibitor S63845 is tolerable and effective in diverse cancer models. *Nature* **538**, 477–482 (2016).

177. Mérino, D. *et al.* Bcl-2, Bcl-x(L), and Bcl-w are not equivalent targets of ABT-737 and navitoclax (ABT-263) in lymphoid and leukemic cells. *Blood* **119**, 5807–5816 (2012).

178. Thaler, S. *et al.* The proteasome inhibitor Bortezomib (Velcade) as potential inhibitor of estrogen receptor-positive breast cancer. *Int. J. Cancer* **137**, 686–697 (2015).

179. Goss, P. E. *et al.* Extending Aromatase-Inhibitor Adjuvant Therapy to 10 Years. *N. Engl. J. Med.* **375**, 209–219 (2016).

180. Davies, C. *et al.* Long-term effects of continuing adjuvant tamoxifen to 10 years versus stopping at 5 years after diagnosis of oestrogen receptor-positive breast cancer: ATLAS, a randomised trial. *Lancet Lond. Engl.* **381**, 805–816 (2013).

181. Ghajar, C. M. Metastasis prevention by targeting the dormant niche. *Nat. Rev. Cancer* **15**, 238–247 (2015).

182. Gao, X., Zhang, M., Tang, Y. & Liang, X. Cancer cell dormancy: mechanisms and implications of cancer recurrence and metastasis. *OncoTargets Ther.* **10**, 5219–5228 (2017).

183. Sosa, M. S., Bragado, P. & Aguirre-Ghiso, J. A. Mechanisms of disseminated cancer cell dormancy: an awakening field. *Nat. Rev. Cancer* **14**, 611–622 (2014).

184. Elmore, L. W., Di, X., Dumur, C., Holt, S. E. & Gewirtz, D. A. Evasion of a single-step, chemotherapy-induced senescence in breast cancer cells: implications for treatment response. *Clin. Cancer Res. Off. J. Am. Assoc. Cancer Res.* **11**, 2637–2643 (2005).

185. Ranganathan, A. C., Adam, A. P., Zhang, L. & Aguirre-Ghiso, J. A. Tumor cell dormancy induced by p38SAPK and ER-stress signaling: an adaptive advantage for metastatic cells? *Cancer Biol. Ther.* **5**, 729–735 (2006).

186. Aguirre-Ghiso, J. A., Estrada, Y., Liu, D. & Ossowski, L. ERK(MAPK) activity as a determinant of tumor growth and dormancy; regulation by p38(SAPK). *Cancer Res.* **63**, 1684–1695 (2003).

187. Aguirre-Ghiso, J. A., Liu, D., Mignatti, A., Kovalski, K. & Ossowski, L. Urokinase receptor and fibronectin regulate the ERK(MAPK) to p38(MAPK) activity ratios that determine carcinoma cell proliferation or dormancy in vivo. *Mol. Biol. Cell* **12**, 863–879 (2001).

188. Ranganathan, A. C., Zhang, L., Adam, A. P. & Aguirre-Ghiso, J. A. Functional coupling of p38-induced up-regulation of BiP and activation of RNA-dependent protein kinase-like endoplasmic reticulum kinase to drug resistance of dormant carcinoma cells. *Cancer Res.* **66**, 1702–1711 (2006).

189. Recasens, A. & Munoz, L. Targeting Cancer Cell Dormancy. *Trends Pharmacol. Sci.* **40**, 128–141 (2019).

190. Dittmer, J. Mechanisms governing metastatic dormancy in breast cancer. *Semin. Cancer Biol.* **44**, 72–82 (2017).

191. Bose, P., Simmons, G. L. & Grant, S. Cyclin-dependent kinase inhibitor therapy for hematologic malignancies. *Expert Opin. Investig. Drugs* **22**, 723–738 (2013).

192. Blum, K. A. *et al.* Risk Factors for Tumor Lysis Syndrome in patients with Chronic Lymphocytic Leukemia Treated with the Cyclin Dependent Kinase Inhibitor, Flavopiridol. *Leukemia* **25**, 1444–1451 (2011).

193. Le Tourneau, C. *et al.* Phase I evaluation of seliciclib (R-roscovitine), a novel oral cyclin-dependent kinase inhibitor, in patients with advanced malignancies. *Eur. J. Cancer Oxf. Engl. 1990* **46**, 3243–3250 (2010).

194. Byrd, J. C. *et al.* Flavopiridol administered using a pharmacologically derived schedule is associated with marked clinical efficacy in refractory, genetically high-risk chronic lymphocytic leukemia. *Blood* **109**, 399–404 (2007).

195. Nemunaitis, J. J. *et al.* A first-in-human, phase 1, dose-escalation study of dinaciclib, a novel cyclin-dependent kinase inhibitor, administered weekly in subjects with advanced malignancies. *J. Transl. Med.* **11**, 259 (2013).

196. Asghar, U., Witkiewicz, A. K., Turner, N. C. & Knudsen, E. S. The history and future of targeting cyclin-dependent kinases in cancer therapy. *Nat. Rev. Drug Discov.* **14**, 130–146 (2015).

197. Mita, M. M. *et al.* Randomized phase II trial of the cyclin-dependent kinase inhibitor dinaciclib (MK-7965) versus capecitabine in patients with advanced breast cancer. *Clin. Breast Cancer* **14**, 169–176 (2014).

198. Stephenson, J. J. *et al.* Randomized phase 2 study of the cyclin-dependent kinase inhibitor dinaciclib (MK-7965) versus erlotinib in patients with non-small cell lung cancer. *Lung Cancer Amst. Neth.* **83**, 219–223 (2014).

199. Gojo, I. *et al.* Phase II Study of the Cyclin-Dependent Kinase (CDK) Inhibitor Dinaciclib (SCH 727965) In Patients with Advanced Acute Leukemias. *Blood* **116**, 3287 (2010).

200. Hortobagyi, G. N. *et al.* Ribociclib as First-Line Therapy for HR-Positive, Advanced Breast Cancer. *N. Engl. J. Med.* **375**, 1738–1748 (2016).

201. Hortobagyi, G. N. *et al.* Updated results from MONALEESA-2, a phase 3 trial of first-line ribociclib + letrozole in hormone receptor-positive (HR+), HER2-negative (HER2–), advanced breast cancer (ABC). *J. Clin. Oncol.* **35**, 1038–1038 (2017).

202. Leo, A. D. *et al.* MONARCH 3: Abemaciclib as initial therapy for patients with HR+/HER2- advanced breast cancer. *Ann. Oncol.* **28**, v609 (2017).

203. Chen, P. *et al.* Spectrum and Degree of CDK Drug Interactions Predicts Clinical Performance. *Mol. Cancer Ther.* **15**, 2273–2281 (2016).

204. Knudsen, E. S., Hutcheson, J., Vail, P. & Witkiewicz, A. K. Biological specificity of CDK4/6 inhibitors: dose response relationship, in vivo signaling, and composite response signature. *Oncotarget* **8**, 43678–43691 (2017).

205. Franco, J., Balaji, U., Freinkman, E., Witkiewicz, A. K. & Knudsen, E. S. Metabolic Reprogramming of Pancreatic Cancer Mediated by CDK4/6 Inhibition Elicits Unique Vulnerabilities. *Cell Rep.* **14**, 979–990 (2016).

206. Lopez-Mejia, I. C. *et al.* CDK4 Phosphorylates AMPKα2 to Inhibit Its Activity and Repress Fatty Acid Oxidation. *Mol. Cell* **68**, 336-349.e6 (2017).

207. Lee, Y. *et al.* Cyclin D1-Cdk4 controls glucose metabolism independently of cell cycle progression. *Nature* **510**, 547–551 (2014).

208. Klein, M. E., Kovatcheva, M., Davis, L. E., Tap, W. D. & Koff, A. CDK4/6 Inhibitors: The Mechanism of Action May Not Be as Simple as Once Thought. *Cancer Cell* **34**, 9–20 (2018).

209. Hampsch, R. A. *et al.* AMPK activation by metformin promotes survival of dormant ER+ breast cancer cells. *Clin. Cancer Res. Off. J. Am. Assoc. Cancer Res.* **26**, 3707–3719 (2020).

210. Torres-Guzmán, R. *et al.* Preclinical characterization of abemaciclib in hormone receptor positive breast cancer. *Oncotarget* **8**, 69493–69507 (2017).

211. Ahn, B.-C. Applications of molecular imaging in drug discovery and development process. *Curr. Pharm. Biotechnol.* **12**, 459–468 (2011).

212. Hong, S.-Y. *et al.* Stabilization of AURKA by the E3 ubiquitin ligase CBLC in lung adenocarcinoma. *Oncogene* **41**, 1907–1917 (2022).

213. Mahlokozera, T. *et al.* Competitive binding of E3 ligases TRIM26 and WWP2 controls SOX2 in glioblastoma. *Nat. Commun.* **12**, 6321 (2021).

214. Xu, G. & Jaffrey, S. R. Proteomic Identification of Protein Ubiquitination Events. *Biotechnol. Genet. Eng. Rev.* **29**, 73–109 (2013).

215. Dunbier, A. K. *et al.* Molecular profiling of aromatase inhibitor-treated postmenopausal breast tumors identifies immune-related correlates of resistance. *Clin. Cancer Res. Off. J. Am. Assoc. Cancer Res.* **19**, 2775–2786 (2013).

216. Bielskienė, K., Bagdonienė, L., Mozūraitienė, J., Kazbarienė, B. & Janulionis, E. E3 ubiquitin ligases as drug targets and prognostic biomarkers in melanoma. *Medicina (Mex.)* **51**, 1–9 (2015).

217. Gigantino, V. *et al.* Identification of Antiestrogen-Bound Estrogen Receptor α Interactomes in Hormone-Responsive Human Breast Cancer Cell Nuclei. *Proteomics* **20**, e2000135 (2020).

218. Cirillo, F. *et al.* Molecular Mechanisms of Selective Estrogen Receptor Modulator Activity in Human Breast Cancer Cells: Identification of Novel Nuclear Cofactors of Antiestrogen–ERα Complexes by Interaction Proteomics. *J. Proteome Res.* **12**, 421–431 (2013).

219. Kaminska, K. *et al.* Distinct mechanisms of resistance to fulvestrant treatment dictate level of ER independence and selective response to CDK inhibitors in metastatic breast cancer. *Breast Cancer Res.* **23**, 26 (2021).

220. Hutcheson, I. R. *et al.* Fulvestrant-induced expression of ErbB3 and ErbB4 receptors sensitizes oestrogen receptor-positive breast cancer cells to heregulin β1. *Breast Cancer Res.* **13**, R29 (2011).

221. Sas, L. *et al.* The interaction between ER and NFκB in resistance to endocrine therapy. *Breast Cancer Res. BCR* **14**, 212 (2012).

222. Lavinsky, R. M. *et al.* Diverse signaling pathways modulate nuclear receptor recruitment of N-CoR and SMRT complexes. *Proc. Natl. Acad. Sci. U. S. A.* **95**, 2920–2925 (1998).

223. Smith, C. L., Nawaz, Z. & O'Malley, B. W. Coactivator and corepressor regulation of the agonist/antagonist activity of the mixed antiestrogen, 4-hydroxytamoxifen. *Mol. Endocrinol. Baltim. Md* **11**, 657–666 (1997).

224. Norris, J. D. *et al.* Peptide antagonists of the human estrogen receptor. *Science* **285**, 744–746 (1999).

225. Lamm, N., Rogers, S. & Cesare, A. J. The mTOR pathway: Implications for DNA replication. *Prog. Biophys. Mol. Biol.* **147**, 17–25 (2019).

226. Villafañez, F. *et al.* AKT inhibition impairs PCNA ubiquitylation and triggers synthetic lethality in homologous recombination-deficient cells submitted to replication stress. *Oncogene* **38**, 4310–4324 (2019).